2007

In-vivo radiation diode dosimetry for therapeutic photon beams

Amarjit Singh Saini
University of South Florida

In-Vivo Radiation Diode Dosimetry for Therapeutic Photon Beams

by

Amarjit Singh Saini

A dissertation submitted in partial fulfillment
of the requirements for the degree of
Doctor of Philosophy
Department of Chemical Engineering
College of Engineering
University of South Florida

Co-Major Professor: William E. Lee III, Ph.D.
Co-Major Professor: Harvey M. Greenberg, M.D.
Timothy C. Zhu, Ph.D.
Kent H. Larsen, Ph.D.
Paris H. Wiley, Ph.D.

Date of Approval:
October 17, 2007

Keywords: Quality assurance, silicon detectors, temperature dependence, dose rate dependence, and energy dependence

DEDICATION

To my family

ACKNOWLEDGEMENTS

I would like to thank my advisor Timothy Zhu, Ph.D. for giving me the opportunity to work on this project and guiding me throughout my graduate career. His guidance has been invaluable. I am thankful to William E. Lee III, Ph.D. and Harvey Greenberg, M.D. for serving as co-major professor and their encouraging support throughout this work. Dr. Lee has provided tremendous support and advice for this project. I would like to thank Kent Larsen, Ph.D. and Paris Wiley, Ph.D. for serving on my supervisory committee and their encouraging support.

I am grateful to my current employer H. Lee Moffitt Cancer Center & Research Institute for providing me the time, support, and resources for this work. I would like to thank Jie Shi from Sun Nuclear Corporation for his in depth critiques and many helpful comments on temperature and dose rate studies.

Thanks to Bill Simon and Jie Shi of Sun Nuclear Corporation, Bill Zimmermann of Fluke biomedical, and Camilla Rönnqvist of Scanditronix Wellhöfer for providing the diodes used in this study.

Above all, I can not thank enough my uncle Daljit Saini who has provided guidance, support, and encouragement throughout my undergraduate and graduate studies.

TABLE OF CONTENTS

LIST OF TABLES iv

LIST OF FIGURES v

ABSTRACT vii

CHAPTER 1 INTRODUCTION 1
- 1.1 Radiation Dosimetry and Diodes 1
- 1.2 Basics of Diode Detectors (n-type and p-type) 2
- 1.3 Diode Detectors for In-vivo Dosimetry 4
- 1.4 Correction Factors Methodology for Diode Dosimetry 6
  - 1.4.1 Sensitivity Variation with Temperature (*SVWT*) 7
  - 1.4.2 Dose Rate and Source-to-Detector Distance (SDD) 9
  - 1.4.3 Energy 10
  - 1.4.4 Field Size 11
  - 1.4.5 Angular Dependence 11
  - 1.4.6 Sensitivity Variation with Accumulated Dose (SVWAD) 12
- 1.5 Objective of the Study 13
- 1.6 Dissertation Outline 13
- 1.7 Limitation of this Work 14

CHAPTER 2 THEORY 16
- 2.1 Electric Transport 16
  - 2.1.1 R-G Centers 16
  - 2.1.2 P-N Junction 22
  - 2.1.3 Steady State and Transient Current in Radiation Diode Detector 23
  - 2.1.4 Diode Sensitivity 26
- 2.2 Radiation Transport 29
  - 2.2.1 Monte Carlo Simulation 29
  - 2.2.2 Analytical Calculation for Diode-to-Water Dose Ratio Using Brag Gray Cavity Theory 30

CHAPTER 3 PAPER I: TEMPERATURE DEPENDENCE OF COMMERCIALLY AVAILABLE DIODE DETECTORS 34
- 3.1 Synopsis 34
- 3.2 Introduction 35

3.3 Material and Methods 36
3.3.1 Description of Diodes 36
3.3.2 Experiment Setup 39
3.3.3 Theory 43
3.4 Results & Discussion 45
3.4.1 Unirradiated N-Type 45
3.4.2 Preirradiated N-Type 47
3.4.3 Unirradiated P-Type 48
3.4.4 Preirradiated P-Type 50
3.5 Conclusion 55

CHAPTER 4 PAPER II: DOSE RATE AND SDD DEPENDENCE OF COMMERCIALLY AVIALABLE DIODE DETECTORS 57
4.1 Synopsis 57
4.2 Introduction 58
4.3 Materials and Methods 60
4.3.1 Description of Diodes 60
4.3.2 Experiment Setup 61
4.3.3 Theory 66
4.4 Results 69
4.5 Discussion 74
4.5.1 Unirradiated and Preirradiated N-Type 74
4.5.2 Unirradiated and Preirradiated P-Type 78
4.5.3 Comparison with Literature 79
4.5.4 Comparison Between N-Type and P-Type Diodes 82
4.6 Conclusion 84

CHAPTER 5 PAPER III: ENERGY DEPENDENCE OF COMMERCIALLY AVAILABLE DIODE DETECTORS FOR IN-VIVO DOSIMETRY 85
5.1 Synopsis 85
5.2 Introduction 86
5.3 Material and Methods 87
5.3.1 Description of Diodes 87
5.3.2 Experimental Setup 89
5.3.3 Monte Carlo Simulation 92
5.4 Results and Discussion 95
5.5 Conclusion 102

CHAPTER 6 PAPER IV: DOSIMETRIC STUDY OF NEW PT-DOPED N-TYPE DIODE DETECTORS USED FOR IN-VIVO DOSIMETRY 103
6.1 Synopsis 103
6.2 Introduction 104
6.3 Materials and Methods 105
6.3.1 Description of Diodes 105
6.3.2 Experimental Setup 107

6.4 Results and Discussion 112
6.5 Conclusion 121

CHAPTER 7 CONCLUDING REMARKS..... 122

REFERENCES 125

APPENDICES 130
Appendix A Mat Lab Codes for Temperature Dependence Study (Paper I)..... 131
Appendix B Mat Lab Codes for Dose Rate Dependence Study (Paper II)..... 139
Appendix C Mat Lab Codes for Energy Dependence Study (Paper III) 166
Appendix D Mat Lab Codes for the Dosimetric Study (Paper IV)..... 173

ABOUT THE AUTHOR ..... End Page

LIST OF TABLES

Table 1. Specification of different diode detectors. 37
Table 2. Dose rate of radiation sources (Paper I)..... 42
Table 3. Temperature coefficients for n-type and p-type diodes. 47
Table 4. Package (a) and device (b) specification of the different diode detectors. 63
Table 5. Dose rate of the radiation sources (Paper II). 65
Table 6. Fitting parameters for the commercial diodes. 75
Table 7. Package specification of the different diode detectors. 88
Table 8. Summary of correction factors. 90
Table 9. Measured diode normalized sensitivity vs. nominal accelerating energy. 96
Table 10. Results of MC simulation for the normalized diode sensitivity. 99
Table 11. Results of the analytical cavity theory calculation. 101
Table 12. Specification of different diode detectors used in this study. 105
Table 13. The field size correction factors for different diodes..... 115
Table 14. Temperature Coefficient (%/^{o}C) for different diodes. 118

LIST OF FIGURES

Figure 1. Schematic for relating diode radiation current with the incident radiation 3
Figure 2. Possible electronic transitions. 17
Figure 3. Schematics of diode current in the p^+-n junction. 23
Figure 4. Schematics of radiation generation shape vs. time. 25
Figure 5. The schematics of the patient dosimetry diode detectors. 38
Figure 6. Temperature dependence for n-type (Isorad) unirradiated photon diodes. 46
Figure 7. Temperature dependence for Isorad Red (n-type) preirradiated diode. 48
Figure 8. Temperature dependence for QED (p-type) unirradiated photon diode. 49
Figure 9. Temperature dependence for p-type (QED) preirradiated photon diodes. 51
Figure 10. Temperature dependence for p-type (EDP) preirradiated photon diodes. 52
Figure 11. Dose rate dependence of the relative diode sensitivity, S/S_0, for 6 MV. 53
Figure 12. SDD correction factors for n-type diodes under pulsed beams. 71
Figure 13. SDD correction factors for p-type diodes under pulsed beams. 72
Figure 14. SDD dependence of different diodes under Co-60 radiation. 73
Figure 15. Dose rate dependence of the diode detectors under pulsed radiation. 76
Figure 16. Dose rate dependence of an n-type and a p-type diode detectors. 77
Figure 17. Comparison of SDD CF at the surface and in miniphantom. 83
Figure 18. Schematics of the geometry of the diode detector for MC simulation. 93
Figure 19. Energy dependence for different (new) diodes. 97
Figure 20. Energy dependence for different (old) diodes. 98
Figure 21. Monte Carlo simulation results. 100
Figure 22. Schematics of n-type pt-doped diodes (a) Isorad-3 (b) QED (n-type). 106

Figure 23. SSD dependence of pt-doped diode detectors. 113
Figure 24. Dose rate dependence of pt-doped diode detectors (6 and 18 MV). 114
Figure 25. Field size dependence correction factors for different diodes. 116
Figure 26. Angular dependence for different diode detectors. 117
Figure 27. Temperature dependence for different diode detectors. 120

IN-VIVO RADIATION DIODE DOSIMETRY FOR THERAPEUTIC PHOTON BEAMS

Amarjit Singh Saini

ABSTRACT

In-vivo dosimetry with diode detectors is used in radiation therapy as a quality assurance tool. The diode sensitivity under radiation depends upon temperature, dose rate and SDD (source-to-detector distance), field size, beam angle, and energy. This dissertation presents the first systematic and quantitative study of dosimetric characteristics for most of the commercial radiation diodes (n-type and p-type) under different radiation beams.

In the temperature dependence study, the systematic study on the dose rate dependence of *svwt* (sensitivity variation with temperature) was performed. It was concluded that sufficient preirradiation can eliminate dose rate dependence of *svwt*. However, preirradiation cannot eliminate dose rate dependence of the diode sensitivity, *S*, itself. In the dose rate and SDD dependence study, it was shown that the p-type diodes do not always show less dose rate dependence than the n-type diodes. Preirradiation does not always reduce diode dose rate dependence. SDD dependence of diode sensitivity can be explained by the instantaneous dose rate dependence if sufficient buildup is provided to eliminate electron contamination. An empirical formula was proposed to fit the dose rate dependence of diode sensitivity. In the energy dependence study, the energy dependence diode detectors are quantified. The empirical theory to quantify this effect was developed. Monte Carlo simulation and the cavity theory are used to predict the energy dependence. It was concluded that the energy dependence does not depend on whether the diode is n- or p- type but rather depends mainly on the material around the die

(buildup and its geometry). A systematic study of the correction factors for accurate diode dosimetry is presented in this dissertation.

This dissertation has established a theoretical foundation for the modeling of the transient electric and radiation properties of the diode detectors, separately. We believe that the Monte Carlo simulations code for radiation transport should be coupled with the continuity equations to describe the charge transport in the diode detector, and thus provides a complete quantitative description of dosimetric characteristics of the diode detectors. The ultimate goal is to use the diode detector as an absolute dosimeter, rather than as a relative dosimeter.

CHAPTER 1 INTRODUCTION

1.1 Radiation Dosimetry and Diodes

Absorbed dose (Gy) in radiation therapy is defined as total energy absorbed (J) per unit mass (kg) of the patient or water.[1-4] Absolute radiation dosimetry is the way of measuring the absorbed dose at a point in a fixed geometry (e.g. field size, distance, and depth) under certain conditions (e.g. temperature, pressure, and humidity).[1-4] Relative radiation dosimetry allows one to determine the dose at any point of interest under the particular conditions for the irradiation, compared to the dose at the reference point under reference geometric conditions. One can determine the dose for any geometric setups by performing absolute dosimetry at the reference condition and relative dosimetry for all other points.

The diode is a good relative dosimeter for in-vivo dosimetery because it exhibits certain characteristics. Compared to ionization chamber, the diode has the advantages of high sensitivity (charge collected per unit dose to the diode) and quick response time. Other major advantages of semiconductor detectors are excellent reproducibility, good mechanical stability, absence of external bias, small size, and the energy independence of mass collision stopping power ratios (between silicon and water for clinically usable electron beams with energy between 4-20 MeV).[5] The real-time in-vivo dosimetry allows one to check the prescribed dose for dynamic beam immediately and make it possible to correct the treatment errors interactively.[5-7]

To perform absolute dosimetry, it is necessary to determine the relationship between the absorbed dose and the measured quantity using the fundamental physics quantities. This

dissertation established some of the preliminary relationship so that it is hoped that the diodes may be used as an absolute dosimeter in addition to relative dosimeter.

1.2 Basics of Diode Detectors (n-type and p-type)

The structure in the silicon diode used for in-vivo dosimetry is p-n junction. The p-n junction can be manufactured in many different ways. The most common device manufacturing technique is to lightly dope a pure silicon substrate to become either n-type (10^{14} to 10^{16} atoms cm^{-3} of phosphorous) or p-type (10^{15} to 10^{17} atoms cm^{-3} of boron), and then heavily doping impurities with the opposite type (with a concentration of more than two orders of magnitude than the substrate) in the surface region to form a p-n junction. This spatially charged p n junction region is also called the depletion region. For the diodes used for in-vivo dosimetry the depletion layer thickness is a few micrometers.

The p^+-n junction diode detector is shown in figure 1 under the incident radiation beam. The diode exhibits radiation electrical current generated by radiation, which is then measured using an electrometer. The diode radiation current is proportional to the radiation dose generated by radiation which depends upon electric and radiation transport properties. The diode sensitivity, i.e. S=M/D, depends on incident dose rate, diode temperature, and incident energy. *M* is the total charge collected by the diode during the irradiation and *D* is the absorbed dose. These can be modeled using radiation and electric transport of the diode detector.

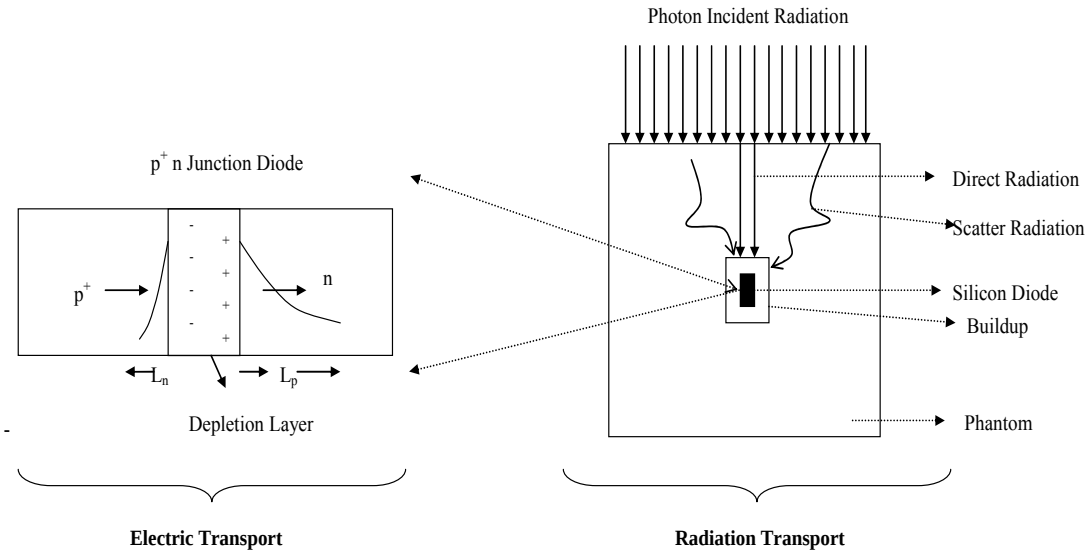

Figure 1. Schematic for relating diode radiation current with the incident radiation.

There are two types of diodes: n-type and p-type. The radiation current generated in diodes is primarily determined by the semiconductor properties in the lightly doped area (the substrate). Thus the diode is termed n-type or p-type depending upon whether the silicon substrate is doped with phosphorous where majority carriers are electrons or boron where majority carriers are holes, respectively.[8]

The high electrical field across the p-n junction makes the charge collection possible for diode without an external bias. The incident ionizing radiation generates electron-hole pairs throughout the diode. The minority carriers (electrons on the p side and holes on the n side) diffuse toward the p n junction. Some of those carriers within one diffusion length from the junction edge are able to reach it before they recombine. The thickness of the diffusion length is determined by the life time of the minority carriers. The lifetime determines the mean time for the electrons and holes to recombine. This finite life time for the minority carriers is due to recombination centers (R-G centers) trapped in the crystal (more detailed in chapter 2). The carriers are swept across the junction by the natural built in potential. The total current consists of the radiation current and the

electrical leakage current of the diode. The construction of the diode (or die), including size, composition of doping, forming of p-n junction by diffusion, and any other lattice defects present (before or after the irradiation), determine of the characteristics of the detector response to radiation.

1.3 Diode Detectors for In-vivo Dosimetry

In-vivo dosimetry in radiation therapy refers to measuring radiation dose directly in a patient during radiation treatment. It can be done invasively by implanting the dosimeter at the point of interest or non-invasively by placing the dosimeter on the patient entrance (or exit) surface. The later is used as part of the quality assurance (QA) program in radiotherapy. It allows indirect comparison between prescribed dose and delivered dose for a particular treatment field, which provides additional safeguards against major setup errors, calculation or transcription errors, which were missed during the initial patient chart checks.[9-14] In the absence of errors, it provides documentation that the treatment was delivered correctly within the user specified tolerances. In-vivo dosimetry is also useful in supporting the high accuracy in dose delivery expected from complex and conformal radiotherapy treatments.[11,15] The AAPM TG40[16] highly recommends that the clinics "should have access to TLD or other in-vivo systems." A well defined in-vivo dosimetry program should be able to catch most of the errors without increasing the treatment time.

In a review from Europe[17], the patients undergoing radiotherapy treatments at three different institutions reported 120 treatment errors exceeding 5% were found with their in-vivo dosimetry system. IAEA has concluded in their report[17] that the well placed in-vivo dosimetry program could have prevented the recent overexposure of 28 patients in Panama. In their report they have recommended that "in-vivo dosimetry should be promoted as far as practicable in radiotherapy departments, but proper preparation for such program is necessary."[17]

The dosimeters are usually placed on the patient's skin to perform either entrance dose or exit dose measurements. The purpose of the entrance dose measurements is to detect any errors due to equipment malfunctioning and human mistake. The purpose of the exit dose is to detect additional dose delivery uncertainties due to tissue heterogeneities (e.g. bone, air cavity, or lung). The measured dose is then compared with the calculated dose. If the measured dose and calculated dose differs greater than the user-specified range, the difference may be used to detect many serious errors after further investigation. Some publications have also reported that the errors in machine calibration were caught using in-vivo dosimetry. The specified range between the measured dose and the calculated dose depend upon the institution and how the in-vivo dosimetry program is setup, but some of the publications have suggested ±5% action level for all the entrance dose measurements performed.[12,18-21]

These days most of the in-vivo radiation dosimetry is performed with silicon diodes, thermoluminescent dosimeters (TLDs), and metal–oxide–semiconductor field-effect transistor (MOSFET). For in-vivo entrance dose measurements, the diode is calibrated under some standard conditions before it is used as a relative dosimeter. The treatment conditions are always different than the standard conditions. Therefore further correction factors are then applied to account for variation in diode response in situations deviating from the standard calibration conditions. The main correction factors which influence the diode response during the entrance dose measurements are temperature, field size, source to skin distance (SSD), and presence of other beam modifiers such as wedges and trays.

The diode die (chip) usually has inherent buildup material placed around the die. The buildup material type and its thickness are chosen in such a way that the effective depth of the measurements is closer to the depth of the maximum dose of the megavoltage photon energy used. The inherent buildup material is usually made of high Z material so that the physical thickness can be less than that of water-equivalent thickness. Normally, the higher the megavoltage photon energy, the thicker the inherent buildup is needed. The buildup material affects the diode's energy response to radiation. For entrance dose

measurements, it is recommended that diodes should be used for the energy range it is designed for.[15] The low-energy range diode detector for high energy beams can be a problem as it increases the affect for the contaminant electrons. The use of a high energy designed diode detector (thicker effective buildup) can be used for lower megavoltage energy beams as long as it is not used in the buildup region, however the significant energy dependence can be observed if the buildup of the diode is too thick.[15]

1.4 Correction Factors Methodology for Diode Dosimetry

The diode sensitivity is defined as the ionization charge per unit radiation dose (usually in unit of nC/cGy). The sensitivity of semiconductor diode detectors depend on the construction of the diodes and the surrounding structures (including inherent buildup material). The temperature[6,22-25], dose rate[6,22,26-30], and accumulated dose are caused by the die (bare diode) itself. The energy [6,7,31], field size, and directional dependency are mainly caused by the construction of the surrounding buildup structures. The absorbed dose measured at a particular point measured by the silicon diode detector can be calculated as:

$$D = \frac{M_{diode}}{S} \tag{1}$$

M_{diode} is the charge collected in nC by the silicon diode detector and S is the total diode sensitivity. D is the absorbed dose at a particular point without the diode. One can also define the sensitivity of the bare diode, S_{diode}, as:

$$S_0 = M_{diode} / D_{diode}. \tag{2}$$

S_o is the ideal sensitivity with all correction factors taken out. D_{diode} is the dose measured with the silicon diode before all the correction factors are applied. Sensitivity of the

diode detector, S depends upon the temperature, dose rate, energy, field size, and beam angle i.e.

$$S = CF_{total} \cdot S_0 . \quad (3)$$

and,

$$CF_{total} = CF_{temp} \times CF_{dose.rate} \times CF_{energy} \times CF_{field.size} \times CF_{beam.angle} \times ..... \quad (4)$$

CF_{total} accounts for all the correction factors for the diode detector. CF_{temp}, $CF_{dose.rate}$, CF_{energy}, $CF_{field.size}$, and $CF_{beam.angle}$ are the correction factors for the diode detector for temperature, dose rate, energy, field size, and beam angle. Another term, S_{diode}, is the sensitivity of the bare diode defined in nC/cGy. $S_{diode} = CF_{temp} \times CF_{dose.rate} \times \cdot S_0$. The literature review of these factors is discussed below.

1.4.1 Sensitivity Variation with Temperature (*SVWT*)

Temperature is an important factor because when the diode is placed on the patient, its temperature can rise to skin temperature within a few minutes.[23,25] Welsh and Reinstein have recently quantified the rising time of temperature and the equilibrium temperature for many commercial diodes.[25] This can produce an inaccuracy in dose measurement up to 9% depending on the type of diode used, photon energy, dose rate, and pre-irradiation.[25]

The radiation current generated in a diode may increase or decrease with temperature. The "temperature coefficient" is the percent change in sensitivity per degree of temperature increase. The temperature dependence generally depends upon the carrier mobility and the lifetime. The carrier mobility generally decreases as temperature increases due to high crystal lattice scatter.[15,32,33] The carrier lifetime appears to increase

with increasing temperature due to increased probability of carrier leaving from the recombination-generation (R-G) centers and traps (discussed in chapter 2). Most of the diodes used in radiotherapy have positive temperature coefficient. The sensitivity variation with temperature (*svwt*) first increases with large (>kGy) accumulated dose and then stabilizes with further doses probably due to additional RG centers and traps so that more carriers are released as the temperature increases.[5,15,22,24,27] The dependence of carrier lifetime on temperature is the dominant effect for these diodes.

Rikner has noted that the sensitivity is dependent on the temperature of the detector and the sensitivity variation with temperature (*svwt*) depends upon the accumulated dose in the detector.[6,23] Different authors have reported the temperature coefficient, also called sensitivity variation with temperature (*svwt*), for n- and p-type diodes.[22,23] Grusell and Rikner have shown in their paper that the sensitivity variation with temperature increases linearly and the temperature coefficient was larger after the detectors were preirradiated, but still linear with respect to temperature.[23] The temperature coefficient was 0.3%/^{o}C for a p-type diode with an accumulated dose of 6kGy of 20 MeV electrons.[5] They have shown that temperature coefficient increases for up to about 6kGy accumulated dose and is then stays constant.[5] Some authors have pointed out the dose rate dependence for *svwt* using a model of two R-G centers with different energy levels [27] in the case where multiple mechanisms of R-G processes exist (e.g., R-G centers caused by defects, Au or Pt impurities exist simultaneously). The commercial diodes used for in-vivo dosimetry show a temperature coefficient of +0.1%^{o}C to 0.5%/^{o}C.[22,24,34,35]

The diode leakage current has a large temperature coefficient. Normally leakage current is much smaller than the radiation current, but the leakage can contribute significantly to the temperature dependence for the diodes with relative large leakage current.

1.4.2 Dose Rate and Source-to-Detector Distance (SDD)

The dose rate could vary due to source–to-detector distance (SDD) change, placement of transmission blocks, or transmission through the patient. In clinical application, the diode is usually placed either at a patient's entrance or exit surface to measure the dose rate. The SDD for patient treatment can vary from 70 cm (for isocentric SAD setup) to 140 cm (for mantle treatment), or even more than 300 cm (for total body irradiation). These changes of treatment setup can affect the results of diode measurements. The change in the SDD and the placement of the beam modifier can change the dose rate at the diode, which thus changes the probability of the indirect recombination. The magnitude of the instantaneous dose rate depends upon the characteristics of the diode die and the dominant R-G center.

The defects and impurities in the semiconductor crystal introduce recombination (R-G) centers. The indirect recombination is the most dominant of charge recombination in silicon diodes. It occurs when a minority carrier (holes for n-type and electron for p-type) is captured by the R-G center and then recombines with the majority carrier. The fraction of minority carriers which recombine depends upon the concentration of the R-G centers, on the capture cross sections for the minority carriers, and excess carrier concentration which is proportional to the instantaneous dose rate. For a single radiation exposure, the number of R-G centers remains constant. The rate of minority carrier increases when the instantaneous rate is increased (short SDD). In case the R-G center concentration is insufficient to keep the recombining fraction of carriers constant, the diode sensitivity increases.[15] This happens because a larger fraction of charge produced by radiation is available to be collected with an electrometer. For linear accelerators, the dose is delivered in pulses and the dose in a single pulse determines the rate of charge generation.

The dose rate has been reported to be a problem in n-type semiconductor detectors but not for preirradiated p-type diodes.[6,7,30] Rikner and Grusell have reported that the p-type

Si detector preirradiated to 25 kGy displays a flat dose rate dependence.[26] Rikner has also shown that the response of n-type detector (in house diode, without any Au or Pt doping) shows more dose rate dependence than p-type detectors.[6] It has also been shown that the linearity of p-type detector depends upon the resistivity or doping level of the diode (higher the doping level, the lower the resistivity, and vice versa).[27] A high doped (low resistivity) p-type detector shows linear response (no dose rate dependence).[27] In a recent paper by Wilkins, it has been shown that the one of the preirradiated p-type diode shows dose rate dependence even after a high level of preirradiation (~25 kGy) where as the other diode shows very little dependence (after ~ 8kGy of preirradiation).[30] In our study, we will show that this condition is not generally true and some n-type diodes can have small dose rate dependence so long as the doping level for the minority carrier is substantially higher than the conventional doping level (10^{14} cm^{-3}).

1.4.3 Energy

The diode response depends on the energy.[6,7,36] Most of the energy dependence in silicon diodes is caused by the materials around the diode. The electrode attachment, protective housing, and buildup material (usually high Z material) can contribute to the energy dependence of the diode. These high Z materials in close proximity to the die alter the dose (or ionization) in the Si die in amounts that depend on the construction of the diode geometry. For in-vivo radiation measurements, the buildup material on the diode is chosen so that the effective depth of the diode is close to the depth of the maximum dose of the megavoltage photon beams. This affects it's energy response to the radiation. At present, the different vendors provide different detectors dedicated to different energy ranges. For clinical use, it is recommended that the diode be used for the energy range it is designed for. It is possible to use a photon diode designed for higher photon energy for in-vivo dosimetry of lower photon energies as long as the diode is not used in the buildup region for the photon energy. However, significant energy dependence is observed if the buildup of the diode is too thick.

1.4.4 Field Size

The diode reading increases with increasing field size for photon entrance dose measurements. The field size correction factors are usually measured by taking the ratio of the normalized diode reading at the surface to the normalized ion chamber reading at the depth of maximum dose. These two dosimeters receive different scattered dose contribution from the incident beam which can cause some field size dependence. The field size dependence reported by many authors is mainly due to the diode's buildup materials and buildup thickness.[10,12,20,31,34] For large field sizes, the diode field size correction factors can differ by as much as 5% from the ion chamber measurements of field size dependence.[34,37,38] The ion chamber measurements of field size dependence are often also called the output ratio in water. For diodes with insufficient buildup, electron contamination contribute to the field size dependence.[39]

1.4.5 Angular Dependence

The diode reading when placed on the patient surface or on the phantom surface depends upon the orientation with respect to the incident beam. This direction dependence is caused by the construction (mainly buildup) of the diode detector and by the back scattering from the patient or phantom surface. For a cylindrical detector the plane of the die is mounted normal to the cable axis and the die is surrounded by a cylindrical sleeve of buildup. For in-vivo dose measurements, the side of the cylinder is usually placed against the patient with the beam axis as nearly normal to the cylinder axis as possible so that the plane of the site is approximately parallel to the beam axis. In general, the cylindrical design shows smaller angular dependence than the flat detector when the beam axis rotated in the axial direction.[15,19,38] The effective sensitivity change for the cylindrical detector is less that 2% for beam angles less than $\pm 70^{o}$.[15,38] For the diode with flat design the die is mounted with the plane of the die parallel to the cable axis. One side of the die is covered with hemispherical buildup and the other side is covered with thin protective covering. This type of detector is designed to be placed with

the flat side on the patient and the central axis of the beam approximately normal to the plane of the die. The flat detectors normally show larger directional dependence, which can exceed 5% for beam angles exceeding ±40°. It is recommended that particular attention needs to be given when this type of detector is placed for entrance dose measurements.[15]

1.4.6 Sensitivity Variation with Accumulated Dose (SVWAD)

The mechanisms such as doping and impurities such as gold, platinum, and ionizing radiation result in sensitivity variation with accumulated dose. The defects from the ionizing radiation create R-G centers and carrier traps. These are the defects which capture the carriers but have small probability of recombination. With accumulated dose, the increase in RG centers and traps reduces the minority carrier lifetime and therefore reduces the carrier lifetime, which thus reduces the diode sensitivity. The SVWAD also affects the instantaneous dose rate or SDD dependence.

The sensitivity drop by the irradiation beam is called the damage coefficient. The damage depends upon the radiation quality.[5] The damage coefficient is low for the electron energies below 0.7 MeV and the coefficient increases more rapidly for between 0.7 MeV and 2 MeV and plateaus at above 2 MeV.[15,40] The sensitivity drop after preirradiation is more pronounced for n-type than p-type diodes of the same resistivity.[26] The photon beams with energies greater than 10 MV cause greater damage than expected from recoil energy of the electrons. This could be because of neutron contamination in the photon beam. The neutrons have much higher damage coefficient than the photon beam.[15,27] The rate SVWAD is reduced with the increase in the defect density. The manufacturer often preirradiates the diode with electron energy or uses the platinum doped silicon to increase the defect density. By increasing the defect density, the diode response changes less with clinical use.[15,41] We did not study this affect because this is well established and SVWAD is provided by all commercial vendors.

1.5 Objective of the Study

As discussed in section 1.4, there are many factors which influence the diode response to radiation for in-vivo dosimetry. In order to achieve the best possible accuracy between the prescribed dose and the measured dose, the proper correction factors need to be applied to the diode in-vivo measurements. This can allow us to catch the human made errors more easily.

In this study, the first systematic and quantitative study of dosimetric characteristics of most of the commercial radiation diodes (n-type and p-type) was performed including, but not limited to temperature, dose rate and SDD, and energy dependence under different radiation beams. The other relevant dosimetric characteristics were also studied for some of the diode detectors. These studies can help us better quantify the dosimetric characteristics of different diode detectors and obtain greater accuracy for relative in-vivo dose measurements in the clinic.

The diode detectors have been used as a relative dosimeters rather than as an absolute dosimeter in the radiation therapy clinics. The other objective of this dissertation was to establish a theoretical foundation for the modeling of the transient electric and radiation properties of the diode detectors, separately. This can help us to achieve the ultimate goal which is to use the diode detector as an absolute dosimeter rather than a relative dosimeter in the future.

1.6 Dissertation Outline

The European format of compiling the body of this document from peer reviewed journals has been adopted for this dissertation. Therefore, there will be overlapping text in various chapters of this work. This format is most efficient for this dissertation which will preserve the overall quality of this work.

Chapter 2 discusses the theory related to the semiconductor diodes and it's radiation properties. The recombination-generation theory, continuity equations, and diode sensitivity will be discussed in this chapter. This chapter will also cover the radiation transport properties of the diode detector under radiation.

In chapter 3, the temperature dependence of different commercially available diode detectors for in-vivo dosimetry was studied. The dose rate effect on sensitivity variation with temperature (*svwt*) of diodes was studied for different preirradiation conditions and for both types (n and p).

Chapter 4 parameterizes the dose rate dependence of different commercially available diode detectors. The dose-rate dependence measured by adjusting radiation pulse height was compared to that measured by changing source-to-detector distance (SDD). A photon energy independent formula was proposed to fit the dose rate dependence of diode sensitivity.

Chapter 5 investigates the energy dependence of different diode detectors with different buildup materials for different energies. Monte Carlo simulations were performed to confirm the observed energy dependence.

Chapter 6 is a systematic study of the correction factors required for pt-doped diodes used in in-vivo dosimetry. Chapter 7 concludes this work and discusses possible directions for future studies.

1.7 Limitation of this Work

For the commercial diode detectors used in this study the device properties of most of the detectors were unknown. As a result, only empirical models derived from experimental measurements are developed for most of the commercial diodes. Some efforts are made to correlate measured results with more fundamental physical quantities required by the

electric transport equation such as the recombination time for minority carriers. However, substantial further work is necessary to completely model the transient properties of diode detectors (e.g. dose rate) using the fundamental equations used in the study.

CHAPTER 2 THEORY

2.1 Electric Transport

2.1.1 R-G Centers

Recombination is a process in which electrons and holes are destroyed or annihilated in a semiconductor. Recombination decreases the charge generated by radiation. The Generation is a process in which electrons and holes are created. There are different types of recombination process. The most common recombination mechanism for a radiation diode detector is via Recombination-Generation (R-G) centers. The R-G centers are deep energy levels in the middle of the semiconductor band gap. These are created by crystal defects or by some impurities of atoms such as platinum and Gold. These impurities are intentionally used as dopants to reduce the transient response of the diodes.[29,42] The created R-G centers act as intermediaries in the envisioned recombination process. The empty R-G center captures a minority carrier and this minority carrier stays there until the R-G center captures a majority carrier to recombine with it. In radiation, the R-G center is the main mechanism where generated electron and hole excess carriers are recombined to reach thermal equilibrium.

There are four possible R-G center transitions possible. They are (1) electron capture at an R-G center, (2) electron emission from an R-G center (3) hole capture at an R-G center, and (4) hole emission from an R-G center. The latter two transitions can also be thought of as an electron trapped at an R-G center falling into vacant valence band state and a vacant band electron being excited to the R-G level, respectively.[42]

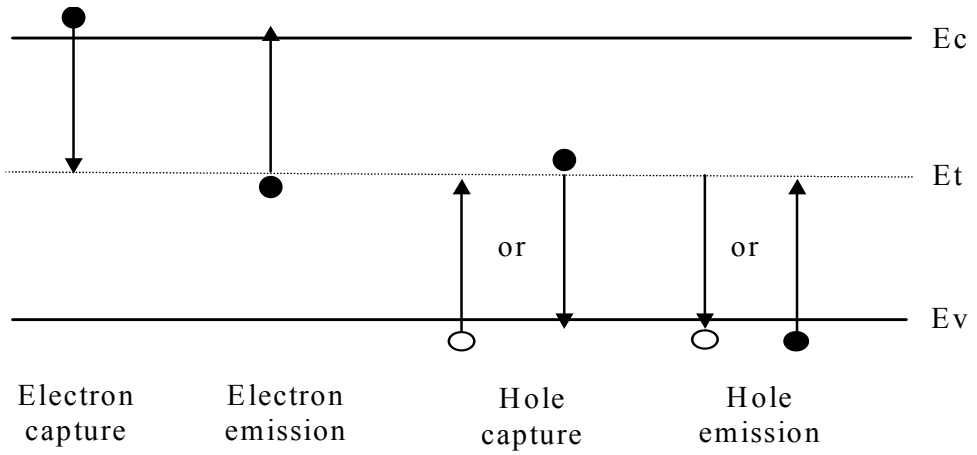

Figure 2. Possible electronic transitions.
These possible transitions are between a single-level R-G center and energy bands.[42]

When radiation is applied, the equilibrium is broken and the net recombination rates do not vanish under steady-state conditions. There are established interrelationships between the net rates. The net steady-state recombination for a single energy level of R-G center (E_t) can be derived as:[29,42]

$$R = \frac{np - n_i^2}{\tau_p(n + n_1) + \tau_n(p + p_1)} \tag{5}$$

Where $n = \Delta n + n_0$ and $p = \Delta p + p_0$ are the electron and hole concentration, respectively. n_0 and p_0 are the equilibrium electron and hole concentration and depend upon the device parameters, n_i is the intrinsic carrier concentration of the material, n_1 and p_1 are computable constants. τ_n and τ_p are the minority carrier lifetime for the electrons and holes in the p- type and n-type materials, respectively. n_0 and p_0 can generally be determined as:

$$n_0 = n_i e^{(E_F - E_i)/kT} \tag{6a}$$

and

$$p_0 = n_i e^{(E_i - E_F)/kT} \tag{6b}$$

When a semiconductor is maintained at extrinsic temperature region, $N_D >> n_i$ in a donor doped ($N_D >> N_A$) semiconductor and $N_A >> n_i$ in an acceptor-doped ($N_A >> N_D$) semiconductor. The majority carrier is determined by doping and do not change by temperature.

$$n_0 \cong N_D \qquad \text{Donor-doped, extrinsic T } (N_D >> N_A,\ N_D >> n_i) \qquad (7a)$$

$$p_0 \cong N_A \qquad \text{Acceptor-doped, extrinsic T, } (N_A >> N_D,\ N_A >> n_i) \qquad (7b)$$

Where N_D and N_A are the donor and acceptor impurity concentration. n_1 and p_1 can be calculated as:

$$n_1 = n_i e^{(E_{T'} - E_i)/kT} \qquad (8a)$$

Similarly,

$$p_1 = n_i e^{(E_i - E_{T'})/kT} \qquad (8b)$$

Where $E_{T'} = E_T \pm kT\, ln g_T$, E_T is the energy level of the introduced R-G center. The (+) is used if R-G centers are acceptors and the (-) is used if the centers are donor-like. g_T is the degeneracy factor. Using equations (6) and (8), $n_0 p_0 = n_1 p_1 = n_i^2$.

For the case of radiation, the excess carrier concentration is in pairs, $\Delta n = \Delta p$ and substituting $n = n_0 + \Delta n$, $p = p_0 + \Delta p$, and $n_0 p_0 = n_i^2$, equation (5) can be simplified as:[29,42]

$$R = \frac{\Delta p(n_0 + p_0 + \Delta p)}{\tau_p(n_0 + \Delta p + n_1) + \tau_n(p_0 + \Delta p + p_1)} \qquad (9)$$

If the excessive carriers recombine before reaching the active region, they will not contribute to the radiation current signal. If the dose rate (excessive carriers) concentrations are increased, the excessive carriers do not completely recombine, and thus increase the sensitivity.

If the excess-carrier concentration generated by radiation is relatively small (compared to the majority-carrier concentration n_0 or p_0 and the single mechanism of recombination and generation (R-G) dominates, the excess minority carrier life time τ generated by radiation can be simplified from a net recombination rate for n-type diode as:[29,33,42]

$$\tau = \frac{\Delta p}{R} = \tau_p \frac{(n_0 + \Delta p + n_1) + \zeta(p_0 + \Delta p + p_1)}{n_0 + p_0 + \Delta p} \tag{10a}$$

and for p-type diode:

$$\tau = \frac{\Delta n}{R} = \tau_n \frac{\zeta^{-1}(n_0 + \Delta n + n_1) + (p_0 + \Delta n + p_1)}{n_0 + p_0 + \Delta n} \tag{10b}$$

ζ is equal to the ratio of the minority carrier life time of electrons to the minority carrier life time holes: $\zeta = \tau_n / \tau_p$. Again, τ_n is the lifetime of the minority carrier (electrons) in the p-type material and the τ_p is the lifetime of the minority carrier (holes) in the n-type material. This ratio is a constant and its value depends upon the level of doping and the crystal defect produced by the manufacturer. The minority carrier life time for holes or electrons can be expressed as:[29,33,42]

$$\tau_p = \frac{1}{\sigma_{cp} \nu_{th_p} N_t}, \tag{11a}$$

$$\tau_n = \frac{1}{\sigma_{cn} \nu_{th_n} N_t}, \tag{11b}$$

σ_{cp} and σ_{cn} are the capture cross sections for the holes and the electrons, respectively. ν_{th} is the thermal velocity for the holes or electrons. N_t is the recombination and generation (R-G) density, i.e. the number of R-G centers per cm^3. N_t is proportional to the total dose

received by the diode. $v_{th_p} = \sqrt{3kT/m_p^*}$ and $v_{th_n} = \sqrt{3kT/m_n^*}$ are thermal velocities of the hole and electron, respectively. m_p^* and m_n^* are the effective masses for hole and electron. These effective masses are constant for Si. T is the temperature in Kelvin. By using equation (12), ζ can be represented as:

$$\zeta = \frac{\tau_n}{\tau_p} = \frac{\dfrac{1}{\sigma_{cn} v_{th_n} N_t}}{\dfrac{1}{\sigma_{cp} v_{th_p} N_t}} = \frac{\sigma_{cp} v_{th_p} N_t}{\sigma_{cn} v_{th_n} N_t} = \frac{\sigma_{cp}\sqrt{3kT/m_p^*}}{\sigma_{cn}\sqrt{3kT/m_n^*}} = \frac{\sigma_{cp}}{\sigma_{cn}}\sqrt{\frac{m_n^*}{m_p^*}} \qquad (12)$$

For n-type diode, using $n_0 >> p_0$, equation (10a) can be simplified as:

$$\tau = \frac{\Delta p}{R} = \tau_p \frac{(n_0 + \Delta p + n_1) + \zeta(\Delta p + p_1)}{n_0 + \Delta p} \qquad (13a)$$

and, for p-type diodes, by using $p_0 >> n_0$, equation (10b) can be written as:

$$\tau = \frac{\Delta n}{R} = \tau_n \frac{\zeta^{-1}(\Delta n + n_1) + (p_0 + \Delta n + p_1)}{p_0 + \Delta n} \qquad (13b)$$

Since the energy of the R-G centers, E_t is in the middle of the energy gap of the Si semiconductor. Further assuming, for n-type diode, $\Delta p >> p_0$, $\Delta p >> p_1$, *and* $n_0 >> n_1$ equation (13) can be further simplified to:[29,33]

$$\tau = \tau_p \frac{(n_0 + \Delta p) + \zeta \Delta p}{n_0 + \Delta p} = \tau_p (1 + \frac{\zeta \Delta p}{n_0 + \Delta p}) \qquad (14a)$$

and for p-type diode, assuming $\Delta n = \Delta p >> n_0$, $\Delta n = \Delta p >> n_1$, and $p_0 >> p_1$:

$$\tau = \frac{\Delta n}{R} = \tau_n \frac{\zeta^{-1}\Delta n + (p_0 + \Delta n)}{p_0 + \Delta n} = \tau_n (1 + \frac{\Delta n}{\zeta (p_0 + \Delta n}) \qquad (14b)$$

$\Delta n = \Delta p$ is the excessive minority carrier mean concentration generated by single radiation pulse (or within the lifetime of the minority carrier for a continuous beam) and is proportional to the instantaneous dose rate. This value can be estimated from the total excess minority carriers generated by radiation. The excessive minority carrier concentration generated by the radiation can be estimated as:

$$\Delta n = \Delta p = \frac{\rho}{e\beta\left(\frac{W}{e}\right)} \int InstDRdt \equiv g \int InstDRdt \qquad (15)$$

Here β is the dose-to-kerma ratio. It is 1.005 for Co-60 and 1.0 for megavoltage photon beams.[3] Using density (ρ = 2.5 g/cm^3) and the energy required to produce an electron-hole pair (W=3.6 eV) for Silicon,[1] we calculated $g = 4.35\times10^{13}$ 1/cGy (Si) assuming β = 1. To calculate the mean excess minority-carrier concentration Δn (or Δp) suitable for equation (14), one has to solve a continuity equation to account for the rate of recombination in a p-n junction.[29] The approximate solution[29] can be estimated as equation (15) with $\int InstDR \cdot dt = InstDR \cdot PW$ when the pulse width PW is shorter than the lifetime of the excess carrier τ, otherwise $\int InstDR \cdot dt = InstDR \cdot \tau$.[29]

There are different possible injection levels for radiation used in radiotherapy. 1. Low injection level: When the excessive carrier concentration Δn or Δp is much smaller compared (generated by small instantaneous dose rate) to n_0 or p_0 and a single mechanism of recombination-generation (R-G) center dominates, then τ can be simplified from an equation (14) to τ_p for n-type and τ_n for p-type diode. 2. Small deviation from low injection: If the charge generated by radiation is only a little larger than the low level injection, is that for n-type, $n_0 > p_0$ and n_1 and $\Delta p >> p_1$ and p_0. The equation (15a) can be reduced to:[29,33]

$$\tau = \tau_p(1 + \frac{\zeta \Delta p}{n_0}) \quad (16a)$$

Similarly for p-type, $p_0 > n_0$ and p_1. $\Delta n >> n_1$ and n_0. The equation (15b) can be reduced to:[29,33]

$$\tau = \tau_n(1 + \frac{\Delta n}{\zeta p_0}) \quad (16b)$$

n_1, p_1, ζ, and τ_p depend upon the characteristics of the dominant R-G center such as capture cross section, energy level, and the concentration. Usually their values are quite different before and after irradiation. n_0 and p_0 depend upon the diode resistivity and are approximately equal to N_d and N_a for n-type and p-type respectively.

2.1.2 P-N Junction

The electrical properties (conductivity) of a semiconductor material such as silicon can be changed by introducing impurities into the crystal. This process is commonly called doping. The n-type (mostly electrons) silicon is made by doping silicon with Group V (P, As, or Sb) element called donors and p-type (mostly holes) by doping with Group III (B, Al, Ga, or In) element called acceptors.[43]

A p-n junction is an internal boundary between the p-type and n-type regions in a single crystal as shown in figure 3. The n-type material has a large concentration of electrons and few holes, while the opposite is true for the p-type material. When these two regions are joined together, diffusion of carriers takes place because of the large gradient of carrier concentration at the junction. Due to this gradient, electrons in the n side diffuse to the p side, and holes in the p side diffuse to the n side. Electron diffusing from n to p region leaves behind uncompensated donor ions (Nd^+) in the n region, and holes diffusing

from p region leaves uncompensated acceptors (Na^-). So, there is positive space charge near the n side, and negative space charge near the p side of the material. The charged ions left on both sides form a depletion region (space charge) over which a built in voltage drop of about 0.7V is created for a normal silicon over a distance of few micrometers.[42] The p-n junction is formed when equilibrium is reached. There is no net current flow across the junction at equilibrium. [43]

2.1.3 Steady State and Transient Current in Radiation Diode Detector

For in-vivo dosimetry, the diode is placed on the patient surface to measure the absorbed dose delivered during radiation treatment. During irradiation, electron-hole pairs are created in the diode, generating a radiation current due to movement of the charges created in the depletion region and by the diffusion of minority carriers (electrons in p-type and holes in n-type) created in the base of the material.[44] For in-vivo dosimetry, the diode is under zero-voltage external bias. In this configuration, a leakage current may be generated without radiation. The diode current thus consists of irradiation current and electrical leakage current.[15,29,33]

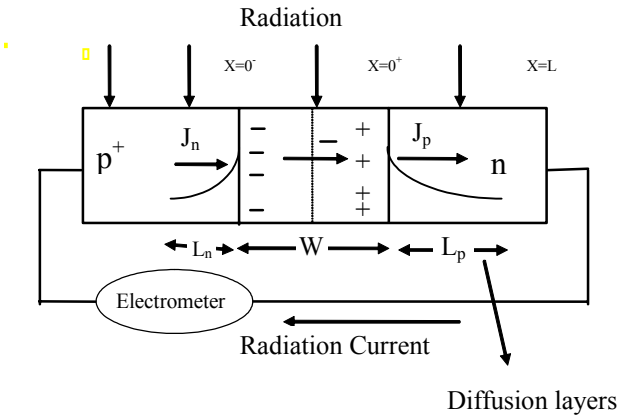

Figure 3. Schematics of diode current in the p^+-n junction.

When a semiconductor is irradiated by electron or photon radiation, electron-hole pairs are generated. In most of the regions, these electrons and holes recombine locally and do

not contribute to radiation current. The electrons and holes generated in the depletion and diffusion regions will contribute to electrical current. As shown in figure 3, carriers generated within the depletion region W are swept across W by the strong electrical field, generating a current J_W. In addition minority carrier generated within diffusion length of each side of the junction diffuse to the depletion region by the diffusion process generating another current (J_n or J_p).

The total radiation current density is the sum of the contributions from diffusion regions in n- and p-side and the depletion region is: $J_{total} = J_p + J_n + J_w$.[45] Subscripts p and n represents the minority carrier current densities in n- and p-side. We assume that there is no applied field in the junction. For n-type, the diffusion radiation current density for holes, J_p, can be obtained from the continuity equation.[29,42]

$$\frac{\partial \Delta p}{\partial t} = \kappa_p \nabla^2 \Delta p - R + G = \kappa_p \nabla^2 \Delta p - \frac{\Delta p}{\tau} + g_o \cdot r(t) \qquad (17)$$

Where $G = g_0.r(t)$ is the charge generation rate. $g_0 = 4.2\times10^{13}$ *pairs/cGy-cm*^{3} is the generation constant for silicon under ionizing radiation and $r(t)$ is the instantaneous dose rate. $x = 0$ is the boundry between the n-side and the depletion layer, W. $R = \Delta p/\tau$ is the net recombination rate.[29,42] κ_p is the diffusion coefficient for holes. κ_p depends upon only temperature and the resistivity.[29,42] τ is the excess minority carrier lifetime and the Δp is the excessive minority carrier mean concentration generated by single radiation pulse (or within the lifetime of the minority carrier for a continuous beam). The solution of the equation (17) for Δp is a function of x and t is used to drive the current density, J_p. The solution of the equation (17) can be solved numerically because τ is a nonlinear function of excess minority carriers concentration Δp.

The solution to the continuity equation (17) for rectangular pulsed radiation was solved by Wirth and Rogers[46] under the condition that the lifetime of the excess minority carrier, τ, is equal to a constant value, e.g., τ_p (life time of the minority carrier (hole) in n-type

material in μs). The transient radiation current density can be calculated from the solution for a step radiation by using:[46]

$$J_p^{pulsed} = J_p^{step}(t) - J_p^{step}(t - t_p) \tag{18}$$

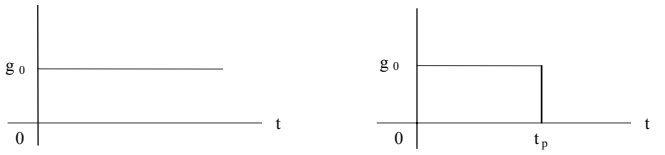

(a) step radiation (b) pulsed radiation

Figure 4. Schematics of radiation generation shape vs. time.
(a) step radiation starting at $t=0$ (b) pulsed radiation with pulse width t_p.

Thus for rectangular pulsed radiation beam with pulse width t_p, and one assumes τ is constant, the transient analytical solution is:[29,45]

$$J_p = q\kappa_p \nabla(\Delta p)\,|_{X=0} = qg_o r(t) L_p erf\left(\sqrt{\frac{t}{\tau}}\right) \qquad 0 < t \le t_p \tag{19a}$$

$$J_p = qg_0 r(t) L_p \left[erf\left(\sqrt{\frac{t}{\tau}}\right) - erf\left(\sqrt{\frac{(t-t_p)}{\tau}}\right)\right] \qquad t > t_p \tag{19b}$$

t_p is the width of the rectangular pulse for a pulsed beam and is the exposure time for the continuous beam. q is the electron charge of 1.6×10^{-19} C. *erf(t)* is the error function. *r(t)* is the instantaneous dose rate. It is interesting to notice that for $t \to \infty$, $J_p = 0$, i.e. there is no steady state current for pulsed radiation.

For continuous beam, the steady state solution of equation (19) becomes:

$$J_p = qg_0 r(t) L_p \qquad t_p >> \tau \tag{20}$$

L_p is the diffusion length for holes in the n-type diode and can be calculated as:[29,33,46]

$$L_p = \sqrt{\kappa_p \tau} \tag{21}$$

Again, κ_p is the diffusion coefficient for holes and τ is the excess minority carrier lifetime.[29,42] $\kappa_p = \mu_p kT/q$ (Einstein's relationship) is the hole diffusion constant. μ_p is the hole mobility which depend upon the resistivity and the temperature.[42] k is Boltzman constant, T is temperature, and q is the electron charge. kT/q = 0.026 V at room temperature. For p-type materials subscripts can be changed to n (which refers to electrons) to determine J_n.

2.1.4 Diode Sensitivity

The diode sensitivity is defined as the number of electron-hole pairs generated in the diode corresponding to the radiation dose or defined as the average charge collected per unit absorbed dose. For most of the diode, the depletion layer is so small that the sensitivity is mostly determined by the diffusion current in the side of lightly doped substrate. The sensitivity $S_{diode}(nC/Gy)$ can be calculated for n-type diode as:[29,33]

$$S_{diode} = \frac{M}{D} = \frac{A\int_0^{\infty} J_p(t)dt}{\int_0^{t_p} r(t)dt} \tag{22a}$$

and similarly for p-type diodes

$$S_{diode} = \frac{M}{D} = \frac{A\int_0^{\infty} J_n(t)dt}{\int_0^{t_p} r(t)dt} \tag{22b}$$

J_p and J_n are the radiation current densities (A/cm^2) for the holes and electron for n-type and p-type materials, respectively. A is the active area of the diode, t_p is pulse width for the pulsed beam and the exposure time for the continuous (Co-60) beam, and $r(t)$ is the instantaneous dose rate of the radiation beam.

If the excess minority carrier concentration Δp is small, τ is close to the constant value of τ_p (low injection minority carrier life time of the holes) for the n-type material. For this case, the equation (22) can be approximated as:[29]

$$S_{diode} \cong \frac{Aqg_0 rt_p L_p}{rt_p} = Aqg_0 L_p \qquad \text{(n-type)} \qquad (23a)$$

$$S_{diode} \cong \frac{Aqg_0 rt_p L_n}{rt_p} = Aqg_0 L_n \qquad \text{(p-type)} \qquad (23b)$$

and using equation (21):[23,24,28,29]

$$S_{diode} = Aqg_0 \sqrt{\kappa_p \tau} = K\sqrt{\kappa_p \tau} \qquad \text{(n-type)} \qquad (24a)$$

$$S_{diode} = Aqg_0 \sqrt{\kappa_n \tau} = K\sqrt{\kappa_n \tau} \qquad \text{(p-type)} \qquad (24b)$$

Where κ_p is the diffusion coefficient for holes in equation 24a and κ_n is the diffusion coefficient for electrons in equation 24b. τ is the excess minority carrier lifetime.[29,42] $K=qg_0A = 6.72\times10^{-6}$ A (C/cGy/cm) for a bare silicon diode.[29] and A is the cross-section area of the diode (in cm^2). For the commercial diodes, the value of the K becomes energy dependent because of the buildup material. The equation is generally true only for continuous (Co-60) radiation beam, but has been verified[23,24,28,29] that it is also true for rectangular pulsed beam for commercial diodes of interest in this study.

Thus the normalized sensitivity ratio can be written as using:

$$\frac{S}{S_{ref}} = \sqrt{\frac{\tau}{\tau_{ref}}} \tag{25}$$

Here, S_{ref} and τ_{ref} are the normalized sensitivity and life time at the reference conditions. The equation (25) is mainly true for when there is one type of R-G center and may be invalid for multiple R-G centers.[7,29] By using equation (14) and (15), the normalized sensitivity ratio can be further written for n-type diodes as:

$$\frac{S}{S(InstDR_{ref})} = \sqrt{\frac{\left(1+\frac{\varsigma\Delta p}{n_0+\Delta p}\right)}{\left(1+\frac{\varsigma\Delta p_{ref}}{n_0+\Delta p_{ref}}\right)}} \tag{26}$$

Where $InstDR_{ref}$, and Δp_{ref} is the instantaneous dose rate and excess minority-carrier concentration at the reference condition (e.g. SDD = 100 cm). This equation is strictly only valid for low current injection condition $(\Delta P << n_0)$.

For very high dose rates (>10^4 cGy/s), τ is non linear function of dose rate. The approximate solution of equation (17), given in equation (19), might not be valid. In these cases, one has to solve the non-linear solution of the continuity equation numerically.

2.2 Radiation Transport

2.2.1 Monte Carlo Simulation

Monte Carlo simulation is a numerical solution to a problem that models objects interacting with other objects or their environment based upon simple object-object or object environment relationships. A solution is determined from the random sampling of the relationships. The use of the Monte Carlo method has been used in many different fields such as social sciences, traffic flow, quantum chemistry, radiotherapy, and radiation dosimetry.

In the field of radiation dosimetry, the Monte Carlo techniques are useful for predicting the trajectories of high energy particles through detectors and other complex assemblies of materials. The EGS is general purpose computer code for the Monte Carlo simulation of the coupled transport of electrons and photon in an arbitrary geometry of particles with energies above a few keV up to several MeV.[47] The EGS Monte Carlo system is structured in such a way so that users can write their own subroutines to handle all of the physics in the simulation geometry and scoring method without actually touching the core of the EGS system itself. The geometry is defined by writing the routines using simple general interface (HOWFAR and HOWNEAR) and a scoring routine (AUSGAB) which is called under well-specified conditions which allow scoring virtually any parameter of interest.[47] The scoring routine can be called before and/or after any class of interaction, to score where they occur, how often they occur, what happened during the interaction, etc.

The EGS system models all the following processes during the calculations: annihilation of positrons at rest or in flight; inelastic Moller and Bhabha scattering of electrons and positrons (respectively) from atomic electrons; bremsstrahlung production by positrons and electrons from interactions with the nucleus and atomic electrons; elastic multiple and single scattering of electrons and positrons from nuclei and atomic electrons; pair

production by photons; Compton scattering of photons from bound atomic electrons; photoelectric interactions of photons with atomic electrons; Rayleigh coherent scattering of photons from atoms; and relaxation of the atom by production of fluorescent x-rays and Auger electrons. These processes are discussed in various radiation transport books.

The cross-section interaction data for EGSnrc system can be prepared ahead of time by the PEGS4 data preparation package. All of these interaction data are picked up by the routine HATCH.

The MC simulation calculations in Chapter 3 were performed using DOSRZnrc user code that comes with EGSnrc v4.2.2.6.[47,48] Only diodes with flat design are used for simulations. Mohan energy spectra were used for pulsed radiation beams and energy spectrum given in EGSnrc was used for Co-60 beam. No variance reduction techniques were used. PRESTA-(Parameter Reduced Electron-Step Transport Algorithm) II was enabled for all electron transport. The particles are transported with a cutoff energy of AP = ECUT = 10 keV for photons and AE = ECUT = 521 keV for the electrons. Photon and electron interaction cross section data (PEGS data set 521icru.dat) from ICRU 37 was used.[49]

2.2.2 Analytical Calculation for Diode-to-Water Dose Ratio Using Brag Gray Cavity Theory

The Bragg-Gray cavity theory relates the dose in the diode (Silicon) to that in the surrounding medium (water). In order to use the Bragg-Gray cavity theory, some conditions have to be assumed: 1. The size of the cavity is small so that it does not perturb the charged-particle field. 2. The dose in the cavity is assumed to be deposited entirely by electrons crossing it.

The ratio of dose to the medium (buildup) to dose to the diode (Si) can be calculated as:[1]

$$\frac{D_{buildup}}{D_{diode}} = (\frac{\overline{S}_{col}}{\rho})_{Si}^{buildup} \cdot \tag{27}$$

$(\frac{\overline{S}_{col}}{\rho})_{Si}^{buildup}$ is the collision stopping power ratio between buildup and diode (Si) according to the Bragg-Gray cavity theory,[1,50] the dose to water to buildup further can be related for photon beams as:[1]

$$\frac{D_{water}}{D_{buildup}} = (\frac{\overline{\mu}_{en}}{\rho})_{buildup}^{water} \cdot A(d_{buildup}) \tag{28}$$

$(\frac{\overline{\mu}_{en}}{\rho})_{buildup}^{water}$ is the mass energy coefficient ratio between the water and the buildup material. [1,50] $A(d_{buildup})$ is the attenuation factor due to the buildup material with thickness $d_{buildup}$. Combining equation (27) and (28), and introducing another factor, P, we can calculate:

$$D_{H_2O}^{diode} = (\frac{\overline{S}_{col}}{\rho})_{buildup}^{Si} \cdot (\frac{\overline{\mu}_{en}}{\rho})_{water}^{buildup} \cdot A(d_{buildup}) \cdot P \tag{29}$$

$D_{H_2O}^{diode}$ is the diode-to-water ratio and is defined as the ratio of dose scored in the silicon (with or without buildup materials) to that in water at the same location without the diode for the same incident photon energy fluence. Where $(\frac{\overline{S}_{col}}{\rho})_{buildup}^{Si}$ is the collision stopping power ratio between silicon and buildup according to the Bragg-Gray cavity theory,[1,50] $(\frac{\overline{\mu}_{en}}{\rho})_{water}^{buildup}$ is the mass energy coefficient ratio between the buildup material and water. The secondary electron fluence in the Si die is ignored since the diode is very thin. $P = 1$

in equation 29, if one assumes that the buildup material is sufficiently thick that electron equilibrium is established and the perturbation of the secondary electron fluence is ignored. Otherwise, there is an additional correction factor, *P,* is introduced to account for the disturbance to the primary dose by the buildup structures and that is not accounted for in the Bragg-Gray cavity theory. For Si diode without buildup, $(\frac{\overline{S}_{col}}{\rho})^{Si}_{water}$ can used because the buildup is replaced by water.

The total stopping power ratio, the mass energy coefficient ratio, and the attenuation function for the buildup material can be calculated using the published data in ICRU 37. The mass energy coefficient ratios between buildup material and water for a particular photon energy spectrum can be calculated using:

$$(\frac{\overline{\mu}_{en}}{\rho})^{buildup}_{water} = \int (\frac{\overline{\mu}_{en}(E)}{\rho})^{buildup}_{water} \psi(E)dE / \int \Psi(E)dE \qquad (30)$$

and the attenuation function, *A* is calculated using:

$$A = \int e^{-\mu(E)\cdot d_{buildup}} \psi(E)dE / \int \Psi(E)dE \qquad (31)$$

where *ψ(E)* is the photon energy spectrum. The diode sensitivity *S* is proportional to $D^{diode}_{H_2O}$, the normalized sensitivity (to Co) can be determined from the calculated diode-to-water dose ratio as:

$$S_{norm} = \frac{D^{diode}_{H_2O}(E)}{D^{diode}_{H_2O}(Co)}. \qquad (32)$$

This analytical equation assumes that the secondary electrons are not disturbed by the structures around the detector. If there is complicated geometry, the results might not be

accurate. Nevertheless, it can demonstrate the magnitude of the energy dependence at least for the bare Si diode. Comparison of results from experimental measurements, Monte Carlo simulation, and analytical solution are shown in chapter 5. When there is complicated geometry Monte Carlo (MC) simulation, discussed in section 2.2.1, is the preferred way.

CHAPTER 3 PAPER I: TEMPERATURE DEPENDENCE OF COMMERCIALLY AVAILABLE DIODE DETECTORS

Temperature is an important factor in calculating the dose measured by the diode because when the diode is placed on the patient, its temperature can rise up to skin temperature within a few minutes. This can produce an inaccuracy in dose measurement up to 9% depending on the type of diode used, photon energy, dose rate, and pre-irradiation. Different studies have reported the temperature coefficient, also called sensitivity variation with temperature (*svwt*), for n- and p-type diodes in the literature. However, few publications, if any, examine the dose rate effect on *svwt* of diodes for various preirradiation conditions and types (n or p). In this study, we examined dose rate dependence of *svwt* for various commercial diodes in the temperature range between 10 and 35°C.

Medical Physics, 29(4):622-30 (2002)

3.1 Synopsis

Temperature dependence of commercially available n- and p-type diodes were studied experimentally under both high instantaneous dose rate (pulsed) and continuous radiation. The sensitivity vs. temperature was measured at SSD = 80 or 100 cm, 10×10 cm^2, and 5-cm depth in a 30×30×30 cm^3 water phantom between 10 and 35°C. The response was linear for all the diode detectors. The temperature coefficient (or sensitivity variation with temperature, *svwt*) was dose rate independent for preirradiated diodes. They were (0.30±0.01)%/°C, (0.36±0.03)%/°C, and (0.29±0.08)%/°C for QED p-type, EDP p-type, and Isorad n-type diodes, respectively. The temperature coefficient for unirradiated n-type diodes was different under low dose rate ((0.16 to 0.45)%/°C,

continuous, cobalt) and high instantaneous dose rate ((0.07±0.02)%/°C, pulsed radiation). Moreover, the temperature coefficient varies among individual diodes. Similarly, the temperature coefficient for a special unirradiated QED p-type diode was different under low dose rate (0.34%/°C, cobalt) and high instantaneous dose rate ((0.26±0.01)%/°C, pulsed radiation). Sufficient preirradiation can eliminate dose rate dependence of temperature coefficient. In contrary, preirradiation cannot eliminate dose rate dependence of the diode sensitivity itself.

3.2 Introduction

Semiconductor detectors became popular in patient dosimetry for photon and electron beams in the early 80's due to their quick processing time (seconds compared to TLD's hours) and high sensitivity (more than 18,000 times higher than that of air filled ionization chamber with the same volume).[5-7] Other major advantages of semiconductor detectors are excellent reproducibility, good mechanical stability, absence of external bias, small size, and the energy independence of mass collision stopping power ratios (between silicon and water for clinically usable electron beams with energy between 4-20 MeV).[5]

Most p-n junction semiconductor detectors are made of Si diodes. The p-n junction can be manufactured in many different ways. The most common device manufacturing technique is to lightly dope a pure silicon substrate to become either n-type (10^{14} to 10^{16} atoms cm^{-3} of phosphorous) or p-type (10^{15} to 10^{17} atoms cm^{-3} of boron), and then heavily doping impurities with opposite type (with a concentration of more than two orders of magnitude than the substrate) in the surface region to form a p-n junction. The radiation current generated in this type of device is primarily determined by the semiconductor properties in the lightly doped area (the substrate). Thus the diode is termed n-type or p-type depending upon whether the silicon substrate is doped with phosphorous where majority carriers are electrons or boron where majority carriers are holes, respectively.

The sensitivity of semiconductor detectors depends on temperature, dose rate, field size, and energy.[5-7,23,33] Temperature is an important factor because when the diode is placed on the patient, its temperature can rise up to skin temperature within a few minutes.[23] Welsh and Reinstein have recently quantified the rising time of temperature and the equilibrium temperature for many commercial diodes.[25] This can produce an inaccuracy in dose measurement up to 9% depending on the type of diode used, photon energy, dose rate, and pre-irradiation.[25] Different authors have reported the temperature coefficient, also called sensitivity variation with temperature (*svwt*), for n- and p-type diodes.[22,23,34] However, few publications, if any, examine the dose rate effect on *svwt* of diodes for various preirradiation conditions and types (n or p).

In this study, we examined dose rate dependence of *svwt* for various commercial diodes in the temperature range between 10 and 35°C.

3.3 Material and Methods

3.3.1 Description of Diodes

Eight different n- and p-type detectors were used in this study. Three Isorad n-type diodes and three QED p-type diodes, both from Sun Nuclear Corporation (Sun Nuclear Corporation, 425 A Pineda Ct., Melbourne, FL 32940) and two p-type diodes were from Scanditronix (Scanditronix AB, Husbyborg, S-752 29 Uppsala, Sweden). The diodes used in this study are summarized in table 1. Note: Two of the diodes (unirradiated QED and Isorad Gold 2) from Sun Nuclear were special made for this study, and were not commercially available.

Table 1. Specification of different diode detectors.

Diode Symbol	Manufacturer Code	Type	Buildup Material, Total buildup thickness (g/cm^2)	Suitable Energy Range	Preirradiation
Isorad 1 Gold	114300	n-type	1.1 mm Brass , 1.534	6–12 MV	none
Isorad 2 Gold	114300	n-type	1.1 mm Brass , 1.534	6–12 MV	none
Isorad Red	114200	n-type	1.1 mm Tungsten , 2.75	15–25 MV	10 kGy, 3 MeV
QED unirradiated*	111300	p-type	—	—	none
QED Blue	111400-0	p-type	3.4 mm Aluminum, 1.03	1–4 MV	10 kGy at 10 MeV
QED Red	111600-0	p-type	3.4 mm Brass, 3.04	15–25 MV	10 kGy at 10 MeV
Scanditronix EDP 10	EDP10	p-type	0.75 mm stainless cap + epoxy, 1	6–12 MV	8 kGy at 10 MeV
Scanditronix EDP 30	EDP30	p-type	1 mm Tantalum + epoxy, 2	20–30 MV	8 kGy at 10 MeV

* Not commercially available, special made for this study.

Figure 5 shows the schematics of packages for the three types of diodes. The Isorad n-type detector has a cylindrical design (Fig. 5a), with the die plane mounted normal to the detector axis, inside the cylinder of buildup which is composed of aluminum (for 1 to 4 MV, Blue); brass (for 6 to 12 MV, Gold); tungsten (for 15 to 25 MV, Red). Radiation is incident along the plane of the die (from side of the p-n junction). This design reduces angular dependence of diode sensitivity and provides uniform buildup in the radial direction. Both QED (Fig. 5b) and Scanditronix detectors (Fig. 5c) use a flat design, with radiation incident normal to the plane of the die (in the direction of p-n junction). The flat design has the advantage of well-defined buildup and less heterogeneous structures around the diode. QED detectors use aluminum (for 1 to 4 MV, Blue); or brass (for 6 to 12 MV, Gold) and (for 15 to 25 MV, Red) as buildup. Scanditronix detectors use steel or tantalum as buildup. The Scanditronix EDP10 diode, which has a 0.75-mm thick stainless steel buildup cap, is designed for lower energy beams because of its thinner build up. The Scanditronix EDP30 diode has thicker buildup and is commonly used for higher energy beams.

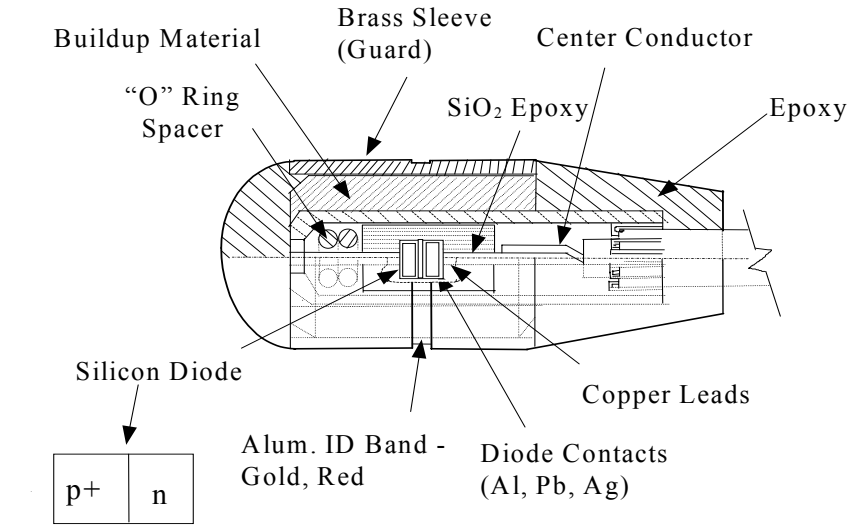

(a)

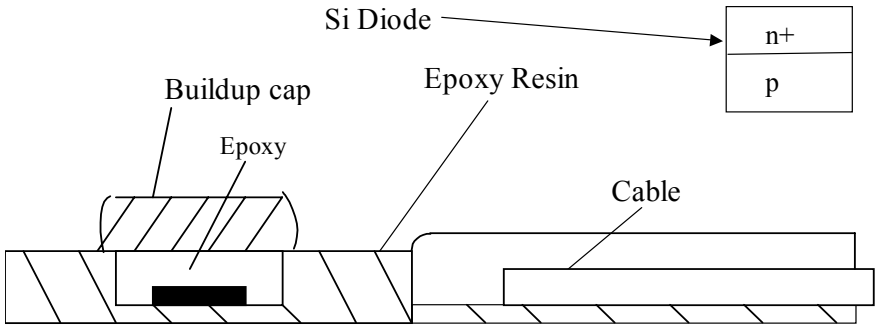

(b)

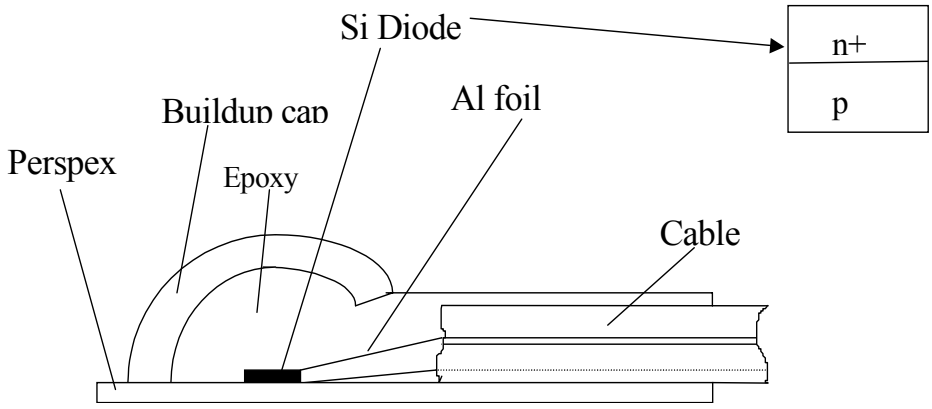

(c)

Figure 5. The schematics of the patient dosimetry diode detectors.
(a) Isorad, (b) QED, (c) EDP.

All commercial p-type diode detectors from the same manufacturer use the same die (chip) for different buildup thicknesses appropriate for the photon energies used. This is also true for all commercial n-type diode detectors. However, Isorad Gold 2 diode has a different diode die from that of Isorad Gold 1 diode, which uses the same die for all commercial Isorad diodes.

Prior to about 1996, commercial Blue and Gold Isorads were not pre-irradiated, but commercial Red Isorad was pre-irradiated to 10 kGy with 3 MeV electrons. Since 1999, all commercial Isorad-p detectors are pre-irradiated to 10 kGy with 10 MeV electrons, and the Isorad n-type detectors were discontinued by the manufacturer. All the QED diodes are made of p-type semiconductor and all the commercially available QED diodes are pre-irradiated to 10-kGy radiation with 10 MeV electrons. The QED unirradiated diode was specially packaged for this study only and is not commercially available. All the Scanditronix diodes were preirradiated to 8 kGy by 10 MeV electrons.

All the diodes were connected to electrometers to measure the relative charge. An adapter was placed between the diode and the electrometer to convert BNC connection from the diode to Triax connection of the electrometer. Charge was measured without applying any bias voltage.

3.3.2 Experiment Setup

The temperature dependence of the diodes was measured under both high instantaneous linear accelerator pulsed beam and low constant Co-60 dose rate radiations. Other than changing radiation machines, the same physical set-up was used throughout the study. The diodes were placed in a $30\times30\times30$ cm^3 water phantom at a depth of 5 cm along the central axis of the beam, so the point of measurement was beyond the range of contamination electrons. The water surface was 100 cm from the x-ray target and the field size was set to 10×10 cm^2 at isocenter, defined as 100 cm from the x-ray source**.** The diodes were placed in a very thin rubber sleeve (0.33 mm thick) to make them

waterproof. Four aquarium water heaters were placed on the corners of the water phantom to raise the temperature of the water. A water pump was used to homogenize the water temperature. Small thermometers were placed on the four inside walls of the water tank to monitor the uniformity of the water temperature. A mercury thermometer was used to determine the actual water temperature.

The temperature was cooled to 10°C using ice, and then the temperature was slowly increased from 10°C to 40°C at a rate of approximately 0.25°C/minute. After the water temperature was raised, the water pump was turned on to circulate the water for at least 10 to 15 minutes. Once the temperature in the phantom was completely stabilized, the radiation was applied. Normally one hundred-monitor units for pulsed radiation and one-minute exposure for Co-60 was used. Three to four readings were taken and the average value was used for analyzing the data. Leakage was measured for each temperature and was subtracted from the reading. Since the water volume was large, the temperature remained constant during the measurement. The water temperature was recorded at each successive step.

The charge collected by the diode was measured for each temperature and normalized to the linear fit value at 22°C. We did not measure the charge at 22°C, instead the expected charge value at 22°C was obtained from a linear fit to the measured data. The results were plotted as normalized charge vs. the temperature. The temperature coefficient, defined as $\frac{1}{S}\frac{dS}{dT}$ where S is the diode sensitivity, was then determined by linear regression of the data. The error bar for the measurement is based on the worst deviation between measurement and the linear fit (Fig. 6) and is set to be ±0.5% for all measurements.

For pulsed dose rate measurements, Elekta SL20 accelerator was used for n-type Isorad and p-type EDP diodes, and Siemens KD2 accelerator was used for p-type QED diodes. For continuous radiation measurements (Co-60), Theratron 1000 (SSD=100 cm) was

used for n-type Isorad and p-type EDP, Theratron 780 (SSD=80 cm) was used for p-type QED diode, and Theratron Phoenix (SSD= 80 cm) was used for p-type unirradiated QED diode. The average dose rate for Elekta SL20 was 337-351 MU/min for 6 MV and 374-378 MU/min for 20 MV at SSD of 100 cm. The instantaneous dose rates at 5 cm depth, SSD of 100 cm, and field size of 10×10 cm^2 were 3941-4105 cGy/s for 6 MV and 9050-9143 cGy/s for 20 MV. For Siemens KD2, the average dose rate for 6 and 15 MV were 200 MU/min and 300 MU/min, respectively at SSD of 100 cm and field size of 10×10 cm^2. The instantaneous dose rates were approximately 5800 cGy/s and 11200 cGy/s for 6 and 15 MV at depth of 5 cm, SSD of 100 cm and field size of 10×10 cm^2. The average dose rate for Theratron 1000, Theratron 780, and Theratron Phoenix were approximately 1.74 cGy/s, 1.52 cGy/s, 2.11 cGy/sec, respectively, at the time of measurements. Table 2 lists parameters for the radiation sources used in the study.

The instantaneous dose rate for pulsed radiation at a depth of 5 cm in water phantom (SSD=100cm and field size of 10×10 cm^2) was calculated as:

$$InstDR = \frac{DR_{100}}{PW \cdot PRF} \cdot PDD(c = 10, d = 5) \cdot IS\,, \tag{33}$$

where *PW* is the pulse width (in seconds) and *PRF* is the pulse repetition frequency (in Hz). They are listed in Table 2. *PDD(c=10,d=5)* is the percentage depth dose [9] for *SSD*=100 cm, 10×10 cm^2 at depth 5 cm, $IS=(100/(SSD+d_{ref}))^2$ is the inverse-square factor to convert calibration setup from *SAD*=100 cm to *SSD*=100 cm. The accelerators were calibrated in SAD geometry so that *D/MU = 1 cGy/MU* at *SAD*=100 cm, 10× 10 cm^2, and $d=d_{ref}$, where the reference depths, d_{ref}, are 0.5 cm for Co-60, 1.5 cm for 6 MV, 2.5 cm for 15 MV, and 3 cm for 20 MV. DR_{100} is the mean dose rate at the reference condition (SAD = 100 cm, $d=d_{ref}$, 10×10 cm^2) and is expressed as MU/sec. The instantaneous dose rate for Co-60 radiation (expressed in cGy/sec) is the same as the mean dose rate at a depth of 5 cm in water phantom (SSD=100 cm or 80 cm), i.e.,

$$InstDR = DR_{100\,or\,80} \cdot PDD_{100\,or\,80}(c = 10, d = 5) \cdot IS\,. \tag{34}$$

The instantaneous dose rates for all radiation sources are listed in table 2. In order to compare with measurements in the literature, the dose per pulse (Gy/pulse), calculated by *InstDR·PW*, is also listed in table 2.

Table 2. Dose rate of radiation sources (Paper I).
Depth of 5 cm, 10 x 10 cm^2, SSD = 100 cm (SSD = 80 cm for T780 and T Phoenix), where all temperature coefficients of diodes were measured. *PRF* is the pulse repetition frequency and *PW* is the pulse width.

Radiation source	Instantaneous dose rate (cGy/sec)	Dose per pulse (Gy/pulse)	*PRF*, *PW*
T780 and T1000, T Phoenix (Co-60)	1.52, 1.74, and 2.11	—	Continuous
Elekta SL20 (6 MV)	3941 – 4105	$1.26 – 1.31 \times 10^{-4}$	400 Hz, 3.2 μs
Siemens KD2 (6 MV)	5655 – 5945	$1.58 – 1.66 \times 10^{-4}$	192 Hz, 2.4 μs
Siemens KD2 (15 MV)	11162 – 11461	$3.40 – 3.49 \times 10^{-4}$	161 Hz, 2.6 μs
Elekta SL20 (20 MV)	9050 – 9143	$2.90 – 2.92 \times 10^{-4}$	200 Hz, 3.2 μs

To check if there is any correlation between dose rate dependence of the diode sensitivity itself and the *svwt*, we also measured dose rate dependence of various diodes at different source-to-detector distance SDD for 6 MV photon beams. All measurements were made in a 5-cm thick Lucite minipantom with sufficient thickness to eliminate electron contamination. Diode reading was compared to ionization chamber reading at the same SDD (70 – 350 cm) and field size (10×10 cm^2). The ratio between diode reading and ionization chamber reading for a fixed SDD is then normalized to be 1 at *SDD*=100 cm. This ratio is proportional to the diode sensitivity at the dose rate of the corresponding SDD. The instantaneous dose rate at different SDD was calculated from the normalized ionization chamber measurement, together with the known dose rate at SDD = 100 cm using the expression:

$$InstDR_{SAD} = \frac{M(SDD)}{M(100)} \cdot InstDR_{100}\,, \tag{35}$$

Where *M(SDD)* and *M(100)* is the total charge measured by an ionization chamber in the same miniphantom for the source-to-detector distance (SDD) of interest and SDD = 100 cm, respectively. $InstDR_{100}$ is the instantaneous dose rate at *SDD* = 100 cm and can be calculated according to:

$$InstDR_{100} = \frac{DR_{100}}{PW \cdot PRF} \cdot TMR(s=4, d=5) \cdot S_p(s=4) \cdot S_c(c=10) . \qquad (36)$$

Here *TMR(4,5)* is the tissue maximum ratio [9] for the miniphantom square field size of 4 cm^2 and depth of 5 cm in the miniphantom. $S_p(4)$ is the phantom scatter factor [9] for the miniphantom with square cross-section of 4 cm^2. $S_c(10)$ is the collimator scatter factor [9] for collimator setting of 10×10 cm^2. Most of diodes were measured using the Elekta SL20 accelerator, except for the QED diodes, which were measured using a Siemens KD2 accelerator. To plot data for dose rate dependence of diode sensitivity measured from different accelerators, all data were normalized to be 1 for instantaneous dose rate of 4000 cGy/s.

3.3.3 Theory

The sensitivity, *S*, of the diode detector can be defined as the radiation current generated per unit absorbed dose rate, i.e., *S=M/D*, where *M* is the total charge collected by the diode during the irradiation and *D* is the absorbed dose. Grusell and Rikner pointed out that *S* can be expressed as:[23]

$$S = K \cdot \sqrt{\kappa \cdot \tau} , \qquad (37)$$

where $K = 6.72 \times 10^{-7} \cdot A$ (C/cGy/cm) for a silicon diode without any buildup, *A* is the cross-section area of the diode (in cm^2), κ is the diffusion coefficient (cm^2/s) and τ is the minority carrier lifetime (s).

If the excessive carrier generated by radiation is relatively small (compared to n_0 or p_0) and a single mechanism of recombination and generation (R-G) center dominates, then τ can be simplified from a complete expression of net recombination rate[42] as first derived by Shi:[33]

$$\tau = \begin{cases} \tau_p(1+\dfrac{\zeta\Delta p}{n_0}) & (n-type) \\ \tau_n(1+\dfrac{\Delta n}{\zeta \cdot p_0}) & (p-type) \end{cases}, \qquad (38)$$

where τ_p and τ_n is the minority carrier life time for hole and electron, respectively, in silicon substrate. $\Delta p=\Delta n$ is the concentration of the excessive minority carriers proportional to instantaneous radiation rate, n_0 and p_0 are the majority carrier concentrations in the n and p type substrate, respectively. The value of $\zeta = \tau_n / \tau_p$ depends on the characteristics of the dominant R-G centers in the diode and is appreciably larger than 1 in silicon.[3,33] This is one of the reasons to favor p-type over n-type diode since the former has smaller dose rate dependence, as can be clearly demonstrated from Eq. (38) assuming $n_0 = p_0$.[7,27,33] Based on this theoretical model, the temperature coefficient (or sensitivity variation with temperature, *svwt*) is independent of dose rate because ζ and $\Delta n/n_0$ (or $\Delta p/n_0$) can be considered temperature independent, e.g., for p-type diode, we get from Eqs. (37) and (38)

$$svwt = \frac{dS}{SdT} = \frac{d\ln S}{dT} = \frac{d\ln \kappa\tau_n}{2\cdot dT} + \frac{d\ln(1+\Delta n/\zeta\cdot p_0)}{2\cdot dT} = \frac{1}{2}\cdot\frac{d\ln\kappa\tau_n}{dT} \quad . \qquad (39)$$

Where κ and τ_n are device parameters, which are independent of the dose rate. Similar expression can be obtained for n-type diode by replacing τ_n by τ_p in Eq. (39). However, if multiple mechanisms of R-G processes exist (e.g., R-G centers caused by defects, Au or Pt impurities exist simultaneously), then the minority carrier lifetime, τ, cannot be approximated by Eq. (38).[3,33] Under that condition, it may be possible to introduce a

dose rate dependence for *svwt*, as has been pointed out by Grusell and Rikner using a model of two R-G centers with different energy levels.[27]

Equation (39) also indicates that photon energy should not have any effect on *svwt*. This is mainly because the photon energy dependence of the diode sensitivity is included in the *K* of Eq. (37). However, as long as *K* is temperature independent, photon energy has no effect on *svwt* because *K* disappears in Eq. (38).

3.4 Results & Discussion

3.4.1 Unirradiated N-Type

The unirradiated n-type diodes generally showed less temperature dependence under the high instantaneous dose rate (pulsed) radiation than the low dose rate (continuous) Co-60 radiation. As shown in figure 6a, the Isorad Gold 1 has a temperature coefficient of 0.45%/°C under the low dose rate (Co-60) radiation and (0.055 ± 0.005)%/°C under the pulsed (6 and 20 MV) radiation. Figure 6b Shows that the Isorad Gold 2 unirradiated diode has a temperature coefficient of 0.16%/°C under the Co-60 radiation, and (0.09 ± 0.01)%/°C under the pulsed beams (6 and 20 MV). The temperature coefficient was quite different between individual unirradiated diodes of even the same manufacturer under the continuous Co-60 radiation (data for two additional Isorad diodes are not shown here). Based on the measurement, we propose an empirical formula to describe the dose-rate dependence of *svwt* as:

$$svwt = a_1 + a_2 \cdot e^{-br}, \tag{40}$$

Where *r* is the instantaneous dose rate. All others are constant parameters. The parameter *b* describes the degree of dose-rate dependence. When there is no dose rate dependence, $b = 0$ and $svwt = a_1 + a_2$. When one increases the dose rate, *r*, the temperature coefficient will decrease. *svwt* reaches a saturation value a_1 when the dose

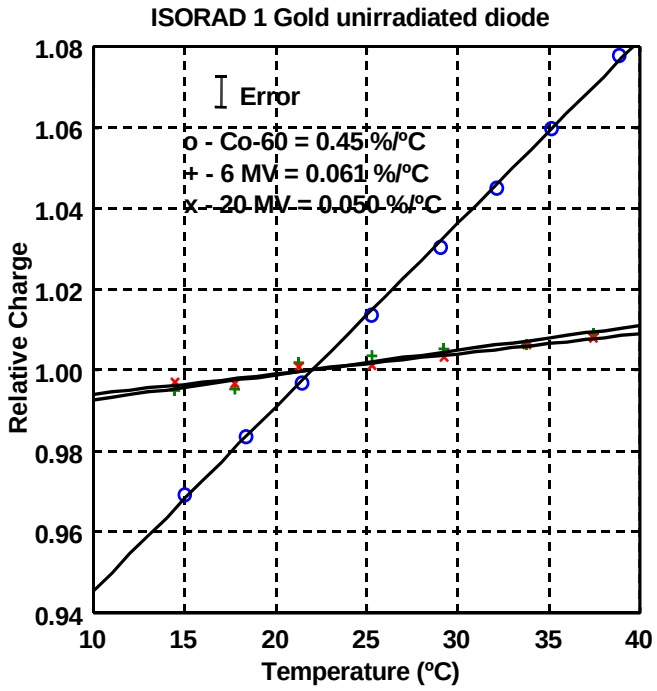

(a)

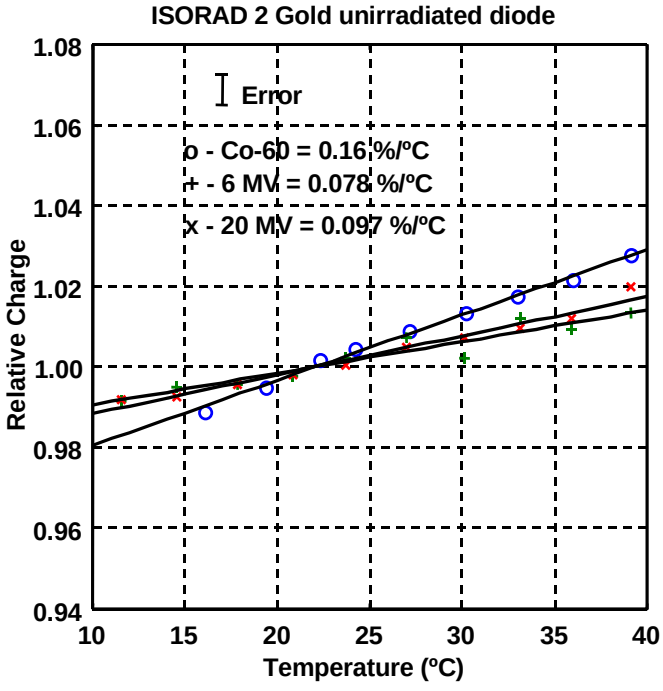

(b)

Figure 6. Temperature dependence for n-type (Isorad) unirradiated photon diodes. (a) Isorad Gold 1 (n-type) and (b) Isorad Gold 2 (n-type).

rate is larger than certain level (e.g, $r > 3/b$). Thus the parameter a_1 describes *svwt* for very high dose rate. a_1 = 0.05%/ºC for the Isorad Gold 1 diode. The parameter a_2 describes the dose rate dependent component of *svwt*. a_2 = 0.4%/ºC for the Isorad Gold 1 diode. From *svwt* for three different dose rates in Table 3, we derived $b = 8 \times 10^{-4}$ $(cGy/s)^{-1}$ for the Isorad Gold 1 diodes.

Table 3. Temperature coefficients for n-type and p-type diodes.
All measurement were made at depth of 5 cm, 10 x 10 cm^2, SSD = 100 cm.

Temperature Coefficient / Diode Type	6 MV (%/°C)	15 or 20 MV (%/°C)	Co-60 (%/°C)
Isorad Gold 1, unirradiated	0.06	0.05 (20 MV)	0.45 (T1000)
Isorad Gold 2, unirradiated	0.08	0.10 (20 MV)	0.16 (T1000)
Isorad Red	0.22	0.21 (20 MV)	0.37 (T1000)
QED unirradiated	0.27	0.25 (15 MV)	0.34 (T Phoenix)
QED Blue Diode	0.30	0.31 (15 MV)	0.30 (T780)
QED Red Diode	0.29	0.29 (15 MV)	0.29 (T780)
Scanditronix EDP 10	0.38	0.33 (20 MV)	0.36 (T1000)
Scanditronix EDP 30	0.36	0.34 (20 MV)	0.39 (T1000)

3.4.2 Preirradiated N-Type

The Isorad Red diode was preirradiated to 10 kGy of radiation under 3 MeV electrons by the manufacturer. Figure 7 shows that the temperature coefficient was 0.37%/°C under the continuous (Co-60) radiation and about 0.22%/°C under the pulsed radiation. Compared with unirradiated n-type Isorad diodes, the temperature coefficient for the pre-irradiated n-type Isorad Red diode is increased under pulsed radiation. Preirradiation reduces the difference in temperature coefficient between pulsed and continuous radiation for the n-type diode. Preirradiation with electrons introduces defects in the semiconductors, which reduces the minority carrier lifetime. Our measurements seem to indicate that the trap centers introduced by preirradiation reduces the dose rate dependence of *svwt*. The *svwt* did not show energy dependence as seen from Figs. 6 and 7 for 6 and 20 MV photons.

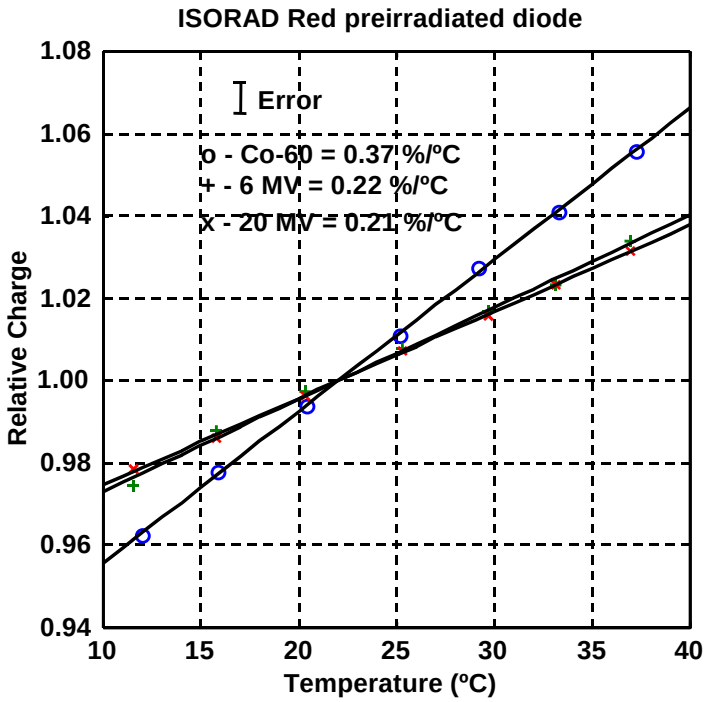

Figure 7. Temperature dependence for Isorad Red (n-type) preirradiated diode.
The diode was preirradiated to 10 kGy by 3 MeV electrons.

The temperature coefficient for all the n-type (Isorad) diodes is given in table 3. The temperature coefficient for all the unirradiated n-type (Isorad) diodes was lower under the pulsed radiation than under the Co-60 radiation.

3.4.3 Unirradiated P-Type

For the QED p-type diodes, the temperature coefficients (*svwt*) for an unirradiated diode* were slightly smaller than the corresponding preirradiated diodes for the same photon beam with pulsed radiation (see Fig. 8). It varied with dose rate and was 0.34%/ºC for Co-60 (dose rate = 2.11 cGy/sec), 0.27%/ºC for 6 MV (dose rate = 5800 cGy/sec) and 0.25%/ºC for 15 MV (dose rate = 11200 cGy/sec). This dose rate dependence was smaller than that observed in unirradiated n-type diode.

* The unirradiated p-type diode is not available commercially and was specially package for this study.

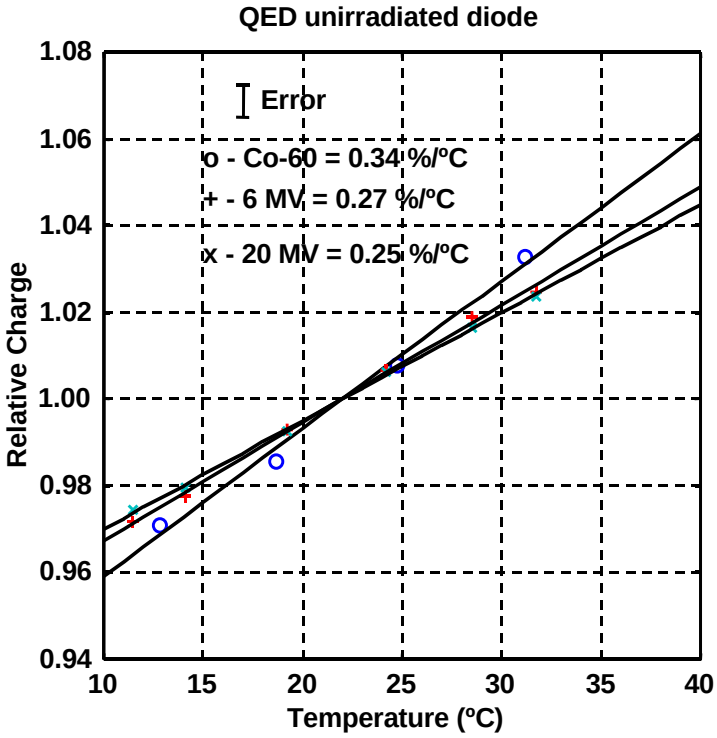

Figure 8. Temperature dependence for QED (p-type) unirradiated photon diode.

For the Scanditronix p-type diodes, we examined the published results of Van Dam *et al*[22], who measured *svwt* for unirradiated p-type diodes from Scanditronix at various cumulative dose levels. These diodes were made in the late 1980s and thus can have different *svwt* from our Scanditronix p-type diodes delivered between 1995 and 2000. Their radiation source was a Saturne-20 accelerator producing 18 MV photon beam with a dose per pulse of 6.5×10^{-4} Gy/pulse. This dose rate per pulse is about twice as high as what was used in this study. They showed *svwt* = 0.03%/ºC for an accumulative dose of 300 Gy, while *svwt* = 0.15 to 0.38%/ºC for an accumulative dose of 4 kGy (Ref. 23, Fig. 1). This range of *svwt* variation is consistent with our result for unirradiated n-type diodes (Table 3, Isorad Gold 1).

3.4.4 Preirradiated P-Type

The temperature coefficient of the preirradiated p-type QED photon diodes remains constant at (0.30±0.01)%/°C with increase in temperature under both high instantaneous dose rate (pulsed) and low dose rate (continuous, cobalt) radiation. The temperature coefficient is independent of the dose rate. Figure 9a and 9b shows the temperature dependence of two of the photon diodes under high instantaneous dose rate (pulsed) and low dose rate (continuous, cobalt) radiation.

In comparison, preirradiated (8kGy) Scanditronix p-type diodes also show that the sensitivity increased linearly with increasing temperature for all the p-type diodes. The temperature coefficient for EDP30 and EDP10 patient diodes was slightly dose rate dependent and was (0.36 ± 0.03)%/°C under the pulsed (6 and 20 MV) as well as continuous (Co-60) radiation. In comparison, temperature coefficient for Scanditronix diode preirradiated with 4kGy varies between 0.19%/ºC and 0.38%/ºC depending on which individual diode was measured (See Ref. 23, Fig. 1). The temperature coefficients for p-type Scanditronix diodes are shown in figures 10a and 10b. Table 3 shows the temperature coefficient measured for the p-type photon diodes.

Our study shows a dose rate dependence for the temperature coefficient, as has been previously reported by Van Dam *et al*.[22] The pre-irradiation reduces (or eliminates) dose rate dependence of *svwt*. This is not true for the dose rate dependence of diode sensitivity. Figure 11 shows that p-type diodes have considerably smaller dose rate dependence than n-type diodes, as discussed previously. For n-type diode, the diode sensitivity increases with increasing dose rate by as much as 8%. Preirradiation does not reduce the dose rate dependence for diode sensitivity, e.g. Isorad Red diode still have strong dose rate dependence even with 10 kGy preirradiation (Fig. 11). However, the temperature coefficient for the Isorad Red diode became less dose-rate dependent because of the preirradiation.

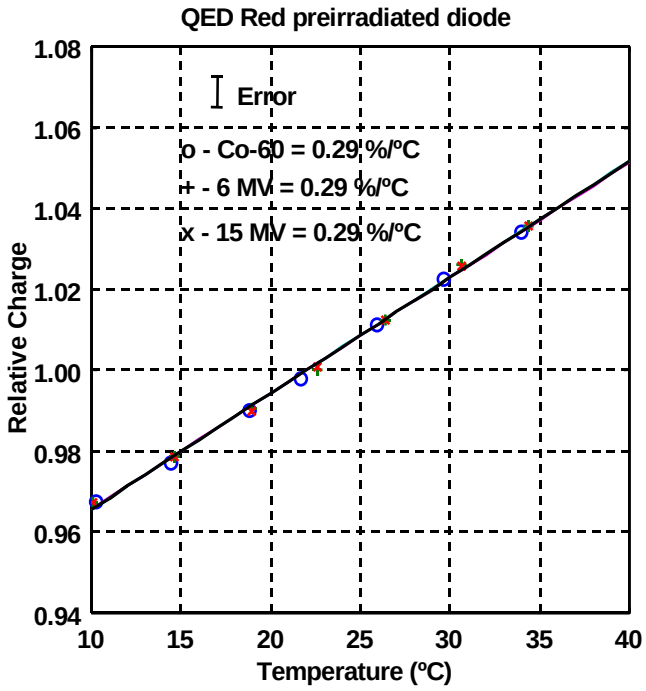

(a)

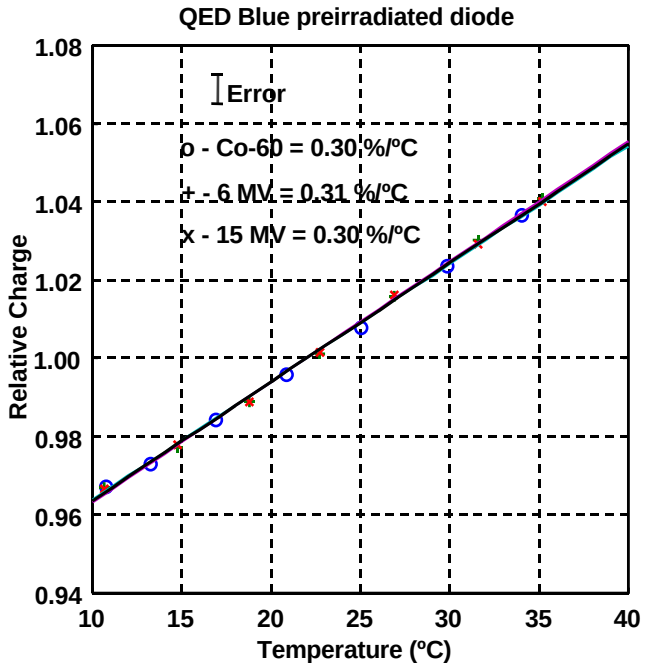

(b)

Figure 9. Temperature dependence for p-type (QED) preirradiated photon diodes. (a) QED Red (p-type) and (b) QED Blue (p-type). The diodes were preirradiated to 10 kGy by 10 MeV electrons.

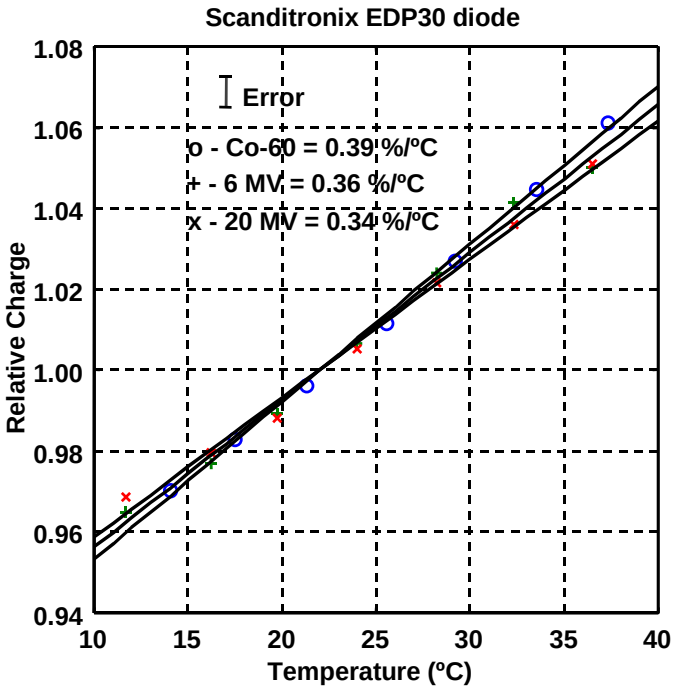

(a)

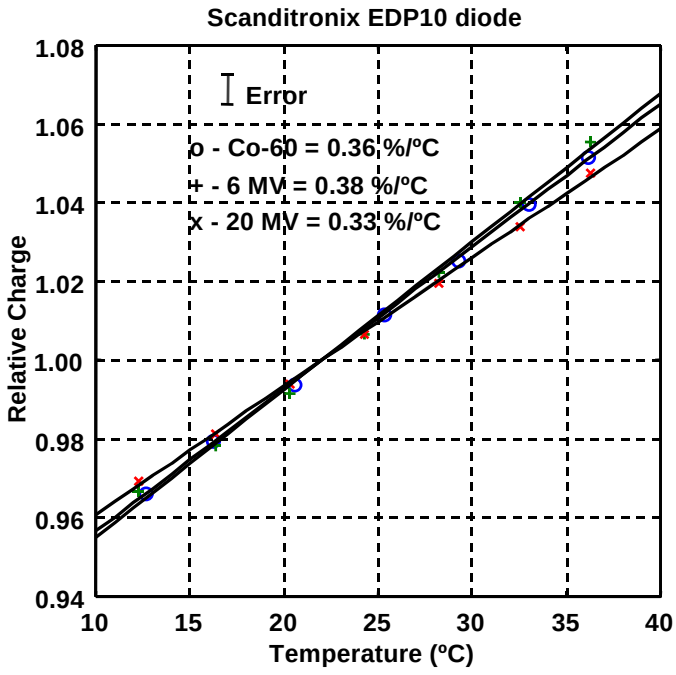

(b)

Figure 10. Temperature dependence for p-type (EDP) preirradiated photon diodes.
(a) EDP30 (p-type) and (b) EDP10 (p-type). The diodes were preirradiated to 8 kGy by 10 MeV electrons.

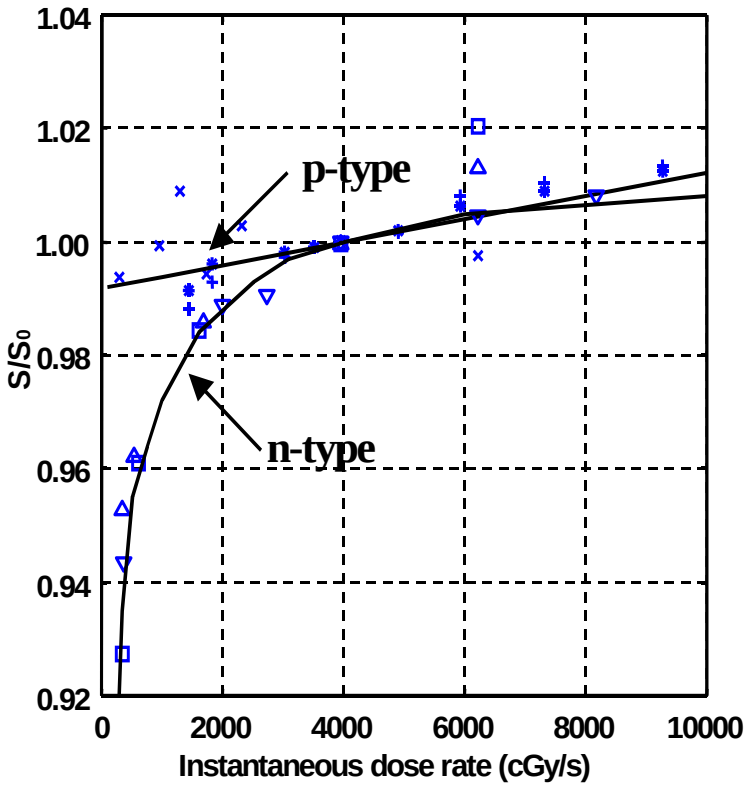

Figure 11. Dose rate dependence of the relative diode sensitivity, S/S_0, for 6 MV.
× – EDP30 (p-type), * – QED Blue (p-type), + – QED Red (p-type), □ – Isorad Gold 1 (n-type), Δ – Isorad Gold 2 (n-type), ∇ – Isorad Red (n-type). S_0 is the diode sensitivity for dose rate of 4000 cGy/s. Notice that the p-type diodes (EDP and QED) have much smaller dose rate dependence than n-type diodes (Isorad). Solid lines are spline lines to show the difference between n- and p-type diodes.

A possible explanation of why pre-irradiation eliminates (or reduces) dose rate dependence of *svwt* but not the diode sensitivity *S* itself can be made from an analysis of the minority carrier lifetime. The minority carrier lifetime can be expressed as[42]

$$\tau_p = \frac{1}{\sigma_{cp} v_{th} N_t}, \tag{41a}$$

or

$$\tau_n = \frac{1}{\sigma_{cn} v_{th} N_t}, \tag{41b}$$

for holes or electrons, respectively. σ_{cp} and σ_{cn} are the capture cross-sections for the holes and electrons, respectively. v_{th} is the thermal velocity for the electrons or holes. N_t is the recombination and generation (R-G) center density, i.e., the number of R-G centers per cm^3. N_t is proportional to the total dose received by the diode. Here, only the thermal velocity $v_{th} = \sqrt{3kT/m^*}$ is a function of temperature T and is approximately 10^7 cm/sec at 300 K (m* is assumed to be the free electron mass).[42] σ_c and N_t are temperature independent. These R-G centers are typically caused by defects, which can be produced by either radiation or by the high-temperature device manufacturing steps. If Au or Pt impurities are introduced, new R-G centers (with different capture cross-section σ, thermal velocity v_{th}, and N_t) are created. When there are multiple mechanisms acting as R-G centers, then the total minority lifetime becomes[42]

$$\tau^{-1} = \tau_1^{-1} + \tau_2^{-1} + \ldots, \tag{42}$$

where τ_i, (i = 1, 2, …) refers to the minority lifetime caused by different types of R-G centers. Notice that the total lifetime depends, for the most part, on the one mechanism that gives the shortest lifetime. We hypothesize that as the diodes were preirradiated, the radiation generated defects becomes the predominat mechanism for the minority lifetime and these R-G centers have similar energy level (E_T). As a result, the influence on minority carrier lifetime from other mechanisms are minimized. Since radiation-induced defects are the only cause, Eq.(38) becomes valid. Combining Eq. (37) and (38) shows that the diode sensitivity S is dose rate dependent because of the dependence on the excessive carrier Δn or Δp. However, Eq. (39), derived from Eqs. (37) and (38), shows no dose rate dependence of *svwt* for either n-type or p-type diodes: $svwt = \frac{1}{2} \cdot \frac{d \ln \kappa \tau_p}{dT}$ for n-type and $svwt = \frac{1}{2} \cdot \frac{d \ln \kappa \tau_n}{dT}$ for p-type. Since the dose rate dependent term, $\Delta n/p_0$ or $\Delta p/n_0$, is temperature independent, its temperature derivative becomes zero in Eq. (39), i.e., $\frac{d \ln(1 + \Delta n / \zeta \cdot p_0)}{2 \cdot dT} = 0$ for n-type diode and $\frac{d \ln(1 + \zeta \cdot \Delta p / n_0)}{2 \cdot dT} = 0$ for p-type diode.

The clinical significance of our finding is two fold: First, preirradiation reduce and even eliminates the dose rate dependence of *svwt*. It is important to preirradiate the diodes so that a consistent value of *svwt* can be established for the same type of diode for temperature correction. For the unirradiated n-type diodes (Table 3), *svwt* is very different between a Co-60 unit and a linear accelerator. This difference can be as much as 0.4%/ºC, or a deviation of 3% assuming the calibration is done at 22ºC and the measurement is done at 29ºC. The later temperature is chosen as the highest equilibrium temperature for package type described in Fig. 5(a) from the thermal study of Welsh and Reinstein [6]. Second, preirradiation increases *svwt* significantly for pulsed radiation. This also favors preirradiation of diode because otherwise the diode *svwt* will change with accumulative dose, which has the same effect as preirradiation. Our measurements for preirradiated p-type diodes indicate that the value of *svwt* will not change once a level-off dose is reached. This is understandable since our previous theoretical analysis (Eqs. (39) and (41)) indicates that $svwt = \frac{d \ln \kappa}{2 \cdot dT} - \frac{d \ln \sigma_c v_{th}}{2 \cdot dT}$ becomes a constant, independent of accumulative dose (or the density of defects N_t) since $\frac{d \ln N_t}{dT} = 0$.

3.5 Conclusion

In this study temperature dependence of n- and p-type diodes were measured under continuous and pulsed radiation. The response was linear with temperature for all the diodes (n- and p-type) under both pulsed and continuous radiation. The temperature coefficient for pre-irradiated p-type diodes was almost the same under low (continuous) and high (pulsed) radiation and their temperature coefficient did not vary much for individual diodes. The unirradiated n- or p- type diodes show different temperature coefficient under pulsed and continuous radiation, and the temperature coefficient varied between each individual diode. The difference in temperature coefficient between pulsed and continuous radiation was reduced with preirradiation (10 kGy) for n-type diode and was almost eliminated with preirradiation (8-10 kGy) for p-type diodes. In contrary, preirradiation cannot eliminate dose rate dependence of the diode sensitivity itself. It was

seen that, compared to unirradiated diodes, the temperature coefficient for a preirradiated diode was larger under pulsed radiation. The pre-irradiated p-type diodes (QED and EDP) showed larger temperature dependence than the unirradiated n-type diodes for the pulsed radiation, but their *svwt* was independent of dose rate.

CHAPTER 4 PAPER II: DOSE RATE AND SDD DEPENDENCE OF COMMERCIALLY AVIALABLE DIODE DETECTORS

In clinical applications, dose rate dependence is the most essential dosimetric parameter for diode dosimetry since unlike ionization chamber ion recombination is inherited in a diode detector. As a result the diode sensitivity changes greatly with the instantaneous dose rate especially for pulsed radiation beam. The dose rate could vary due to source–to-detector distance (SDD) changes, placement of transmission blocks or wedges, or transmission through the patient. In this paper, SDD (or SSD (source-to-surface distance)) and dose rate dependence of diode sensitivity for different commercially available diode detectors were measured under high instantaneous dose rate (pulsed) and low dose rate (continuous) radiation. The dose rate dependence measured by adjusting radiation pulse height directly was compared to that measured by changing SDD. A photon-energy independent empirical formula was proposed to fit the dose rate dependence of diode sensitivity.

Medical Physics, 31 (4):914-24 (2004).

4.1 Synopsis

The dose rate dependence of commercially available diode detectors was measured under both high instantaneous dose rate (pulsed) and low dose rate (continuous, Co-60) radiation. The dose rate dependence was measured in an acrylic miniphantom at 5-cm depth in a 10×10 cm^2 collimator setting, by varying source–to-detector distance (SDD) between at least 80-200 cm. The ratio of normalized diode reading to a normalized ion chamber reading (both at SDD = 100 cm) was used to determine diode sensitivity ratio

for pulsed and continuous radiation at different SDD. The inverse of the diode sensitivity ratio is defined as SDD correction factor (SDD CF). The diode sensitivity ratio increased with increasing instantaneous dose rate (or decreasing SDD). The ratio of diode sensitivity, normalized to 4000 cGy/s, varied between 0.988 (1490 cGy/s) – 1.023 (38900 cGy/s) for unirradiated n-type Isorad Gold, 0.981 (1460 cGy/s) – 1.026 (39060 cGy/s) for unirradiated QED Red (n-type), 0.972 (1490 cGy/s) – 1.068 (38900 cGy/s) for pre-irradiated Isorad Red (n-type), 0.985 (1490 cGy/s) – 1.012 (38990 cGy/s) for n-type Pt-doped Isorad-3 Gold, 0.995 (1450 cGy/s) – 1.020 (21870 cGy/s) for n-type Veridose Green, 0.978 (1450 cGy/s) – 1.066 (21870 cGy/s) for pre-irradiated Isorad-p Red, 0.994 (1540 cGy/s) – 1.028 (17870 cGy/s) for p-type pre-irradiated QED, 0.998 (1450 cGy/s) – 1.003 (21870 cGy/s) for the p-type pre-irradiated Scanditronix EDP20^{3G}, and 0.998 (1490 cGy/s) – 1.015 (38880 cGy/s) for Scanditronix EDP10^{3G} diodes. The p-type diodes do not always show less dose rate dependence than the n-type diodes. Pre-irradiation does not always reduce diode dose rate dependence. A comparison between the SDD dependence measured at the surface of a full scatter phantom and that in a miniphantom was made. We concluded that the SDD dependence of diode sensitivity can be explained by the instantaneous dose rate dependence if sufficient buildup is provided to eliminate electron contamination. An energy independent empirical formula was proposed to fit the dose rate dependence of diode sensitivity.

4.2 Introduction

Semiconductor detectors are widely used for patient dosimetry for photon and electron beams. They have high sensitivity (~18000 times more sensitive) and high spatial resolution compared to the air filled ionization chamber with the same volume.[5-7] The diode sensitivity is defined as the ionization charge collected per unit absorbed dose (usually in units of nC/cGy). The sensitivity of semiconductor detectors depends on temperature[23,24], dose rate[22,26,27], and energy.[6,7] In clinical applications, the diode is usually placed either at a patient's entrance or exit surface to measure the dose. It is important to characterize the dose rate dependence since the dose rate could vary due to

source–to-detector distance (SDD) changes, placement of transmission blocks or wedges, or transmission through the patient. The SDD for patient treatment can vary from 70 cm (for isocentric SAD setup) to 200 cm (for mantle treatment), or even more than 300 cm (for total body irradiation). These different treatment geometries affect the instantaneous dose rate and thus the diode sensitivity. The instantaneous dose rate refers to the peak dose rate of individual radiation pulses from a linear accelerator, which could be a factor of 1500 times larger than the average dose rate. For a Cobalt unit, average dose rate equals the instantaneous dose rate. For simplicity, we will use "dose rate" to refer to "instantaneous dose rate" throughout the paper. A theoretical analysis of the instantaneous dose rate dependence of diode detectors can be found elsewhere.[29]

Diodes are termed n-type or p-type depending upon whether the silicon substrates are doped with phosphorous (where majority-carriers are electrons) or boron (where majority-carriers are holes).[6,24,29] Dose rate has been reported to be a problem in n-type diodes, but not for pre-irradiated p-type diodes.[7] Rikner and Grusell have reported that a p-type Si detector (Scanditronix diodes) pre-irradiated to 25 kGy displays a flat dose rate dependence.[27] Rikner has also shown that the response of a n-type detector (diodes made in-house, without any Au or Pt doping) shows more dose rate dependence than some p-type detectors.[6] It has also been shown that the dose rate dependence of diode sensitivity of the p-type detector depends upon the resistivity or doping level of the diode (higher the doping level lower the resistivity, and vice versa).[27] A highly doped (low resistivity) p-type detector shows no dose rate dependence. Accumulated dose can reduce dose rate dependence for p-type diodes.[5,29] However, some pre-irradiated (Scanditronix) p-type diodes had increased dose rate dependence after a high level of accumulated irradiation (~25 kGy) with high photon energies (E > 10 MV).[30] For n-type diodes, accumulated dose usually increases the dose rate dependence.[35] However, it is found that the dose rate dependence for some Pt-doped n-type diodes does not depend on the accumulated dose because of the short minority carrier life-time.[29]

In this paper, SDD (or SSD (source-to-surface distance)) and dose rate dependence of diode sensitivity for different commercially available diode detectors were measured under high instantaneous dose rate (pulsed) and low dose rate (continuous) radiation. The dose rate dependence measured by adjusting radiation pulse height directly was compared to that measured by changing SDD. A photon-energy independent empirical formula was proposed to fit the dose rate dependence of diode sensitivity.

4.3 Materials and Methods

4.3.1 Description of Diodes

Eleven different n- and p-type detectors were used in this study: Four n-type and three p-type diodes were from Sun Nuclear Corporation (Sun Nuclear Corporation, 425 A Pineda Ct., Melbourne, FL 32940), three p-type diodes were from Scanditronix (Scanditronix AB, Husbyborg, S-752-29, Uppsala, Sweden), and one n-type diode from Nuclear Associates (Cardinal Health, 6045 Cochran Rd, Cleveland, OH 44139). We initially intended to cover all commercially available diodes for in-vivo radiation dosimetry. However, the final choice of diodes was determined by availability at the time the study began.

The Isorad diodes (two Isorad Gold (#1 and #2), one Isorad Red (n-type), one Isorad-3 Gold and one Isorad-p Red) from Sun Nuclear have cylindrical designs with the die plane mounted normal to the detector axis.[24] The two Isorad Gold diodes were from different batches but were nominally the same. All other diodes (the QED, Veridose, and Scanditronix EDP) use a flat design, with radiation incident normal to the plane of the die (chip). The diodes were all new without any prior clinical irradiation. Isorad-p Red diode uses the same die as is used in p-type QED diodes, but the die plane is mounted normal to the detector's axis. Detailed schematics of some of the diodes used in this study can be found elsewhere.[24] Different thicknesses and materials of inherent buildup are used for

different diode models in order to match the suitable photon energy range used. These physical package details are listed in Table 4a.

The device specification of the diode (chip) determines the response of the diode sensitivity. This includes the type of diodes (n-type or p-type), Pt-doping, substrate resistivity (in Ω-cm), and the level of preirradiation. This information is summarized in Table 4b. Several new n-type diodes (Veridose Green, QED red (n-type), and Isorad-3 Gold) are Pt-doped. Pt doping can drastically reduce the minority carrier lifetime ($\tau < 0.1$ μs) and thus reduce the dose rate dependence of diode sensitivity. The resistivity of substrate is proportional to the majority carrier concentration. The Scanditronix EDP10^{3G} and EDP20^{3G} are new p-type diodes. They have the same resistivity as the EDP30 diode. Pre-irradiation of the diode changes the dose rate dependence. The n-type Isorad Gold diodes and Pt-doped n-type diodes (Isorad-3 Gold and QED Red (n-type)) from Sun Nuclear were not pre-irradiated. The n-type Isorad Red (n-type) diode was pre-irradiated to 10 kGy by 3 MeV electrons. All other diodes were pre-irradiated by 10 MeV electrons except for the Scanditronix EDP10^{3G} and EDP20^{3G} diodes, whose type of pre-irradiation is kept confidential by the manufacturer. All the commercial p-type detectors used in this study are from the same manufacturer. They use the same die (chip) with different buildup thicknesses appropriate for their photon energies.

4.3.2 Experiment Setup

The diode SDD dependence was measured for the diodes with SDD ranging from at least 80 to 200 cm for the pulsed radiation and Co-60 radiation. All the measurements were taken by using the 10 x 10 cm^2 collimator setting. The diode was placed at 5-cm depth in a 4-cm diameter Lucite miniphantom. A thimble-type ionization chamber was used for the inter-comparison, under the same geometric conditions. One hundred monitor units or one-minute time exposures were given for pulsed or Co-60 radiation respectively. Each set of data was completed within about 3 hours, with each diode or ionization chamber measurement completed within an hour, on the same day. Charges from all

diodes were measured using an electrometer under zero-bias. Leakage was subtracted for all the measurements before analyzing the data. The SDD correction factors (SDD CF) were calculated by taking the inverse of normalized ratios between the diode readings (M_{diode}) and the ion chamber readings (M_{ion}):

$$SDD \quad CF = \frac{(M_{diode} / M_{ion})_{100}}{(M_{diode} / M_{ion})_{SDD}}. \tag{43}$$

SDD CF = 1 at SDD=100cm and is a function of SDD. Our SDD CF results should not be directly compared to other published results, which are usually measured with the diode placed at the surface of a full scatter phantom. To differentiate between the two different conditions, we termed SDD CF measured at surface as "SSD CF". For measurements with diode placed at the surface, the same formula (Eq. (43)) was used to calculate SSD CF, except for the ionization chamber was placed at the depth of maximum dose (1.6 cm for 6 MV and 3.2 cm for 18 MV) for the same SDD. To quantify the differences, a comparison of the measured SSD CF for diodes placed at surface and the SDD CF for our setup (in miniphantom) was made for selected diodes.

We chose the miniphantom with a depth of 5 cm to measure SDD dependence because (1) this provides sufficient thickness to eliminate electron contamination, (2) the irradiated volume of the miniphantom will remain the same at different SDDs thus reducing changes caused by the phantom scattered dose, and (3) the depth of the ionization chamber is the same as that of the diode detector. In the conventional method of determining SSD CF, the diode (with intrinsic buildup) is placed at the surface of the phantom while the ionization chamber is placed at the depth of the maximum dose below the surface. This difference in the depth of detector placement introduces uncertainty in determining the actual dose received by the diode.

Table 4. Package (a) and device (b) specification of the different diode detectors.

(a)

Diode Type	Manufacturer Code	Shape	Buildup Material, Total Buildup Thickness (g/cm^2)	Suitable Energy Range	Manufacturing Period
Nuclear Associates Veridose Green	30-474	Flat	1.7 mm Tungsten, 3.574	18-25 MV	1998-
Scanditronix EDP 10^{3G}	$EDP10^{3G}$	Flat	0.75 mm Stainless Steel + epoxy, 1	4-8 MV	2001 -
Scanditronix EDP 20^{3G}	$EDP20^{3G}$	Flat	2.2 mm Stainless Steel + epoxy, 2	10-20 MV	2001 -
Scanditronix EDP 30	EDP30	Flat	1 mm Tantalum + epoxy, 1.3	20–30 MV	1990-2001
Sun Nuclear Isorad Gold	114300	Cylinder	1.1 mm Brass, 1.534	6–12 MV	1993 - 1998
Sun Nuclear Isorad Red (n-type)	114200	Cylinder	1.1 mm Tungsten, 2.75	15–25 MV	1993 - 1998
Sun Nuclear Isorad-p Red	1164000-0	Cylinder	1.13 mm Tungsten, 2.58	15-25 MV	1998 - 2002
Sun Nuclear Isorad-3 Gold	1163000-0	Cylinder	1.13 mm Molybdenum, 1.6	6-12 MV	2003 -
Sun Nuclear QED Red (n-type)	1116000-0	Flat	3.4 mm Brass, 3.04	15-25 MV	2003 -
Sun Nuclear QED Blue (p-type)	111400-0	Flat	3.4 mm Aluminum, 1.03	1–4 MV	1997 - 2002
Sun Nuclear QED Red (p-type)	111600-0	Flat	3.4 mm Brass, 3.04	15–25 MV	1997 - 2002

(b)

Diode Type	Type	With Platinum Doping	Resistivity (Ω-cm)	Preirradiation
Nuclear Associates Veridose Green	n-type	YES	NA	8 kGy, 10MeV
Scanditronix EDP 10^{3G}	p-type	NO	0.2	Yes, Value Confidential
Scanditronix EDP 20^{3G}	p-type	NO	0.2	Yes, Value Confidential
Scanditronix EDP 30	p-type	NO	0.2	8 kGy at 10 MeV
Sun Nuclear Isorad Gold	n-type	NO	35	None
Sun Nuclear Isorad Red (n-type)	n-type	NO	35	10 kGy, 3 MeV
Sun Nuclear Isorad-p Red	p-type	NO	0.8	10 kGy, 10 MeV
Sun Nuclear Isorad-3 Gold	n-type	YES	10	None
Sun Nuclear QED Red (n-type)	n-type	YES	10	None
Sun Nuclear QED Blue (p-type)	p-type	NO	0.8	10 kGy at 10 MeV
Sun Nuclear QED Red (p-type)	p-type	NO	0.8	10 kGy at 10 MeV

The ratio of diode reading to ion chamber reading was plotted against the instantaneous dose rate. This ratio was normalized to be 1 at an instantaneous dose rate of 4000 cGy/s for the pulsed radiation and 1.6 cGy/s for the continuous radiation. The instantaneous dose rate at a depth of 5 cm in the miniphantom for different SDDs was calculated from the normalized ionization chamber measurement, together with the known dose rate at SDD=100cm using the expression:[4]

$$InstDR_{SDD} = \frac{M_{ion}(SDD)}{M_{ion}(100)} \cdot InstDR_{100}. \tag{44}$$

Here M_{ion}(SDD) and M_{ion}(100) are the total charge measured by an ionization chamber in the same miniphantom for the source to detector distance (SDD) of interest and SDD =100 cm, respectively. For pulsed radiation, $InstDR_{100}$ is the instantaneous dose rate at SDD=100 cm for the 10×10 cm^2 collimator setting at a depth of 5-cm in a Lucite miniphantom. It can be calculated according to[4]:

$$InstDR_{100} = \frac{(DR_{100}/60)}{(PW)(PRF)}(S_c(c=10)(S_p(s=4))(TMR(s=4,d=5)), \tag{45}$$

where DR_{100} is expressed in MU/min and the factor 60 is used to convert DR_{100} to MU/sec. PW is the measured pulse width (in seconds) and PRF is the measured pulse repetition frequency (in Hz). Notice 1 MU = 1 cGy at the calibration condition: SAD = 100 cm, 10×10 cm^2 and at a depth of maximum dose (1.5 cm for 6 MV, 2 cm for 8 MV, 3.0 cm for 15, and 3.2 cm for 18 MV). Thus, after conversion DR_{100} (in cGy/sec) is the average dose rate under the calibration condition, while $InstDR_{100}$ (in cGy/sec) is the instantaneous dose rate at a 5-cm depth in the miniphantom at SAD = 100 cm and 10×10 cm^2 collimator setting. For continuous (Co-60) radiation, $InstDR_{100}$ is calculated according to[24]:

$$InstDR_{100} = DR_{100}(S_c(c=10)(S_p(s=4))(TMR(s=4,d=5)). \tag{46}$$

Here $S_c(10)$ is the collimator scatter factor for a collimator setting of 10×10 cm^2, $S_p(4)$ is the phantom scatter factor for a cross section of 4×4 cm^2, and $TMR(4,5)$ is the tissue maximum ratio for a field size of 4×4 cm^2 at a depth of 5 cm in a phantom.[4] DR_{100} is the average dose rate measured at the calibration condition (10×10 cm^2, $d = d_{max}$, SAD = 100 cm), which is usually expressed using units of MU/min. These parameters are listed in Table 5.

Table 5. Dose rate of the radiation sources (Paper II).
Depth of 5 cm in a miniphantom, 4×4 cm^2 at SDD = 100 cm, *PRF* is the pulse repetition frequency and *PW* is the pulse width.

Radiation Source	Average Dose Rate DR_{100} (MU/min)	Instantaneous Dose Rate $InstDR_{100}$ (cGy/sec)	Dose per Pulse (mGy)	*PRF*, *PW*
T1000, Co-60	—	1.6	—	Continuous
Siemens KD2, 6 MV	200	6322	0.152	192 Hz, 2.4 µs
Siemens Primus, 6 MV	297	6169	0.174	263 Hz, 2.8 µs
Varian 2100CD, 8 MV	600	7575	0.318	360 Hz, 4.2 µs
Siemens KD2, 15 MV	300	11448	0.298	161 Hz, 2.6 µs
Siemens Primus, 18 MV	490	13977	0.419	200 Hz, 3.0 µs
Varian 2100CD, 18 MV	600	17361	0.608	180 Hz, 3.5 µs

For pulsed radiation, a Siemens Primus (for Isorad Gold #1, Isorad Red (n-type), Isorad-3 Gold, QED Red (n-type), Isorad-p Red, EDP10^{3G}, EDP20^{3G}, and Veridose Green), and a Siemens KD2 (for QED p-type diodes) were used. For continuous radiation, a Theratronix 1000 was used for n-type Isorad and p-type Scanditronix EDP diodes. The instantaneous dose rate in the miniphantom was calculated from measured data (*PW*, DR_{100} and *PRF*) for each beam at 100 cm SDD according to Eq. 45 and is summarized in Table 5. For the Siemens KD2 accelerator, it was approximately 6322 cGy/s and 11448 cGy/s for 6 and 15 MV, respectively. For Siemens's Primus accelerator, it was approximately 6169 cGy/s and 13977 cGy/s for 6 and 18 MV, respectively. For continuous (Co-60) radiation, it was 1.6 cGy/s. Table 5 lists the parameters for the radiation sources used in this study.

A Varian 2100CD linear accelerator was used to measure the dose rate dependence of diode sensitivity directly by adjusting the radiation pulse height to change the

instantaneous dose rate. Two diodes (the p-type Scanditronix EDP 30 and the n-type Isorad Gold #2) were used. For comparison, SDD dependence of the diodes was measured on the same Varian accelerator at the same time. However, the SDD dependence was measured in a 25 × 25 cm^2 field in a full scatter phantom at a depth of 3.5 cm. The average dose rate (DR_{100}) for the Varian 2100CD was 600 MU/min for both 8 and 18 MV at a source-to-detector distance of 100 cm. The radiation pulse height was adjusted so that the instantaneous dose rate varied between 2710 – 16550 cGy/s and 3966 – 42287 cGy/s for 8 and 18 MV, respectively, at the source-to-detector distance of 67.5 cm. The ionization chamber reading was corrected by P_{ion} to account for the ion recombination effect at a high dose rate. To merge the measured relative diode sensitivity for 8 MV and 18 MV together to cover a wider dose rate range, the relative sensitivity was normalized to be 1 for *InstDR* = 10000 cGy/s. When no data point is available at *InstDR* = 10000 cGy/s, a linear interpolation of the measured data point is used.

4.3.3 Theory

The sensitivity, S, of the diode detector can be expressed as:[23,24,29]

$$S = K \cdot \sqrt{\kappa \cdot \tau}\ , \tag{47}$$

Where κ is the diffusion coefficient (cm^2/s) and τ is the excess minority-carrier lifetime (s). $K = 6.72 \times 10^{-6} \cdot A$ (C/cGy/cm) for a silicon diode without any buildup[29], and A is the cross-section area of the diode (in cm^2). However, since the commercial diode has inherent buildup, K value changes and is energy dependent.

If the excess-carrier concentration generated by radiation is relatively small (compared to the majority-carrier concentration n_0 or p_0) and a single mechanism of recombination and generation (R-G) center dominates, then τ can be simplified from a complete expression

of net recombination rate.[29] For a n-type (or p-type) substrate with majority-carrier concentration n_0 (or p_0), τ can be expressed as:

$$\tau = \begin{cases} \tau_p\left(1+\dfrac{\zeta\Delta p}{n_0+\Delta p}\right) & (n-type) \\ \tau_n\left(1+\dfrac{\Delta n}{\zeta\cdot(p_0+\Delta n)}\right) & (p-type) \end{cases}, \tag{48}$$

where τ_p is the minority-carrier (hole) lifetime in the n-type substrate while τ_n is the minority-carrier (electron) lifetime in the p-type substrate. $\zeta = \tau_n/\tau_p$ is the ratio between the minority carrier lifetimes. Δp or Δn is the mean concentration of the excess minority-carriers generated in a single radiation pulse (or within the lifetime of the minority carrier for a continuous radiation) and is proportional to the instantaneous radiation rate. This value can be estimated from the total excess minority-carriers generated by the radiation,

$$\Delta n = \Delta p = \frac{\rho}{e\beta(W/e)}\int InstDR\cdot dt \equiv g\cdot\int InstDr\cdot dt \tag{49}$$

Here β is the dose-to-kerma ratio. It is 1.005 for Co-60 and 1.0 for megavoltage photon beams. Using density (ρ = 2.5 g/cm^3) and the energy required to produce an electron-hole pair (W=3.6 eV) for Silicon,[1] we calculated $g = 4.35\times10^{13}$ 1/cGy (Si) assuming β = 1. To calculate the mean excess minority-carrier concentration Δn (or Δp) suitable for Eq. 48, one has to solve a continuity equation to account for the rate of recombination in a p-n junction.[29] The approximate solution[29] can be expressed as Eq. 49 with $\int InstDR\cdot dt = InstDR\cdot PW$ when the pulse width PW is shorter than the lifetime of the excess carrier τ, otherwise $\int InstDR\cdot dt = InstDR\cdot\tau$.[29]

Given the definition of diode sensitivity, the readings of the diode and the ionization chamber, under the same geometrical condition, can be expressed as $M_{diode} = S\cdot D$ and $M_{ion} = S_{ion}\cdot D$, respectively, where S is the diode sensitivity and $S_{ion} = 1/N_{ion}$ is a constant

for a given photon energy. As a result, the ratio of the diode and the ionization chamber readings for the same *SDD* and photon energy, normalized to the ratio for *SDD* = 100 cm becomes:

$$\frac{(M_{diode}/M_{ion})_{SDD}}{(M_{diode}/M_{ion})_{100}} = \frac{S}{S_{100}} \tag{50}$$

Here we have assumed that S_{ion} is dose rate independent. Thus the SDD CF is given by S_{100}/S according to Eq. (43). The ratio of diode sensitivity *S* can be replaced by the ratio of the square root of the minority-carrier lifetime according to Eq. 47. For n-type diode, this can be further expressed using Eq. 48 to

$$\frac{S}{S(InstDR_{ref})} = \sqrt{\frac{\tau}{\tau_{ref}}} = \sqrt{\left(1+\frac{\zeta\Delta p}{n_0+\Delta p}\right)\Big/\left(1+\frac{\zeta\Delta p_{ref}}{n_0+\Delta p_{ref}}\right)}, \tag{51}$$

where $InstDR_{ref}$, τ_{ref}, and Δp_{ref} is the instantaneous dose rate, lifetime, and excess minority-carrier concentration at the reference condition (e.g. *SDD* = 100 cm). This relationship is only true when there is one type of R-G centers and may be invalid for multiple R-G centers.[7,29] However, an empirical formula based on this equation can be used to fit the experimental results. Since the excess carrier concentration (Δp) is proportional to the instantaneous dose rate (Eq. 49), Eq. (51) can be rewritten as:

$$\frac{S}{S(InstDR_{ref})} = \sqrt{(1+\frac{\beta_1 \cdot InstDR}{1+\beta_2 \cdot InstDR})/(1+\frac{\beta_1 \cdot InstDR_{ref}}{1+\beta_2 \cdot InstDR_{ref}})}, \tag{52}$$

where β_1 and β_2 are two fitting parameters that are related to the device parameters. The ratio β_1/β_2 is not necessarily equal to ζ as in Eq. 51. For Cobalt, $S/S(InstDR_{ref}) \approx 1$ since $InstDR \approx InstDR_{ref} \approx 0$. For pulsed radiation, the reference dose rate is usually chosen to be the common dose rate for high and low energies of a dual energy accelerator, e.g. $InstDR_{ref}$ = 4000 cGy/s. The fitting parameters (β_1 and β_2) can be made a constant for the

combination of a particular diode and a radiation source, regardless of whether the pulse width of the linear accelerator is smaller or larger than the minority-carrier lifetime (τ_p for n-type). Eq. (52) should also be valid for the p-type diode provided that the device parameters for n-type diode are replaced by those for p-type diode. When the reference dose rate is $InstDR_{ref} = 0$, Eq. (52) can be further simplified to:

$$\frac{S}{S(0)} = \sqrt{1 + \frac{\beta_1 \cdot InstDR}{1 + \beta_2 \cdot InstDR}} \,. \tag{53}$$

This expression is energy independent and allows one to extrapolate data measured for different SDD's and energy to be a function of instantaneous dose rate only. We introduced Eq. 53, because normalizing S to S(0), the minimum value of S, provides the overall range of change of S for a particular diode detector. The parameters β_1 and β_2 can be extrapolated by fitting Eq. (52) (or Eq. (53)) to measured $S/S(InstDR_{ref})$ (or $S/S(0)$) using a differential evolution algorithm.[51]

The empirical formula (Eq. 53) that describes the dose rate dependence of the diode can also be used to determine the SDD dependence, or SDD CF. According to the definition for SDD CF (Eq. 43) and S/S_{100} (Eq. 50), SDD CF is equal to the inverse of S/S_{100}. Thus SDD CF can be calculated as a ratio of Eq. 53 evaluated at SDD = 100 cm and the desired SDD. We will show later that the SDD CF measured in a miniphantom is very similar to the SSD CF measured on the surface of a full scatter phantom for the same diode detector.

4.4 Results

SDD CF was measured for commercial n-type diodes using pulsed radiation from an accelerator with low (Fig. 12a) and high (Fig.12 b) photon energies, respectively, in a miniphantom. The SDD CF of n-type diodes increased with decreased dose rate (by increasing SDD). Both unirradiated and pre-irradiated n-type Isorad diodes showed SDD

dependence under pulsed radiation. For example, at SDD = 150 cm, the SDD CF, normalized to 100 cm, was 1.008 and 1.004 for n-type unirradiated Isorad Gold #1, 1.030 and 1.028 for n-type pre-irradiated Isorad Red (n-type), 1.014 and 1.014 for unirradiated QED Red (n-type), 1.005 and 1.005 for Isorad-3 Gold, and 1.010 and 1.011 for n-type pre-irradiated Veridose Green diode under pulsed radiation for low (6 MV) and high (18 MV) energies, respectively (Fig.12).

Similar measurements of SDD CF were made for p-type diodes using pulsed radiation (Fig. 13). The SDD CF at SDD=150 cm, normalized to 100 cm, was 1.006 and 1.008, 0.999 and 0.999 for p-type pre-irradiated Scanditronix for $EDP10^{3G}$ and $EDP20^{3G}$ under pulsed radiation for low (6MV) and high (18MV) photon energies, respectively. The SDD CF at SDD=150 cm, normalized to 100 cm, was 1.011 and 1.015±0.002 for p-type pre-irradiated QED diodes, and 1.025 and 1.034 for pre-irradiated Isorad-p Red under pulsed radiation for low (6 MV) and high (15 or 18 MV) photon energies, respectively.

SDD CF was also measured under continuous radiation for selected n-type and p-type diodes (Fig. 14). The SDD CF at SDD=150 cm, normalized to 100 cm, was 1.003±0.002 for all the diodes measured under continuous radiation. The SDD CF varied between 1.001 and 1.005 for SDD between 80 and 208 cm for all diodes under continuous radiation.

The diode sensitivity ratio as a function of the instantaneous dose rate was obtained for n-type diodes from the measured SDD CF vs. SDD. The solid lines in Fig. 4 are curve fits using Eq. (52) and the fitting parameters are listed in Table 6. The sensitivity ratio, normalized to 4000 cGy/s for pulsed radiation, increased with dose rate for all n-type diodes. The sensitivity ratio for the dose rate dependence ranged from 0.972 to 1.068 (1490 cGy/s to 38900 cGy/s) for n-type pre-irradiated Isorad Red (n-type) and 0.995 to 1.020 (1450 cGy/s to 21870 cGy/s) for n-type pre-irradiated Veridose Green diode. The sensitivity ratio varied between 0.988 to 1.023 for Isorad Gold #1 when the dose rate was varied between 1490 cGy/s and 38900 cGy/s. The sensitivity ratio varied between 0.985

(1490 cGy/s) – 1.012 (38990 cGy/s) for unirradiated Isorad-3 Gold, and 0.981 (1460 cGy/s) – 1.026 (39059 cGy/s) for unirradiated QED Red (n-type).

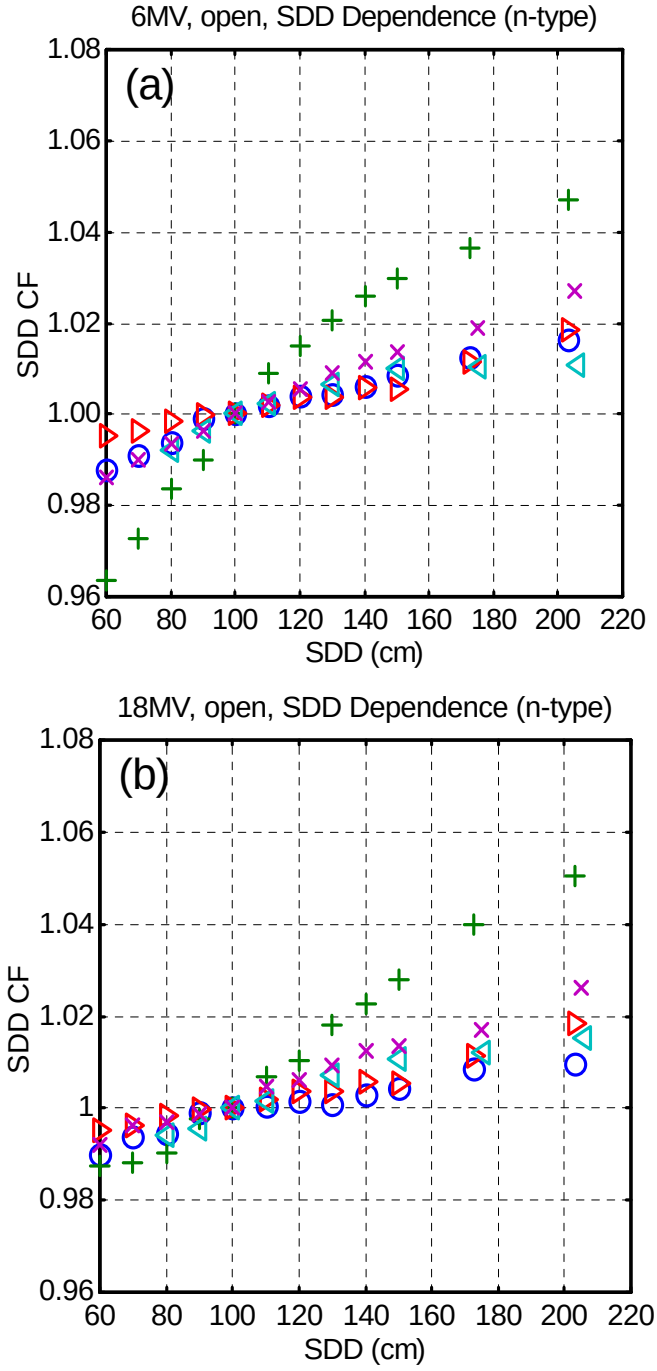

Figure 12. SDD correction factors for n-type diodes under pulsed beams.
(a) 6 MV and (b) 18 MV. o- Isorad Gold #1 , + - Isorad Red (n-type), ▷ - Isorad-3 Gold, ◁ - Veridose Green, and x - QED Red (n-type).

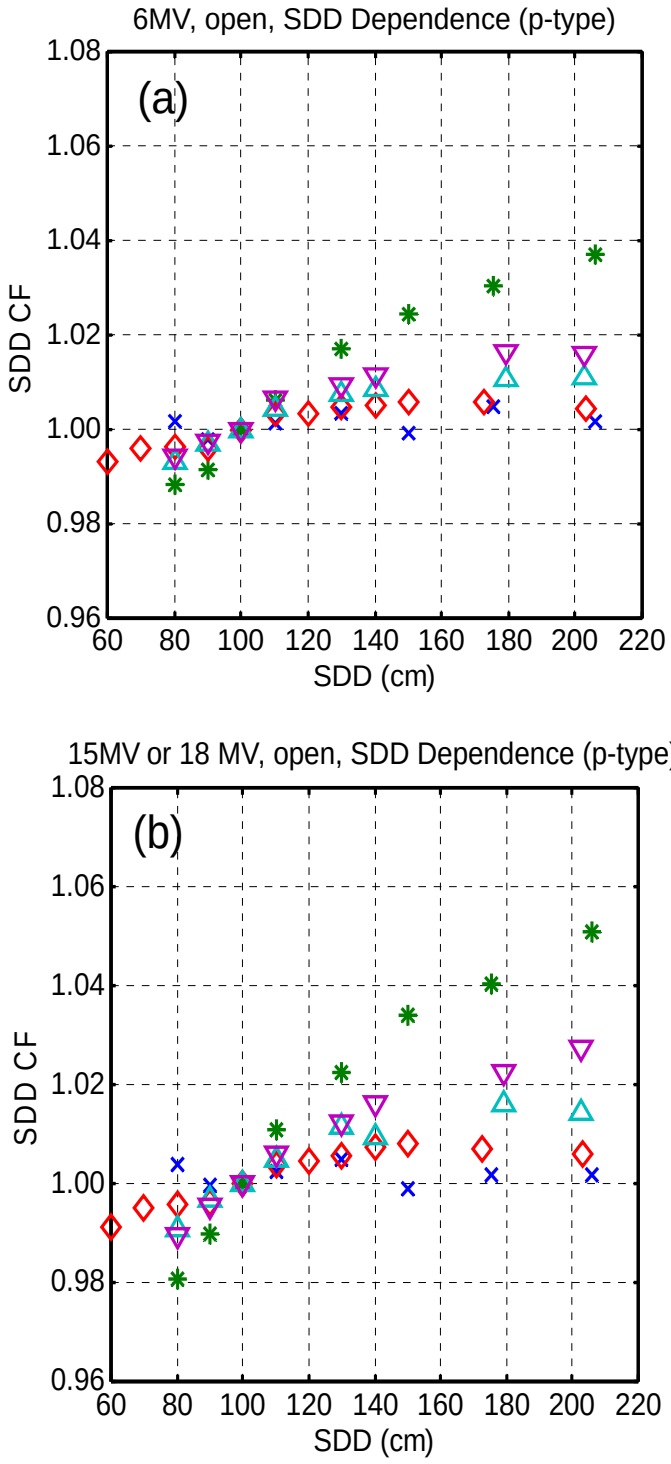

Figure 13. SDD correction factors for p-type diodes under pulsed beams.
(a) 6 MV and (b) 15 or 18 MV. ◊ - EDP10[3G], x- EDP20[3G] , * - Isorad Red (p-type), Δ - QED Red (p-type), and ∇ - QED Blue.

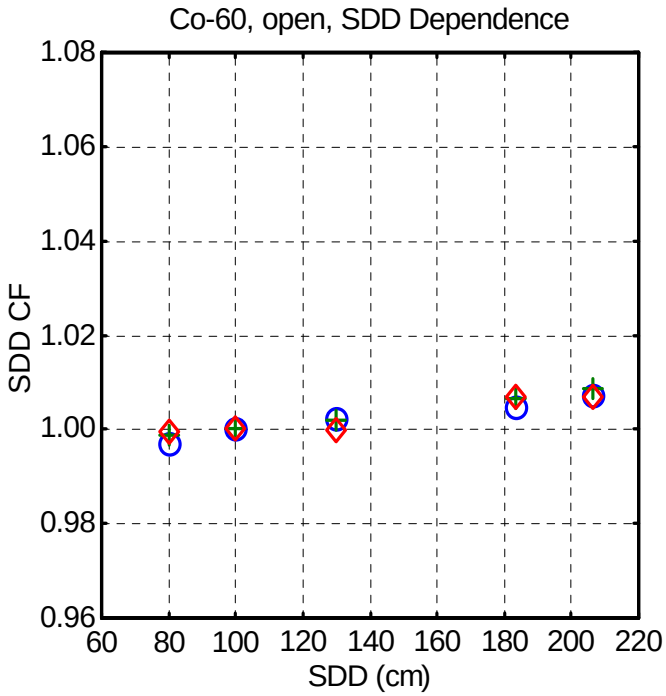

Figure 14. SDD dependence of different diodes under Co-60 radiation.
o - Isorad Gold #2, + - Isorad Red (n-type), and ◊ - EDP30.

Similar results for p-type diodes are shown in Fig. 15b. The sensitivity ratio, normalized to 4000 cGy/s, was 0.998-1.015 (for dose rate 1490 cGy/s-38880 cGy/s) for p-type pre-irradiated EDP10^{3G} and 0.998-1.003 (1470 cGy/s – 21870 cGy/s) for p-type pre-irradiated EDP20^{3G} diodes. The sensitivity ratio varied between 0.996–1.025 for the p-type pre-irradiated QED diodes when the instantaneous dose rate was varied between 1540 cGy/s and 17870 cGy/s (Fig. 15). This ratio varied between 0.978 and 1.066 for pre-irradiated Isorad-p Red diode for the instantaneous dose rate between 1450 cGy/s to 21870 cGy/s.

A comparison was made of the dose rate dependence of diode sensitivity obtained from direct adjustment of radiation pulse height (Fig. 16a) and SDD change (Fig. 16b). The same parameters are used to plot the solid lines in Figs. 16a and 16b using Eq. 53, except that we have to renormalize the diode sensitivity S to $InstDR$ = 10000 cGy/s because of the lack of overlap between the dose rate for 8 MV and 18 MV photon beams. The data

measured with direct radiation pulse height adjustment (Fig. 16a) were renormalized to be 1 for *InstDR* = 0 after fitting Eq. (53).

4.5 Discussion

4.5.1 Unirradiated and Preirradiated N-Type

The SDD CF was between 1.001 – 1.005 for dose rates between 0.375 cGy/s to 2.5 cGy/s for unirradiated and pre-irradiated n-type under continuous radiation (Fig. 14). This result agrees with the empirical expression for diode dose rate dependence (Eqs. 52 and 53) as well as the theoretical prediction.[29]

The unirradiated Isorad Gold #1 diode showed small dose rate dependence (Fig. 15). However, a large variation of dose rate dependence was observed among individual Isorad Gold diodes (Cf. Isorad Gold #1 and #2 in Figs. 15 and 16). Pre-irradiation substantially increases the dose rate dependence of the Isorad Gold diodes, as has been shown by others.[35,38] Most published data showed larger dose rate dependence for Isorad Gold diode than Isorad Gold #1[35,38], with a similar magnitude as that of the Isorad Gold #2. This increased dose rate dependence is probably due to the accumulated dose given in clinic.

Clearly the Veridose Green, Isorad-3 Gold, and QED Red (n-type) diodes have substantially smaller dose rate dependence than other n-type diodes. These diodes are doped by platinum. Heavily platinum doped diodes have very small dose rate dependence due to very small minority-carrier lifetime (< 0.3 μs).[29]

Based on the equation 53, the parameters for the instantaneous dose rate dependence of the n-type diode (Fig. 16) was determined to be $\beta_1 = 2.1 \times 10^{-5}$ s/cGy and $\beta_2 = 3.9 \times 10^{-5}$ s/cGy for Isorad Gold #2 (n-type) using a non-linear global optimization algorithm (the differential evolution algorithm).[1] The solid lines in Fig. 16a are the fit using Eq. 53.

The dose rate dependence of the Isorad Gold (n-type) diode obtained from direct radiation pulse height adjustment agreed with that obtained from SDD change.

Similar fits were performed for the dose rate dependence of diodes in Fig. 15 using Eq. 52, with fitting parameters listed in Table 6. β_1 characterizes the rate of the *S* increase vs. dose rate of a diode detector, while β_2 characterizes the curvature of the dose rate dependence (or the rate S reaches its saturation value).

The saturation value of *S* is determined by β_1/β_2. To compare the magnitude of dose rate dependence between different diodes, β_1/β_2 should be used, i.e. larger β_1/β_2 means larger dose rate dependence. However, it is possible that β_1/β_2 value cannot be extrapolated correctly for some diodes because no saturation occurs in the dose rate range studied (i.e., $\beta_2 \cdot InstDR << 1$). In this case (e.g. for some p-type diodes), β_1 may be a better indicator, i.e., larger β_1 means larger dose rate dependence in the linear region where no saturation occurs. The "saturation" only applies to the empirical formula.

Table 6. Fitting parameters for the commercial diodes.
Using Eqs. (52) (and (53)) for results shown in Figs. 15 (and 16). (Fits to diodes marked by * are plotted in Fig. 16).

Diode Symbol	β_1 (s/cGy)	β_2 (s/cGy)	β_1/β_2	Dose Rate Range (cGy/s)
Isorad Gold (n-type) #1	2.5×10^{-5}	2.4×10^{-4}	0.10	1488-38903
Isorad Gold (n-type) #2 *	2.1×10^{-5}	3.9×10^{-5}	0.54	3987-34856
Isorad Red (n-type)	6.1×10^{-5}	1.6×10^{-4}	0.38	1488-38903
Isorad-3 Gold (n-type, Pt-doped)	9.6×10^{-6}	1.9×10^{-4}	0.05	1486-38986
Isorad-p Red (p-type)	2.1×10^{-5}	5.4×10^{-5}	0.39	1452-21872
Veridose Green (n-type)	8.2×10^{-6}	7.6×10^{-5}	0.11	1450-21868
QED Red (n-type, Pt-doped)	5.8×10^{-5}	3.8×10^{-4}	0.15	1457-39059
QED Blue (p-type)	8.3×10^{-6}	2.9×10^{-5}	0.29	1537-17874
QED Red (p-type)	4.7×10^{-6}	1.1×10^{-5}	0.43	1537-17874
Scanditronix EDP10^{3G} (p-type)	2.3×10^{-6}	3.2×10^{-5}	0.07	1492-38883
Scanditronix EDP 20^{3G} (p-type)	1.0×10^{-6}	2.5×10^{-4}	0.004	1452-21872
Scanditronix EDP 30 (p-type) *	6.0×10^{-7}	1.0×10^{-6} †	0.60 †	3987-34856

† These values are not reliable since the dose rate dependence was virtually linear ($\beta_2 = 0$) in the dose rate range studied.

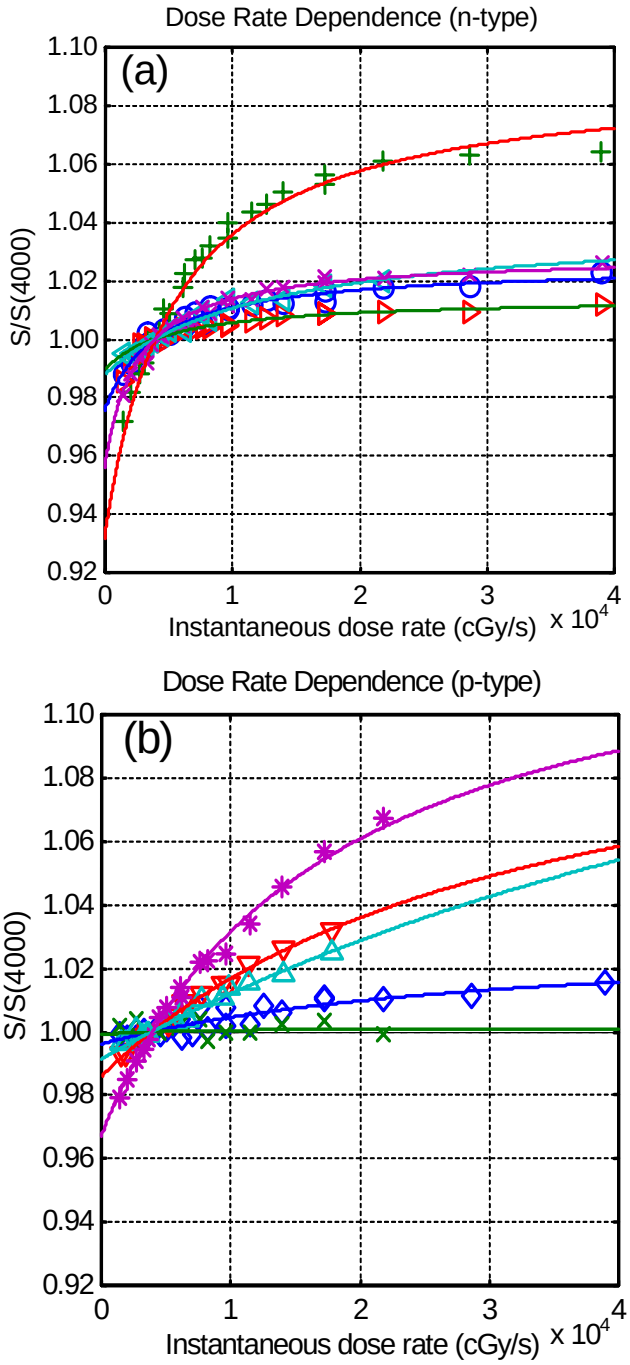

Figure 15. Dose rate dependence of the diode detectors under pulsed radiation.
(a) n-type and (b) p-type. n-type diodes: o-Isorad Gold#1 (6 and 18 MV), + - Isorad Red (n-type) (6 and 18 MV), ▷ - Isorad-3 Gold (6 and 18 MV), ◁ - Veridose Green (6 and 18 MV), and x - QED Red (n-type) (6 and 18 MV). p-type diodes: ◊ - EDP10^{3G} (6 and 18 MV), x- EDP20^{3G} (6 and 18 MV), * - Isorad-p Red (6 and 18 MV), Δ - QED Red (p-type) (6 and 15 MV), and ∇- QED Blue (6 and 15 MV). Solid lines are fit using Eq. (52) and parameters in Table 6. This figure was generated by combining the dose rate dependence from 6 MV and 15 or 18 MV pulsed beams.

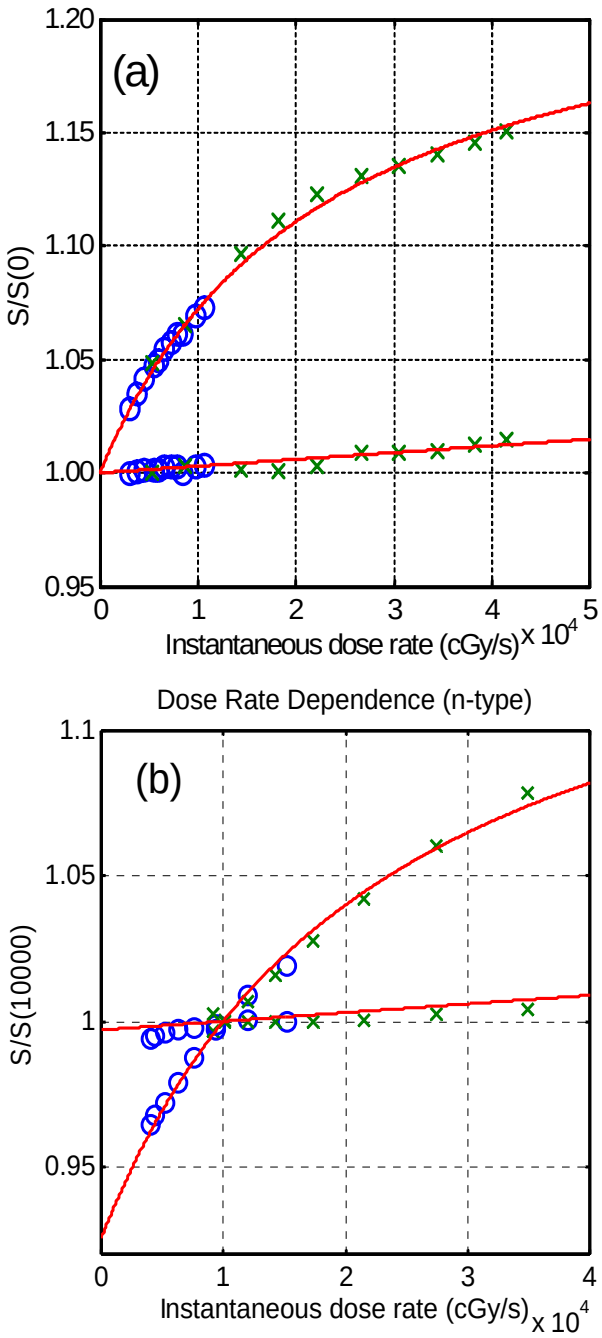

Figure 16. Dose rate dependence of an n-type and a p-type diode detectors.
Measured by (a) adjusting the radiation pulse height directly at a fixed SDD and field size (SDD = 67.5 cm, 25 × 25 cm^2, d = 3.5 cm) and (b) SDD measurement under otherwise the same conditions. From top to bottom, the curves are for Isorad Gold #2 (n-type) and EDP30, p-type. The symbols are for different photon energies: o – 8 MV, x – 18 MV. Solid lines are fits using Eq. (53) (Fig. 16a) and Eq. (52) (Fig. 16b) with the same parameters in Table 6 (see text for details).

4.5.2 Unirradiated and Preirradiated P-Type

Unirradiated p-type diodes were not studied in this study. Rikner and Grusell have compared dose rate dependence of unirradiated and pre-irradiated p-type diodes.[5] They showed variation in relative sensitivity of the p-type unirradiated diode to be about 5% when the dose per pulse was varied between 0.04 mGy and 0.43 mGy.[5] The variation of relative sensitivity was less than 1% for the p-type pre-irradiated diode under the same conditions. Thus, sufficient pre-irradiation reduced the dose rate dependence for the p-type diode. Another publication[30] shows that the dose rate dependence of the p-type diode could increase with accumulated dose substantially, although this is usually for photon energies higher than 10 MV and this points to mechanisms other than the photon and electron radiation. Another publication[22] showed increased dose rate dependence caused by a high level of accumulated dose (~ 25 kGy) with high energy electrons, although those results applied to an earlier version of Scanditronix diodes with higher resistivity (10 Ω-cm) than the resistivity (0.2 Ω-cm) of Scandtironix diodes studied here.

The dose rate dependence of the p-type pre-irradiated QED diodes and the Isorad-p Red diode was larger than that of the p-type pre-irradiated Scanditronix diodes. The p-type pre-irradiated Isorad-p Red diode showed similar dose rate dependence as some of the n-type diodes (e.g. Isorad Red (n-type)). The dose rate dependence of the pre-irradiated p-type QED diodes was larger than some of the n-type diodes (e.g., QED Red (n-type), Isorad-3 Gold, and Veridose Green).

The instantaneous dose rate dependence for p-type EDP30 (Fig. 16) was fitted to Eq. (52) to obtain $\beta_1 = 6.0 \times 10^{-7}$ and $\beta_2 = 1.0 \times 10^{-6}$. Clearly, the dose rate dependence for the p-type diode (EDP-30) is much less than the n-type diode (Isorad Gold #2) since β_1 for p-type diode is much smaller than that for the n-type diode. Since the same fitting agrees with measurements obtained from SDD measurements made on the same accelerator, we have proven that the SDD dependence of the diode detectors is caused mostly by the dose rate dependence. Its behavior can be described by the empirical formula (Eq. (53)).

We have fitted the dose rate dependence of the diode's relative sensitivity (S/S(4000)) by Eq. 52 for all commercial diodes studied. The parameters of the fit are listed in Table 6. The dose rate dependence presented cannot be generally applied to diodes placed at the surface of a phantom, where other effects such as electron contamination and difference between diode and ionization chamber depth of measurement may change the dose rate response.

4.5.3 Comparison with Literature

All published SSD CF was measured with diodes placed at the surface rather than placed at a depth in a miniphantom (our study). To facilitate the comparison, we compared SDD CF and SSD CF measured with the two methods (Fig. 17). In general, overall variation of SDD CF measured with our method is smaller than the SSD CF measured with the conventional method (at surface). However, they agree with each other to within 1% for 6 MV and up to 3% for 18 MV depending on the inherent diode buildup thickness.

There are two possible reasons for the observed difference between the two methods: (1) Using the conventional method, the depth of the ionization chamber placement was different from the depth of the diode placement in a full scatter phantom. If the depth of maximum dose was different from the depth of the inherent buildup of the diode detector (Table 4a), then the actual dose delivered to the diode could be different from the dose measured by the ionization chamber. This difference in scatter conditions may introduce up to 1% error. This is the cause of the difference between SDD CF and SSD CF observed for 6 MV photons and some of the 18 MV photons, provided the inherent diode buildup is thick enough to eliminate electron contamination. (2) Electron contamination and electron disequilibrium increases the variation of SSD CF for surface in-vivo dosimetry if the inherent diode buildup is thinner than the depth of maximum dose.[31,52]

The diode reading measured for the surface placement is lower than the diode reading at dmax because the actual dose received by the diode is less than that assigned to it

(measured by the ionization chamber at dmax). Due to the additional contribution of electron contamination, the variation of SSD CF for the surface placement is larger than SDD CF measured in the miniphantom. This was confirmed in our comparison. For diodes with inherent buildup thickness not suitable for the 18 MV photon energy (EDP10^{3G} and Isorad-3 Gold), the variation of SSD CF measured on the surface was substantially larger (>2%) than that measured in miniphantom (Fig. 17b).

Rikner and Grusell have reported sensitivity ratio to be between 1.02 to 1.0 for EDP30 diode for 6 MV when the SDD was varied between 80 to 135 cm.[53] For 16 MV beams, the sensitivity ratio for the EDP30 diode varied 1.02 to 0.98.[31] Gerog *et. al.* has reported that the sensitivity ratio for the EDP20^{3G} diode varied between 1.03 and 0.985 when the distance was varied between 80 and 120 cm under 18 MV beam.[31] Our measurements for EDP30, EDP10^{3G}, and EDP20^{3G} showed smaller dose rate dependence, with a maximum variation of 0.995 and 1.006 for all photon energies studied. This is most likely because we have used sufficient buildup (5 cm water equivalent) to eliminate the additional SDD dependence caused by electron contamination.

Nuclear Associates have reported the SSD CF of the Veridose Green diode varies between 1.000 and 1.015 when the SDD is changed between 100-150 cm (Nuclear Associates operation and instruction manual, 1997). In comparison, our measurements showed a variation between 1.000 and 1.011 over the same SDD change.

The unirradiated n-type Isorad Gold SSD CF varied between 0.960 – 1.020 for 6 MV and pre-irradiated Isorad Red (n-type) SSD CF varied between and 0.940 – 1.02 for 18 MV when the SDD was changed between 70 and 130 cm.[38] This is in agreement with our measurement for Isorad Gold #2 and Isorad Red (n-type). However, most unirradiated Isorad Gold diodes had much smaller dose rate dependence, similar to our measurement for Isorad Gold #1. The SDD CF for unirradiated n-type Isorad Gold #1 diode varied between 0.991 – 1.004 for 6 MV and 0.994 – 1.002 for 18 MV for SDD change of 70 to 130 cm. This smaller dose rate dependence is also observed elsewhere.[35] This variation

can be caused by variation among individual Isorad (n-type) diodes (Gold #1 and Gold #2). In addition, the dose rate and the accumulated dose to the diodes used in the publications were unknown, which could affect the dose rate dependence. The dose rate dependence of the Isorad (n-type) diodes increases with accumulated doses given in the clinic.[35]

The QED Red (p-type) diode SSD CF varied between 0.980 – 1.02 for 18 MV over the SDD range of 80-130 cm.[38] Another publication showed that the SSD CF for p-type QED Blue varied between 0.983-1.009 for 4 MV and QED Red (p-type) varied between 0.973-1.035 for 18 MV pulsed beams when the SDD was changed from 80 to 130 cm.[8] Our measurements showed smaller variations than the published results. The pre-irradiated p-type QED Blue diode SDD CF varied between 0.994 – 1.010 (for 6 MV) and 0.989 – 1.012 (for 15 MV) for the SDD range of 80-130 cm where as SDD CF for QED Red (p-type) varied between 0.993 – 1.008 (for 6 MV) and 0.990 – 1.011 (for 15 MV) for the same SDD range.

The SSD CF for the Isorad-p Red were between 0.970-1.02 for 18 MV under the SDD change of 80-130-cm.[38] The Isorad-p Red diode SSD CF varied between 0.998 – 1.003 for 6 MV and 0.970 – 1.029 for the SDD range of 80-130 cm.[53] In comparison, our measurement showed the pre-irradiated p-type SDD CF Isorad-p Red varied between 0.989 – 1.017 for 6 MV and 0.981 – 1.022 for 18 MV, respectively, for the SDD range of 80-130 cm.

All published studies were performed by placing the diodes on the surface of a solid phantom (corresponding to the depth of maximum dose), while our study was performed at a depth of 5-cm, well beyond range of electron contamination. In general, the Isorad Red (or some Gold) n-type diodes have the largest dose rate dependence while the Scanditronix p-type diodes showed the smallest dose rate dependence. Generally, our SDD CF were somewhat smaller for Scanditronix EDP diodes, Sun Nuclear pre-irradiated p-type QED and Isorad-p diodes, than the SSD CF measured at surface for high

energy beams, which could include the additional effect of electron contamination. In addition, the difference could also be caused by dose rate dependence variations among individual diodes of the same type from the same manufacturer, especially from different batches.

4.5.4 Comparison Between N-Type and P-Type Diodes

The value of $\zeta = \tau_n / \tau_p$ depends on the characteristics of the dominant R-G centers in the diode and is appreciably larger than 1 in silicon[24,29] for the dominant R-G centers generated by electron radiation or platinum doping. This is the reason to favor p-type over n-type diodes, as can be clearly demonstrated from Eq. (48) assuming $n_0 = p_0$ and other device parameters are the same.[7,29] n_0 and p_0 are inversely proportional to the resistivity of the diode substrate.

In most instances, we have seen larger dose rate dependence for n-type diodes than the p-type diodes for pulsed radiation. However, this is not generally true, as the pre-irradiated p-type diodes do not necessarily show less dose rate dependence than the unirradiated and pre-irradiated n-type diodes. In this study, we showed that pre-irradiated Isorad-p Red diode showed similar or larger dose rate dependence than the unirradiated n-type and pre-irradiated n-type diodes. The n-type pre-irradiated Veridose Green, unirradiated Isorad-3 Gold, and unirradiated QED Red (n-type) diodes did show less dose rate dependence than the unirradiated and pre-irradiated n-type Isorad, pre-irradiated p-type QED, and Isorad-p Red diodes. The p-type pre-irradiated Scanditronix EDP diodes showed the smallest dose rate dependence.

It is noticed that the measured SDD dependence of most diodes for low and high energies from a dual-energy accelerator is almost the same despite the fact that in our measurements the instantaneous dose rate for the high energy beam is about twice as high as the low energy beam. This can be explained by the following reason: the relative change in instantaneous dose rate is the same regardless of energy, since it comes solely

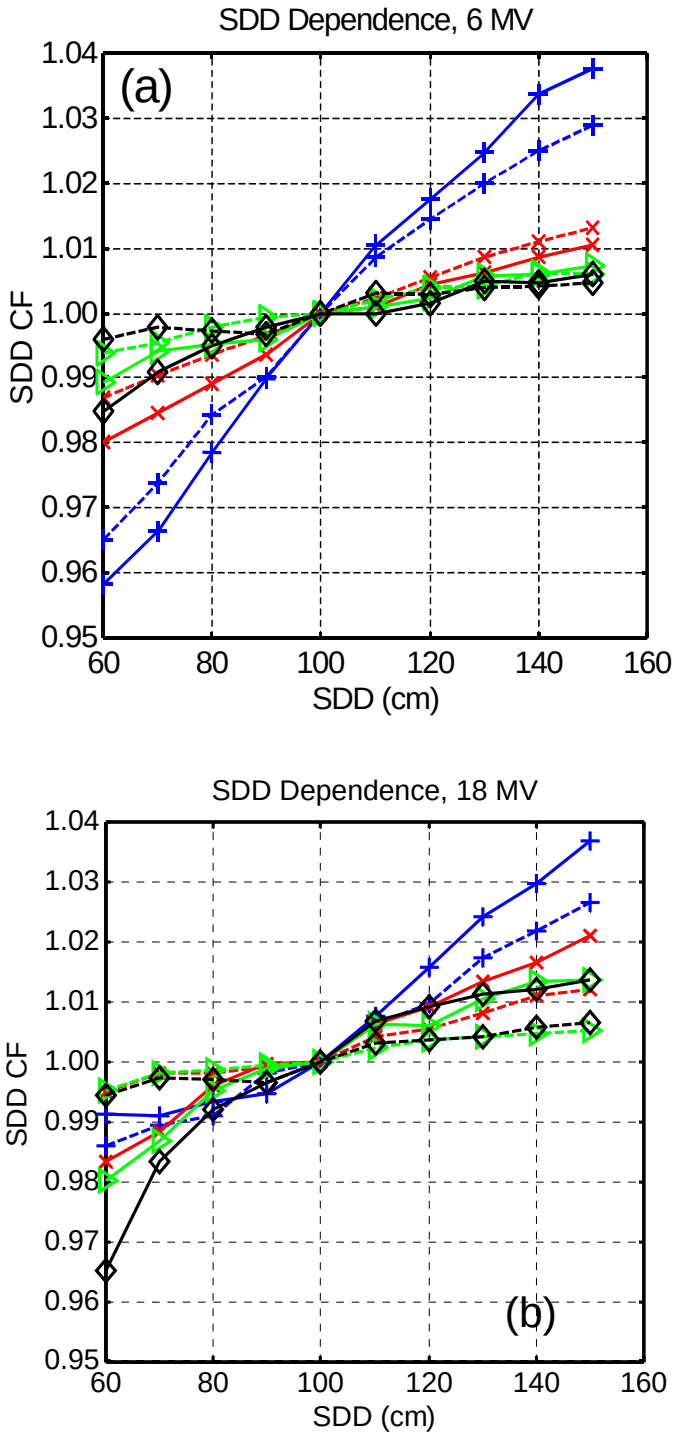

Figure 17. Comparison of SDD CF at the surface and in miniphantom.
The data was measured with diode placed at surface in a full scatter phantom and diode placed at 5-cm depth in a miniphantom. (a) 6 MV and (b) 18 MV. Symbols with solid line are for surface measurements and symbols with dashed line are for miniphantom measurement: + - Isorad Red (n-type), ▷ - Isorad-3 Gold, ◊ - EDP10^{3G}, and x - QED Red (n-type).

from the inverse square law, although the absolute range is smaller for the lower energy than for the higher energy (scaled by the instantaneous dose rate at 100 cm). As a result, the relative change of the diode sensitivity due to the dose rate should be the same for both energies, if the dose rate dependence is linear or whenever the dose rate dependence of *S* is sufficiently small. The dose rate dependence of the diode sensitivity is no longer a linear function of dose rate for diodes with large dose rate dependence (Figs. 15 and 16). As predicted by the empirical model (Eq. 53), the slope of the dose rate dependence of *S* (*dS/dInstDR)* decreases with increasing dose rate. Under this condition, the overall variation of SDD CF for low energy will be larger than the overall variation of SDD CF for high energy for the same range of SDD from a dual energy accelerator.

4.6 Conclusion

The instantaneous dose rate dependence was measured for commercially available diode detectors used in in-vivo dosimetry. The ratio of diode sensitivity, normalized to SDD=100 cm, increased with increasing dose rate (or decreasing distance). The Isorad Red (n-type) and some Isorad Gold (n-type) generally showed the largest SDD and dose rate dependence. However, one of the unirradiated n-type Isorad Gold diodes showed small dose rate dependence. The Scanditronix EDP p-type diodes showed the smallest SDD and dose rate dependence. N-type diodes with platinum doping (e.g., Isorad-3 Gold, QED Red (n-type), and Veridose Green) show less SDD and dose rate dependence than the n-type Isorad and some p-type diodes (Isorad-p Red and QED (p-type)). Thus, p-type diodes are not necessarily better than all the n-type diodes. The dose rate dependence could be quite different for the same type of diode package due to different die used inside, such as for Isorad, Isorad-p, Isorad-3, QED Red (n-type), and QED p-type diodes. Under Co-60 beam radiation, all diodes showed almost no SDD and dose rate dependence. We have proposed an empirical formula to fit the dose rate dependence for all commercially available diodes.

CHAPTER 5 PAPER III: ENERGY DEPENDENCE OF COMMERCIALLY AVAILABLE DIODE DETECTORS FOR IN-VIVO DOSIMETRY

The diode detector used for radiation diode dosimetry is designed for specified energy range. Different high Z buildup materials are placed around the diode detectors, so that the dose is measured is close to the depth of maximum dose. Significant energy dependence is observed when the inherent buildup is too thick. Energy dependence of different commercially available diode detectors was measured for energies ranging between Co-60 and 20 MV pulsed radiation. Monte Carlo simulation and cavity theory is used to predict the energy dependence in consistent with the measurements. We concluded the observed energy dependence was caused mainly by the high Z buildup material around the diode detectors.

Medical Physics, 34 (5):1704-11 (2007).

5.1 Synopsis

The energy dependence of commercially available diode detectors was measured for nominal accelerating potential ranging between Co-60 and 17 MV. The measurements were performed in a liquid water phantom at 5-cm depth for 10 × 10-cm^2 collimator setting and source–to-detector distance (SDD) of 100 cm. The response (nC/Gy) was normalized to Co-60 beam after corrections for the dose rate and temperature dependences for each diode. The energy dependence, calculated by taking the percent difference between the maximum and minimum sensitivity, normalized to Co-60 beam, varied by 39% for the n-type Isorad Red, 26% for n-type Isorad Electron, 19% for the QED Red (p-type), 15% for QED Electron (p-type), 11% for the QED Blue (p-type), and 6% for the EDP10 diode for nominal accelerating potential between Co-60 and 17 MV.

It varied by 34% for Isorad-3 Gold #1 and #2, 35%for Veridose Green, 15% for Veridose Yellow, 9% for Veridose Electron, 21% for n-type QED Gold, 24% for n-type QED Red, 3% for EDP2[3G], 2% for PFD (Photon Field Detector), 7% for EDP10[3G], and 16% for EDP20[3G] for nominal accelerating potential between Co-60 and 15 MV. The magnitude of the energy dependence is verified by Monte Carlo simulation. We concluded that the energy dependence does not depend on whether the diode is n- or p- type but rather depends mainly on the material around the die such as the buildup and the geometry of the buildup material. As a result, the value of the energy dependence can vary for each individual diode depending on the actual geometry and should be used with caution.

5.2 Introduction

Semiconductor detectors are widely used for patient dosimetry for photon and electron beams. They have high sensitivity (~18000 times more sensitive) and high spatial resolution compared to the air filled ionization chamber with the same volume.[5,7,15] The diode sensitivity is defined as the ionization charge collected per unit absorbed dose (usually in units of nC/cGy). The sensitivity of semiconductor detectors depends on temperature[23,24], dose rate[22,26-28], and energy.[6,7] In clinical applications, the diode is calibrated for the each energy separately before it is used for the measurements.

The diode's energy dependence is mainly due to the material around the die, such as electrode attachment, protective housing, and the buildup, which usually contains high Z material. These high Z materials in close proximity to the die (the silicon chip) alter the dose (or ionization) in the die in amounts that depend on the construction of the diode geometry. The buildup material is chosen so that the effective depth of the diode for in-viv*o* dosimetry is close to the depth of the maximum dose of the megavoltage photon beams, which affects its energy response to the radiation.[15]

For clinical use, it is recommended that a diode be used for energy range it is designed for. It is possible to use a photon diode designed for higher photon energy for in-vivo

dosimetry of lower photon energies as long as the diode is not used in the buildup region for the photon energy. However, significant energy dependence is observed when the buildup of the diode is too thick.[15]

In this paper, the energy dependence of different commercially available diode detectors was measured for energies ranging between Co-60 and high energy pulsed radiation, generated by medical linear accelerators. Monte Carlo simulations were performed to confirm that the observed energy dependence is caused mainly by the high Z buildup material around the commercial diode detectors.

5.3 Material and Methods

5.3.1 Description of Diodes

Seventeen n- and p-type detectors were used in this study: Six n-type and three p-type diodes were from Sun Nuclear Corporation (Sun Nuclear Corporation, 425 A Pineda Ct., Melbourne, FL 32940), five p-type diodes were from Scanditronix (Scanditronix AB, Husbyborg, S-752-29, Uppsala, Sweden), and three n-type diode from Nuclear Associates (Fluke Biomedical, 6045 Cochran Rd, Cleveland, OH 44139). A wide range of diodes with different buildup material was covered.

The Isorad diodes (Isorad Red, Isorad Electron, and Isorad 3 Gold #1, and Isorad 3 Gold #2) from Sun Nuclear have cylindrical designs with the die plane mounted normal to the detector axis.[24] Isorad 3 Gold #1 and Isorad 3 Gold #2 n-type diodes were the same type of diodes. All other diodes (Veridose, QED, and Scanditronix EDP, EDP^{3G}, and PFD) use a flat design, with radiation incident normal to the plane of the die. The PFD (Photon Field Detector) is a scanning Scanditronix diode with no buildup material. The diodes were all new without any prior clinical irradiation. Detailed schematics of some of the diodes used in this study can be found elsewhere.[24] The diodes with different thicknesses

and materials of inherent buildup are used to evaluate the energy dependence. The physical package details are listed in Table 7.

Several new n-type diodes (Veridose, QED (n-type), and Isorad-3) are Pt-doped. The Scanditronix EDP2^{3G}, EDP10^{3G}, and EDP20^{3G} are new p-type diodes. The diodes from the same manufacturer use the same die with different buildup thicknesses appropriate for their photon energies.

Table 7. Package specification of the different diode detectors.

Diode Type	Type	Shape	Buildup Material, Total buildup thickness (g/cm^2)	Energy Range	Manufacturing Period
Nuclear Associates Veridose Yellow	n	Flat	1.2 mm Copper, 1.359	5-11 MV	1998-
Nuclear Associates Veridose Green	n	Flat	1.7 mm Tungsten, 3.574	18-25 MV	1998-
Nuclear Associates Veridose Electron	n	Flat	0.89 mm Polystyrene, 0.284	Electrons	1998-
Scanditronix EDP 2^{3G}	p	Flat	Epoxy (0.5mm), 0.2	Electrons	2001 -
Scanditronix EDP 10^{3G}	p	Flat	0.75 mm Stainless Steel + epoxy, 1	4-8 MV	2001 -
Scanditronix EDP 20^{3G}	p	Flat	2.2 mm Stainless Steel + epoxy, 2	10-20 MV	2001 -
Scanditronix PFD	p	Flat	Epoxy (0.5mm), 0.2	Photon Scanning	2001-
Scanditronix EDP10	p	Flat	0.75 mm stainless cap + epoxy, 1	6–12 MV	1990-2001
Sun Nuclear Isorad Red (n-type)	n	Cylinder	1.1 mm Tungsten, 2.75	15–25 MV	1993 - 1998
Sun Nuclear Isorad Electron	n	Cylinder	0.25 mm PMMA, 0.03	Electrons	1993 - 1998
Sun Nuclear Isorad-3 Gold #1	n	Cylinder	1.13 mm Molybdenum, 1.6	6-12 MV	2003 -
Sun Nuclear Isorad-3 Gold #2	n	Cylinder	1.13 mm Molybdenum, 1.6	6-12 MV	2003 -
Sun Nuclear QED Gold (n-type)	n	Flat	2.07 mm Brass, 1.85	6-12 MV	2003 -
Sun Nuclear QED Red (n-type)	n	Flat	3.4 mm Brass, 3.04	15-25 MV	2003 -
Sun Nuclear QED Blue (p-type)	p	Flat	3.4 mm Aluminum, 1.03	1–4 MV	1997 - 2002
Sun Nuclear QED Red (p-type)	p	Flat	3.4 mm Brass, 3.04	15–25 MV	1997 - 2002
Sun Nuclear QED Electron (p-type)	p	Flat	0.25 mm PMMA, 0.03	Electrons	1997 - 2002

5.3.2 Experimental Setup

The diode energy dependence was measured for the diodes using SDD (source-to-detector distance) setup (SDD=100 cm) for the pulsed and Co-60 radiation. All the measurements were taken by using the 10 x 10 cm^2 collimator setting. The diode was placed at 5-cm depth in a full scatter liquid water phantom. A thin rubber protective sleeve was used to prevent water from reaching the diode. One hundred monitor units or one-minute time exposures were given for pulsed or Co-60 radiation respectively. Charges from all diodes were measured using an electrometer under zero-bias. Leakage was subtracted for all the measurements before analyzing the data. The magnitude of the leakage was ~1% for the Veridose diodes, less than 0.5% for the Isorad and QED diodes, and negligible for the Scanditronix diodes. The dose for the diodes used in Fig 19 was measured for linear accelerators calibrated using TG51[54] and that for the diodes used in Fig.20 was measured for linear accelerators calibrated using TG21[55]. Typical dose variation in the output of the beams was within 1%. The readings were also corrected for the temperature dependence using the measured temperature coefficients for the particular diode before the normalization. All the readings were corrected to temperature of 22ºC.[24] The maximum correction factor due to temperature is less than 1.03 since the temperature coefficient (Table 8) is less than 0.63% and the water temperature was in a range of 22 ± 5ºC. The sensitivity (nC/cGy) was calculated for each diode at each energy and was normalized to the Co-60 sensitivity. The sensitivity of the diode for a particular energy at depth of 5 cm and field size of 10×10 cm^2 was determined by:

$$S(E) = \frac{M_{diode}(nC)}{D_{water}(cGy)} \tag{54}$$

Where M_{diode} is the charge collected by the diode at depth of 5 cm and field size of 10×10 cm^2, corrected for temperature and leakage. D_{water} is the dose delivered at depth of 5 cm and field size of 10×10 cm^2. The calculated doses were corrected for the actual dose output of machine at the time of the measurements using the linear accelerator output constancy check.

Table 8. Summary of correction factors.

These correction factors are for the combination of radiation source characteristics (nominal potential, %PDD10, instantaneous dose rate) and commercial diodes. The diode dose rate correction factors[28] and temperature coefficients[24,56] are taken from our previous studies.[24,28,56]. The temperature coefficients for Veridose Green diode were taken from Nuclear Associates Operation and Instruction Manual. (For diodes not listed, the equivalent dose rate and temperature correction factors used are: EDP 2^{3G} = EDP20^{3G}; PFD=EDP20^{3G}; Veridose Yellow = Veridose Green; Veridose Electron= Veridose Green, QED Red (n-type) = QED Gold (n-type); Isorad Electron = Isorad Red (p-type); EDP30=EDP10; QED Electron (p-type) = QED Blue (p-type).)

Diode or Source Parameters					
			Figure 19*		
Radiation Sources	Theratron Co-60	Siemens Oncor 6 MV	Siemens Oncor 10 MV	Siemens KD 15 MV	Siemens Prim. 18MV
Nom. Acc. Poten. (MV)	1.25	4.90	8.90	13.2	15.0
PDD10 (%)	58.7	67.0	73.8	76.8	78.9
Inst. DR (cGy/s)**	1.23	7.00×10^3	1.21×10^4	1.52×10^4	1.39×10^4
			Diode Dose Rate Correction Factor		
Veridose Green	1.000	1.019	1.026	1.029	1.027
EDP 10^{3G}	1.000	1.007	1.010	1.012	1.011
EDP 20^{3G}	1.000	1.001	1.002	1.002	1.002
Isorad 3 Gold	1.000	1.014	1.018	1.019	1.018
QED Gold (n-type)	1.000	1.054	1.061	1.063	1.062
			Diode Temperature Coefficient (%/^{o}C)		
Veridose Green	0.50	0.50	0.50	0.50	0.50
EDP 10^{3G}	0.25	0.25	0.25	0.25	0.25
EDP 20^{3G}	0.25	0.25	0.25	0.25	0.25
Isorad 3 Gold	0.52	0.52	0.52	0.52	0.52
QED Gold (n-type)	0.63	0.63	0.63	0.63	0.63
			Figure 20*		
Radiation Sources	Theratron Co-60	Elekta SL20 6MV	Varian 2100CD 8 MV	Varian 2100CD 18MV	Elekta SL20 20MV
Nom. Acc. Poten. (MV)	1.25	4.80	6.25	16.0	17.0
PDD10 (%)	58.7	66.2	70.7	79.0	78.9
Inst. DR (cGy/s)**	1.90	4.48×10^3	7.58×10^3	1.74×10^4	9.79×10^3
			Diode Dose Rate Correction Factor		
EDP 10	1.000	1.010	1.016	1.034	1.021
QED Blue (p-type)	1.000	1.016	1.026	1.047	1.031
QED Red (p-type)	1.000	1.010	1.016	1.034	1.021
Isorad Red (n-type)	1.000	1.077	1.100	1.132	1.110
			Diode Temperature Coefficient (%/^{o}C)		
EDP 10	0.36	0.36	0.36	0.36	0.36
QED Blue (p-type)	0.30	0.30	0.30	0.30	0.30
QED Red (p-type)	0.30	0.30	0.30	0.30	0.30
Isorad Red (n-type)	0.37	0.20	0.20	0.20	0.20

* Reference to Figures 19 and 20 later in the paper.

** The instantaneous dose rate (cGy/s) is the peak dose rate of individual radiation pulses from a linear accelerator. This could be 1500 times larger than the average dose rate. For a Cobalt unit, average dose rate equals the instantaneous dose rate.[28]

For pulsed radiation, D_{water} is the dose at SDD=100 cm for the 10×10 cm^2 collimator setting at a depth of 5-cm in a water phantom. It can be calculated according to:

$$D_{water}\ (cGy) = MU\ (TMR\ (s = 10, d = 5)).IS\ , \qquad (55)$$

For continuous (Co-60) radiation, D_{water} is calculated according to:

$$D_{water}\ (cGy) = DR_{100}\, Time\ (\min)(\ TMR\ (s = 10, d = 5)) \qquad (56)$$

Here the collimator scatter factor and phantom scatter factor for a collimator setting of 10×10 cm^2, is unity, i.e., $S_c(10) = S_p(10)=1$. $TMR(10,5)$ is the tissue maximum ratio for a field size of 10×10 cm^2 at a depth of 5 cm in a phantom. DR_{100} is the average dose rate measured at the calibration condition (10×10 cm^2, $d = d_{max}$, SDD = 100 cm), which is usually expressed using units of MU/min. For pulsed radiation, the 1 MU=1cGy at the calibration condition (10×10 cm^2, $d = d_{max}$, SDD = 100 cm or source-to-surface distance, SSD=100 cm). For calibration conditions different than SDD=100 cm, additional inverse square factor (IS) was applied to calculate the dose at the desired point.

The normalized sensitivity is calculated by dividing the sensitivity of a particular energy by sensitivity of Co-60 beam, i.e., it is defined as:

$$S_{norm} = \frac{S(E)}{S(Co)} \qquad (57)$$

Where $S(E)$ is the diode sensitivity of the pulsed radiation and the $S(Co)$ is the diode sensitivity for the Co-60 beam. The normalized sensitivity was further corrected for the dose rate dependence of each diode using parameters determined from our previous paper by dividing by the dose rate correction factor.[28] The maximum correction due to instantaneous dose rate is less than 13%. Detailed information about the dose rate correction factors is listed in Table 8.

For pulsed radiation, Siemens Primus, Siemens KD, Siemens Oncor, Elekta SL20, and Varian 2100 CD were used. For Co-60 radiation the Theratronix 1000 was used. The normalized sensitivity was plotted against the nominal accelerating potential. Nominal accelerating potentials were determined by using the TG21 protocol.[55] PDD10 is also listed as it is used in TG51 to determine the photon beam quality.[54] Table 8 lists the parameters for the radiation sources used in this study.

5.3.3 Monte Carlo Simulation

Monte Carlo (MC) simulation is performed using DOSRZnrc user code that comes with EGSnrc v4.2.2.6.[47,48] Cylindrical geometry is used for all the simulations. No variance reduction techniques were used. PRESTA-II is enabled for all electron transport. The particles are transported with a cutoff energy of AP = ECUT = 10 keV for photons and AE = ECUT = 521 keV for the electrons. Photon and electron interaction cross section data (PEGS data set 521icru.dat) from ICRU 37 was used.[49]

Only diodes of flat design are simulated. The die is simulated as a 0.02 cm thick silicon cylinder of 0.05 cm diameter (Fig. 18). The center of the silicon diode is placed at 5 cm depth in a water phantom that has a radius of 50 cm. The build up is placed as a cylinder on top of the diode with thicknesses of 0.12 cm, 0.3 cm of Cu or 0.17 cm and 0.3 cm of Tungsten, respectively. It has a diameter of 1 cm. The back of the diode is composed of 0.2 cm thick PMMA and then 45 cm thick water. Mohan energy spectra (6, 10, 15, 24 MV) simulating the linear accelerators[57] and Co-60 energy spectrum that comes with EGSnrc were used. Each simulation uses parallel photon beams with 5 cm radius. The numbers of incident photons are 100, 60, 40, 30, 20 million for Co-60, 6, 10, 15, 24 MV photon spectrum, respectively. Since the purpose of the MC simulation is to qualitatively verify the experimental results, no great effort is made to match the exact diode geometry with any particular commercial diodes.

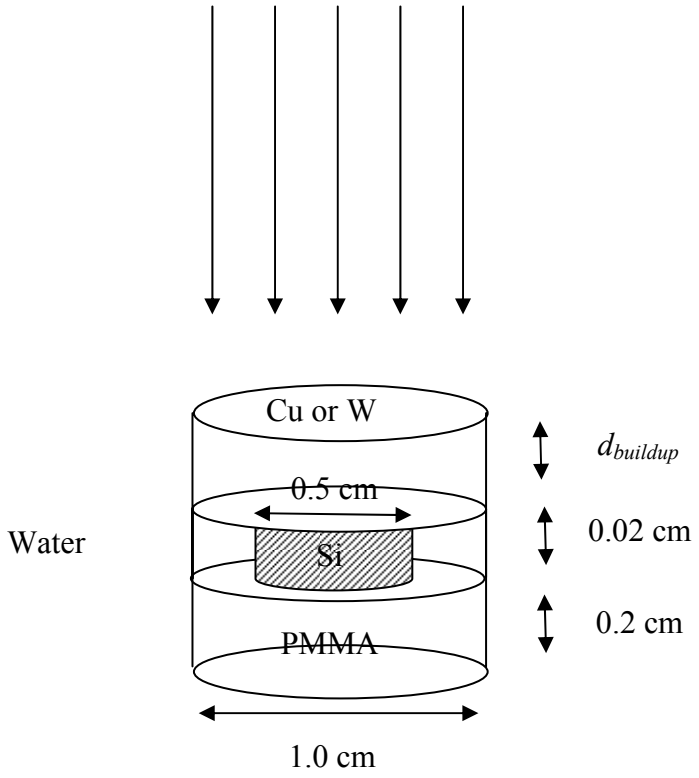

Figure 18. Schematics of the geometry of the diode detector for MC simulation.
The middle of the diode die (shaded cylinder, 0.02 cm thick and 0.5 cm diameter, Si) is placed at 5 cm depth in 50-cm radius water column, with additional 45 cm water behind the detector. The material in the back of the Si die is PMMA, 0.2 cm thick and 1 cm diameter. The thickness of the buildup material, $d_{buildup}$, used in MC simulation is listed in Table 10. Figure is not drawn to the scale.

The diode-to-water dose ratio, $D_{H_2O}^{diode}$, is defined as the ratio of dose scored in the silicon (with or without buildup materials) to that in water at the same location without the diode for the same incident photon energy fluence. Similarly, the normalized sensitivity of the diode is defined as the ratio of $D_{H_2O}^{diode}$ for the particular photon energy to that measured for Co-60, the same as that based on Eq. 57.

The diode-to-water dose ratio can be analytically expressed as:[1]

$$D_{H_2O}^{diode} = (\frac{\overline{S}_{col}}{\rho})_{buildup}^{Si} \cdot (\frac{\overline{\mu}_{en}}{\rho})_{water}^{buildup} \cdot A(d_{buildup}) \cdot P \,. \qquad (58)$$

Where $(\frac{\overline{S}_{col}}{\rho})^{Si}_{buildup}$ is the collision stopping power ratio between silicon and buildup according to the Bragg-Gray cavity theory,[1,50] $(\frac{\overline{\mu}_{en}}{\rho})^{buildup}_{water}$ is the mass energy coefficient ratio between the buildup material and water, and $A(d_{buildup})$ is the attenuation factor due to the buildup material with thickness $d_{buildup}$. We have ignored the attenuation of the secondary electron fluence in the Si die since it is very thin, 0.2 mm. $P = 1$ in Equation 58, if one assumes that the buildup material is sufficiently thick that electron equilibrium is established and the perturbation of the secondary electron fluence is ignored. Otherwise, we introduce an additional correction factor, P, to account for the disturbance to the primary dose by the buildup structures and that is not accounted for in the Bragg-Gray cavity theory. For Si diode without buildup, $(\frac{\overline{S}_{col}}{\rho})^{Si}_{water}$ is used because the buildup is replaced by water. To compare the results between analytical theory and Monte Carlo simulation, we have calculated the total stopping power ratio, the mass energy coefficient ratio, and the attenuation function for the buildup material using the ICRU 37 data. The stopping power ratios for silicon to buildup of different photon energies were calculated for monoenergetic electron energy equal to (1/3) of the nominal accelerating potential of the corresponding photon spectrum. The mass energy coefficient ratios between buildup material and water for a particular photon energy spectrum were calculated using:

$$(\frac{\overline{\mu}_{en}}{\rho})^{buildup}_{water} = \int (\frac{\overline{\mu}_{en}(E)}{\rho})^{buildup}_{water} \psi(E)dE / \int \Psi(E)dE , \tag{59}$$

and the attenuation function, A is calculated using:

$$A = \int e^{-\mu(E)\cdot d_{buildup}} \psi(E)dE / \int \Psi(E)dE , \tag{60}$$

Where ψ(E) is the photon energy spectrum. Since the diode sensitivity *S* is proportional to $D_{H_2O}^{diode}$, the normalized sensitivity can be determined from the calculated diode-to-water dose ratio as:

$$S_{norm} = \frac{D_{H_2O}^{diode}(E)}{D_{H_2O}^{diode}(Co)}. \quad (61)$$

5.4 Results and Discussion

The energy dependence was measured for commercial n and p-type diodes for energies between Co-60 and pulsed radiation. The normalized sensitivities for each diode were plotted against nominal accelerating potential. The data are summarized in Table 9.

The energy dependence was calculated by taking the percent difference, (max-min)/min*100, between the maximum and minimum normalized sensitivity. It varied by 34% for Isorad-3 Gold #1 and #2, 35% for Veridose Green, 15% for Veridose Yellow, 9% for Veridose Electron, 21% for n-type QED Gold, 24% for n-type QED Red, 3% for EDP2^{3G}, 2% for PFD (Photon Field Detector), 7% for EDP10^{3G}, and 16% for EDP20^{3G} for nominal accelerating potential between Co-60 and 15 MV (Fig. 19). Note the exact value of the percentage variation of the energy dependence should only be used as a reference.

It varied by 39% for the n-type Isorad Red, 26% for Isorad Electron, 19% for the QED Red (p-type), 15% for QED Electron (p-type), 11% for the QED Blue (p-type), and 6% for the EDP10 diode for nominal accelerating potential between Co-60 to 17 MV (Fig. 20). Note that we used different linear accelerators (and photon energies) to measure the energy dependence of the diodes plotted in Figures 19 and 20.

Table 9. Measured diode normalized sensitivity vs. nominal accelerating energy.
(Note dose rate and temperature dependences are corrected in the table).

Radiation Sources	Theratron Co-60	Siemens Oncor 6 MV	Siemens Oncor 10 MV	Siemens KD 15 MV	Siemens Prim. 18MV
Nom. Acc. Poten. (MV)	1.25	4.90	8.90	13.2	15.0
			Figure 19*		
EDP10[3G]	1.000	0.936	0.944	0.966	0.999
EDP20[3G]	1.000	0.949	0.999	1.044	1.100
EDP2[3G]	1.000	0.988	0.978	0.976	1.008
PFD	1.000	1.017	1.003	0.994	1.013
Veridose Yellow	1.000	1.023	1.070	1.070	1.147
Veridose Green	1.000	1.028	1.167	1.229	1.346
Veridose Electron	1.000	1.024	1.060	1.022	1.092
Isorad 3 Gold 1	1.000	1.045	1.151	1.259	1.338
Isorad 3 Gold 2	1.000	1.051	1.165	1.258	1.339
QED Gold (n-type)	1.000	0.969	1.028	1.107	1.176
QED Red (n-type)	1.000	0.905	0.962	1.042	1.120
Radiation Sources	Theratron Co-60	Elekta SL20 6MV	Varian 2100CD 8 MV	Varian 2100CD 18MV	Elekta SL20 20MV
Nom. Acc. Poten. (MV)	1.25	4.80	6.25	16.0	17.0
			Figure 20*		
Isorad Electron (n-type)	1.000	0.899	0.861	0.792	0.816
Isorad Red (n-type)	1.000	1.012	1.039	1.299	1.391
EDP10	1.000	0.944	0.943	0.963	0.991
QED Blue (p-type)	1.000	0.949	0.921	0.898	0.919
QED Red (p-type)	1.000	0.965	0.967	1.095	1.151
QED Electron (p-type)	1.000	0.945	0.918	0.866	0.876

* Reference to Figures 19 and 20 later in the paper.

Monte Carlo simulation shows that the diode energy dependence (S_{norm}) increases with increasing buildup thickness for the same high Z material (Fig. 21a and Table 10). The general trend is qualitatively consistent with the analytical calculation (Table 10). Although the energy dependence determined from MC simulation is generally smaller than that predicted by analytical calculation, indicating that there is significant additional correction due to perturbation of secondary electrons, i.e., $P < 1$ in Eq. 58. This effect is expected to be more pronounced when the heterogeneous structure becomes more complicated, e.g., for Isorad diodes. All Scanditronix diodes have less energy dependence than other diode types, probably due to thinner buildup thickness.

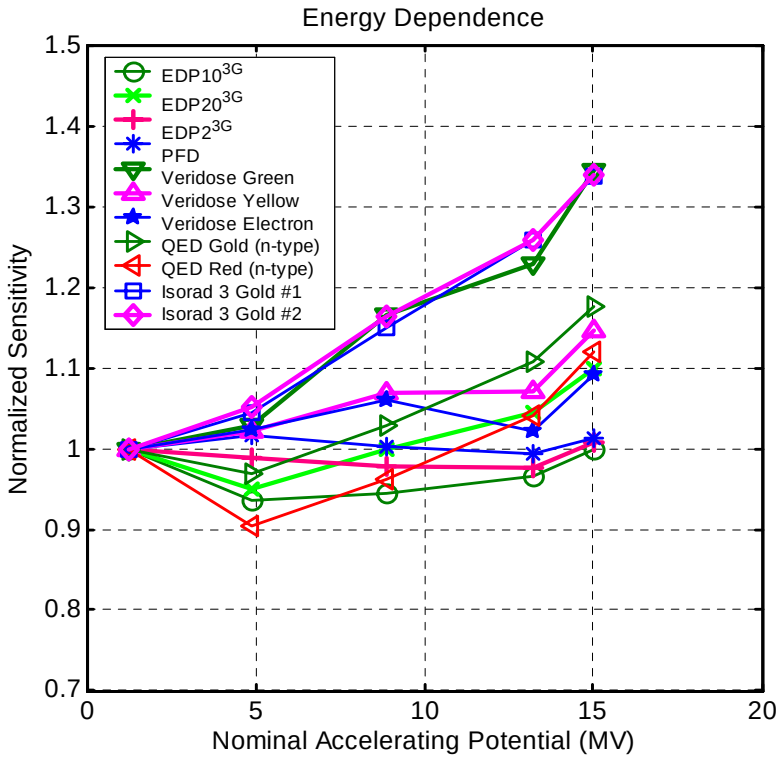

Figure 19. Energy dependence for different (new) diodes.
o- EDP10^{3G}, x- EDP20^{3G}, +-EDP2^{3G}, * - PFD, ∇ - Veridose Green, Δ - Veridose Yellow, ∗ - Veridose Electron, ▷ - QED Gold (n-type), ◁ - QED Red (n-type), - Isorad 3 Gold #2, and ◊ - Isorad 3 Gold #2.

The MC geometry for the buildup of 0.12 cm Cu and 0.17 cm W has similar buildup thickness and material as that of Veridose Yellow and Veridose Green diodes, respectively. The MC results show a normalized sensitivity of 1.22 ± 0.06 and 1.35 ± 0.06 for 0.12 cm Cu and 0.17 cm W at 15 MV (Table 10), while the measured normalized sensitivity was 1.15 and 1.35, respectively, at 15 MV (Fig. 19). The MC calculation agrees with measurement within the uncertainty of MC calculation. Due to limitation of computer resources, the uncertainty of the current MC simulations has an uncertainty of up to 6%, while the experimental measurement has an uncertainty of 1%. There are also some uncertainty caused by the difference in actual beam quality (for the same nominal accelerating potential) and actual diode configuration between the MC simulation and the measurements.

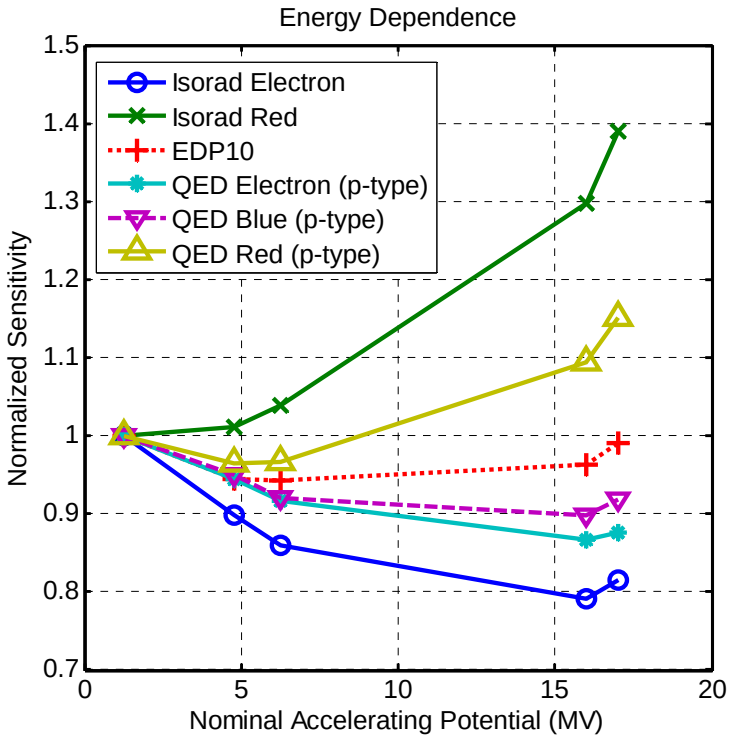

Figure 20. Energy dependence for different (old) diodes.
o- Isorad Electron, x- Isorad Red, +-EDP10 , * - QED Electron (p-type), ∇ - QED Blue (p-type) , Δ -QED Red (p-type).

The energy dependence for the Si die was expected to be less than 10%. This is shown experimentally for the energy dependence of PFD diode (Fig. 19) and QED Electron diode (Fig. 20) detectors, which have negligible buildup. With increasing photon energies, the normalized sensitivity for p-type PFD and QED Electron diodes were 1.013 (Fig. 19) and 0.876 (Fig. 20), respectively, at nominal accelerating potential of 15 and 16 MV, respectively. For the n-type Veridose Electron diode, the normalized sensitivity was 1.092 (Fig 19) at nominal accelerating potential of 15 MV. The MC simulation shows an average value of 0.943 ± 0.054 at 15 MV (Table 10), and it is independent of diode types (n or p) because the concentration (less than 2 parts per million) of the impurities (phosphorous or boron for n or p type semiconductors, respectively) is too low to impact the radiological properties of the silicon, and thus is completely ignored in the MC simulation. The QED Electron (p-type) diodes include 0.03g/cm^2 PMMA (acrylic) buildup, while the PFD diodes include 0.2 g/cm^2 Epoxy buildup. The n-type Veridose

Electron has buildup of 0.284 g/cm^2 polystyrene buildup. It should be noted that the dose rate dependence was excluded in both the MC simulation and the experiment results. The MC simulation is for the Si die without any inherent buildup. Isorad Electron diode has larger energy dependence (0.792 at 16 MV) even though it has the same 0.03 g/cm^2 PMMA buildup as the QED Electron (p-type) diode (Fig. 20). We hypothesize that this is caused by larger disturbance to the secondary electrons because the Isorad Electron diode has a complicated diode geometry, which is not modeled in our current MC simulation.

A Comparison of the diode-to-water dose ratio, $D_{H_2O}^{diode}$, can be made between the MC simulation (Table 10) and the cavity theory (Tables 11). For pure Si die, the predictions of the cavity theory are higher than the MC simulation results, but they agree to within ~ 6%. We attribute this difference to an error made in the cavity theory to calculate the stopping power ratio between Si and water. In the cavity theory, we have approximated

Table 10. Results of MC simulation for the normalized diode sensitivity. ($S_{norm} = D_{H_2O}^{diode}$ *(E) /* $D_{H_2O}^{diode}$ *(Co-60)*) and the diode-to-water dose ratio ($D_{H_2O}^{diode}$) for Si diodes with various buildup. The statistical uncertainty corresponds to 1 SD.

Energy/type	Silicon diode	Diode + 1.2mm Cu	Diode + 3 mm Cu	Diode + 1.7 mm W	Diode + 3 mm W
			$D_{H_2O}^{diode}$		
Co	0.889 ± 4.1%	0.699 ± 4.3%	0.864 ± 4.3%	0.693 ± 4.4%	1.112 ± 4.3%
6 MV	0.870 ± 4.3%	0.764 ± 4.6%	0.972 ± 4.6%	0.787 ± 4.7%	1.266 ± 4.7%
10 MV	0.888 ± 4.2%	0.821 ± 4.4%	1.040 ± 4.9%	0.850 ± 4.7%	1.400 ± 4.8%
15 MV	0.838 ± 4.0%	0.854 ± 4.3%	1.213 ± 4.3%	0.935 ± 4.4%	1.646 ± 4.1%
24 MV	0.877 ± 4.3%	0.958 ± 4.5%	1.374 ± 4.4%	1.259 ± 4.4%	2.148 ± 4.3%
			S_{norm}		
Co	1.000 ± 5.7%	1.000 ± 6.1%	1.000 ± 6.1%	1.000 ± 6.3%	1.000 ± 6.1%
6 MV	0.979± 5.9%	1.094 ± 6.3%	1.126 ± 6.3%	1.136 ± 6.5%	1.139 ± 6.4%
10 MV	0.999 ± 5.8%	1.175 ± 6.2 %	1.204 ± 6.5%	1.226 ± 6.4%	1.259 ± 6.5%
15 MV	0.943 ± 5.7%	1.222 ± 6.1%	1.404 ± 6.1%	1.349 ± 6.3%	1.481 ± 6.0%
24 MV	0.987± 5.9%	1.371 ± 6.2%	1.590 ± 6.2%	1.815 ± 6.3%	1.932 ± 6.1%

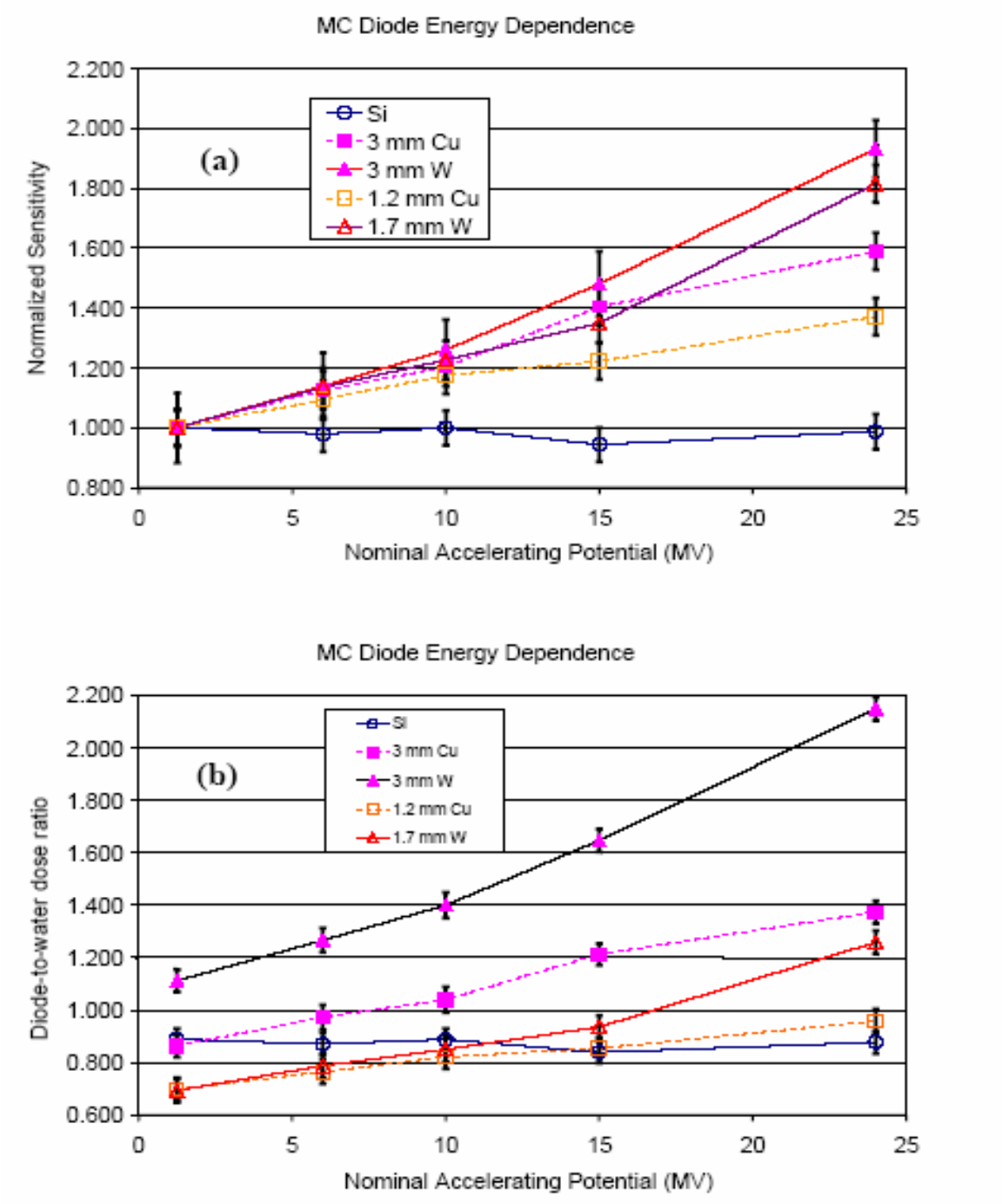

Figure 21. Monte Carlo simulation results.
(a) MC-calculated normalized sensitivity for a typical Si diode detector surrounded with different thickness of buildup materials (Cu and W) for various photon energies; (b) the diode-to-water dose ratio, $D_{H_2O}^{diode}$, calculated using MC simulation for the same conditions. o- Si only, Δ - 0.17 cm W , □ - 0.12 cm Cu, ▲- 0.3 cm W, ■- 0.3 cm Cu. Error bars are for 1 SD (see table 10).

Table 11. Results of the analytical cavity theory calculation.
The calculation included energy dependence of the ratio of stopping power, the ratio of energy absorption coefficient, the total attenuation function of the buildup material, and the normalized diode sensitivity.
The stopping power ratios were calculated using electron energy equal to (1/3) of the nominal accelerating potential of the corresponding photon spectrum. [$D_{H_2O}^{diode}$ is calculated using Eq. 58 assuming $P = 1$ and $S_{norm} = D_{H_2O}^{diode}(E) / D_{H_2O}^{diode}(Co\text{-}60)$ assuming $P = 1$].

Energy/type	Silicon diode	Diode+1.2mm Cu	Diode+3 mm Cu	Diode+1.7 mm W	Diode+3 mm W
		$(\overline{S}_{col}/\rho)_{buildup}^{Si} \times (\mu_{en}/\rho)_{water}^{Buildup}$ *			
Co	0.820×1.000	1.193×0.819	1.193×0.819	1.476×0.931	1.476×0.931
6 MV	0.832×1.000	1.193×0.881	1.193×0.881	1.464×1.040	1.464×1.040
10 MV	0.847×1.000	1.193×0.985	1.193×0.985	1.450×1.223	1.450×1.223
15 MV	0.855×1.000	1.192×1.090	1.192×1.090	1.437×1.399	1.437×1.399
24 MV	0.861×1.000	1.185×1.278	1.185×1.278	1.419×1.742	1.419×1.742
			$A(d_{buildup})$		
Co	0.997	0.945	0.868	0.833	0.724
6 MV	0.998	0.956	0.894	0.856	0.760
10 MV	0.998	0.962	0.907	0.863	0.771
15 MV	0.999	0.964	0.912	0.862	0.770
24 MV	0.999	0.965	0.915	0.853	0.756
			$D_{H_2O}^{diode}$		
Co	0.818	0.923	0.848	1.145	0.995
6 MV	0.830	1.005	0.940	1.303	1.157
10 MV	0.845	1.130	1.066	1.530	1.367
15 MV	0.854	1.253	1.185	1.733	1.548
24 MV	0.860	1.461	1.386	2.109	1.869
			S_{norm}		
Co	1.000	1.000	1.000	1.000	1.000
6 MV	1.015	1.088	1.107	1.138	1.163
10 MV	1.033	1.223	1.256	1.344	1.383
15 MV	1.044	1.355	1.396	1.514	1.555
24 MV	1.051	1.583	1.634	1.843	1.878

* The values are separated as: $(\overline{S}_{col}/\rho)_{buildup}^{Si} \times (\mu_{en}/\rho)_{water}^{Buildup}$

the secondary electron fluence by mono-energetic electron energy equal to 1/3 of the nominal accelerating potential. For the diodes with thick buildup (Diode + 3 mm Cu and Diode + 3 mm W), the $D_{H_2O}^{diode}$ results agree to within 10% between the MC simulation and the cavity theory. This indicated that $P \sim 1$ when there is sufficient buildup material to establish electron equilibrium. (The error in calculating the stopping power ratio between Si and buildup material in the cavity theory probably account for the 10% error.)

For the diodes with thinner buildup (Diode + 1.2 mm Cu and Diode + 1.7 mm W), the cavity theory predicts a much larger $D_{H_2O}^{diode}$ than that from MC simulation. This indicated that $P < 1$ in the cavity theory and there is strong disturbance of secondary electron fluence. Under this condition, the assumption of electron equilibrium in the current cavity theory is no longer valid.

The large energy dependence (35% at 15 MV) observed in Veridose Green is in agreement with the MC simulation but is smaller than the cavity theory using the stopping power ratio, mass energy attenuation coefficient ratio, and photon attenuation of the buildup material. The prediction by MC simulation is 1.35±0.06 (Table 10) while that by the cavity theory is 1.51 (Table 11). The Monte Carlo simulations are more consistent with the measurement, which suggests additional effects due to perturbation of secondary electron spectra (P) caused by the heterogeneous buildup structures around the silicon die.

5.5 Conclusion

The energy dependence for commercially available diodes was measured under high energy radiation beams. The diodes with thicker buildup material showed larger energy dependence, up to 39% for nominal accelerating potential of up to 17 MV. The energy dependence does not depend on the type of the diodes (n- or p-types). The Isorad Red (n-type), Veridose Green, Isorad 3 #1 and #2 diodes showed the largest energy dependence due to either more complex buildup geometry or thicker buildup thickness. The Monte Carlo simulation was used to verify the results for diodes with different buildup thicknesses and materials. We concluded that the material around the Si die such as buildup material causes the energy dependence.

CHAPTER 6 PAPER IV: DOSIMETRIC STUDY OF NEW PT-DOPED N-TYPE DIODE DETECTORS USED FOR IN-VIVO DOSIMETRY

The dosimetric characteristics of commercially available new n-type Pt doped unirradiated Isorad-3 and QED silicon diode detectors were studied under pulsed radiation (6 MV and 18 MV). The SSD (source-to-surface distance), dose rate, field size, angular, and temperature dependence were experimentally studied. This new n-type pt-doped Isorad-3 and QED diodes do show improved characteristics compared to previous n-type and p-type preirradiated Isorad and p-type QED diodes.

(Intend to submit)

6.1 Synopsis

The dosimetric characteristics of commercially available new n-type Pt doped unirradiated Isorad-3 and QED silicon diode detectors were studied under pulsed radiation (6 MV and 18 MV). The SSD (source-to-surface distance), dose rate, field size, angular, and temperature dependence were experimentally studied. The SSD correction factors (SSD CF), normalized to 100-cm SSD, was between 0.977-1.023 for all the n-type pt-doped diodes for SSD=60-150 cm. The dose rate dependence, measured at depth of 5-cm thick acrylic miniphantom, normalized to 10000 cGy/sec, varied between 0.964 (0.146×10^4 cGy/s) – 1.014 (3.90×10^4 cGy/s) for all the n-type pt-doped diodes. The field size correction factors (FS CF), normalized to field size of 10 cm^2, varied from 0.962 to 1.034 for all the pt-doped diodes for field size ranging between 4-40 cm^2. The angular dependence, measured with a square field of 10-cm^2 for beam angles between -75^o and +75^o, was within 2.6% for cylindrical Isorad-3 diodes and within 7.5% for flat geometry QED diodes. The sensitivity vs. temperature was measured at SSD=100 cm, 10×10 cm^2,

and depth of 5-cm in a large water phantom between 10 – 35°C. The response was linear with temperature coefficient of (0.475±0.055)%/°C for Isorad-3 and (0.64±0.02)%/°C for and QED diodes. This new n-type pt-doped Isorad-3 and QED diodes do show improved characteristics compared to previous n-type and p-type preirradiated Isorad and p-type QED diodes.

6.2 Introduction

It is recommended that the radiation dose should be accurately delivered for evaluation of the clinical results.[16] The International Commission on Radiological Units and Measurements (ICRU) recommends that the prescribed dose to a tumor be within 5.0% of the delivered dose.[58] The accuracy of the dose delivered can be checked by using in-vivo dosimetry. The thermoluminescent dosimeters (TLDs) and patient diodes are most commonly being used for patient dosimetry.

The most common p-n junction semiconductor diodes used in patient dosimetry are made of Si diodes. The p-n junction can be manufactured in many different ways. The diode is termed n-type or p-type depending upon whether the silicon substrate is doped with phosphorous (where majority-carriers are electrons) or boron (where majority-carriers are holes). [6,7] The radiation current generated in this type of device is determined by the semiconductor properties in the lightly doped area (the substrate).

The response of the diode detectors used in-vivo dosimetry depends on temperature, SSD (or dose rate), beam angle, field size, and energy. [6,7,15,24,25,28,30,36] In order to achieve the required verification (recommended by ICRU), the corrections factors of the diode detectors have to be determined for each individual diode and energy. The different diode detectors have to be characterized individually due to different construction materials and designs.

The purpose of this study was to evaluate a new n-type pt-doped unirradiated Isorad-3 and QED diode detectors manufactured by Sun Nuclear Corporation under pulsed (6 MV and 18 MV) radiation. Four diodes were used for the evaluation with each diode used for the appropriate range except for the dose rate and temperature measurements where each diode was tested under both 6 MV and 18 MV photon beam. The diode detectors were experimentally evaluated for SSD, dose rate, field size, angular, and temperature dependence. The energy dependence will be discussed from our previous paper.[36] These diode detectors replace the previous designs by this manufacturer. Different authors have investigated the correction factors for different commercially available diodes. However, practical data for these diodes is unavailable in the literature. The new diode detectors will also be compared with the previous detectors from the same manufacturer as well as other detectors being used for in-vivo dosimetry.

6.3 Materials and Methods

6.3.1 Description of Diodes

Four new n-type (Isorad-3 Gold, Isorad-3 Red, QED Gold, QED Red) from Sun Nuclear Corporation (Sun Nuclear Corporation, 425 A Pineda Ct., Melbourne, FL 32940) were used in this study. The diodes specifications are summarized in table 12.

Table 12. Specification of different diode detectors used in this study.

Diode Symbol	Manufacturer Code	Buildup Material, Total buildup thickness (g/cm^2)	Suitable Energy Range	Manufacturing period
Isorad-3 Gold	1163000-0	1.13 mm Molybdenum, 1.6	6-12 MV	2003-
Isorad-3 Red	1164000-0	1.13 mm Tungsten, 2.6	15-25 MV	2003-
QED Gold	111500-0	2.1 mm Brass, 1.85	6-12 MV	2003-
QED Red	111600-0	3.4 mm Brass, 3.04	15-25 MV	2003-

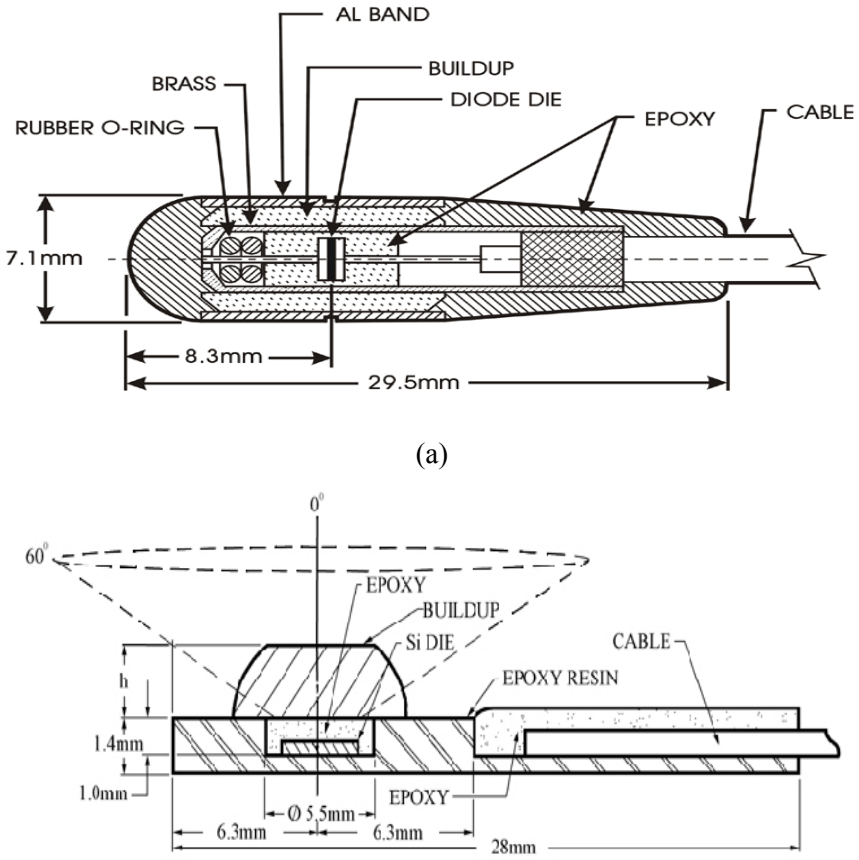

Figure 22. Schematics of n-type pt-doped diodes (a) Isorad-3 (b) QED (n-type).

Figure 22 shows the schematics of packages for the two types of detectors. The n-type Isorad-3 diodes have cylindrical design (Fig. 22(a)) with die plane mounted normal to the detector axis. The Isorad-3 diode is available in the three different energy ranges using build up of: brass (for 1–4 MV, Blue), molybdenum (6-12 MV, Gold), and tungsten (for 15-25 MV, Red). Radiation is incident from the plane of the die (from side of the p-n junction). This type of design reduces the angular dependence of diode sensitivity and provides uniform build up in the radial direction. The n-type QED diodes use flat design (Fig. 22(b)), with radiation incident normal to the plane of the die (in the direction of the p-n junction). The flat design has the advantage of well-defined buildup and less heterogeneous structures around the diode. This type of design usually has larger angular

dependence for angles between 40^{o}-75^{o}. The n-type QED detectors use none (for Co-60, Black), aluminum (1-4 MV, Blue), brass (for 6-12 MV, Gold), and brass (for 15-25 MV, Red) as build up. All of the Isorad-3 and QED are unirradiated n-type diodes with heavy Pt-doping, which has become commercial as of 2003.

6.3.2 Experimental Setup

The following parameters were used for the evaluation on the n-type unirradiated pt-doped Isorad-3 and QED diodes.

1. Source to surface distance (SSD) dependence
2. Dose rate dependence
3. Field size dependence
4. Angular dependence
5. Temperature dependence
6. Energy dependence (reference 37)

All the diodes were connected to an electrometer to measure the relative charge. An adapter was placed between the diode and the electrometer to convert BNC connection from the diode to the triax connection of the electrometer. The charge was measured with an electrometer without applying any bias.

1. Source to Surface Distance (SSD) Dependence

The diode SSD dependence was measured for n-type diodes ranging from 60 to 150 cm under the pulsed radiation (6 and 18 MV). All the measurements were taken using 10×10 cm^2 collimator setting. The charge readings were taken by placing the diode on the surface of polystyrene phantom and ion chamber at depth of maximum dose (1.6-cm for 6 MV and 3.2-cm for 18 MV) on the same phantom. One hundred monitor units were given for both 6 and 18 MV radiation beams. The data set was completed within about 2

hours with each diode and the ionization chamber measurements were completed within an hour on the same day. Leakage was subtracted for all the measurements before analyzing the data. The ratio between the diode reading and the ion chamber reading for a fixed SSD is normalized to be 1 at SSD=100cm. The SSD correction factors (SSD CF) were calculated by taking the inverse of normalized ratios between the diode readings (M_{diode}) and the ion chamber readings (M_{ion}):

$$SSD \quad CF = \frac{(M_{diode} / M_{ion})_{100}}{(M_{diode} / M_{ion})_{SSD}}. \tag{62}$$

SSD CF = 1 at SSD=100-cm and is a function of SSD.

2. Dose Rate Dependence

The dose rate (or instantaneous dose rate) dependence was measured in a 5-cm thick acrylic mini-phantom by changing the source-to-detector distance (SDD). The ratio of diode reading to ion chamber reading was plotted against instantaneous dose rate. The ratio was normalized to be 1 at an instantaneous dose rate of 10000 cGy/s for both 6 and 18 MV pulsed radiation beams. The instantaneous dose rate at a depth of 5 cm in the miniphantom for different SDDs was calculated from the normalized ionization chamber measurement, together with the known dose rate at *SDD*=100-cm using the following expression.[24]

$$InstDR_{SDD} = \frac{M_{ion}(SDD)}{M_{ion}(100)} \cdot InstDR_{100}. \tag{63}$$

Here M_{ion}(SDD) and M_{ion}(100) are the total charge measured by an ionization chamber in the same miniphantom for the source to detector distance (SDD) of interest and SDD =100 cm, respectively. $InstDR_{100}$ is the instantaneous dose rate at SDD=100 cm for the 10×10 cm^2 collimator setting at a depth of 5-cm in a Lucite miniphantom. It can be calculated according to:[24]

$$InstDR_{100} = \frac{(DR_{100}/60)}{(PW)(PRF)}(S_c(c=10)(S_p(s=4))(TMR(s=4,d=5)), \quad (64)$$

Where DR_{100} is expressed in MU/min and the factor 60 is used to convert DR_{100} to MU/sec. PW is the measured pulse width (in seconds) and PRF is the measured pulse repetition frequency (in Hz). Notice 1 MU = 1 cGy at the calibration condition: SAD = 100 cm, 10×10 cm^2 and at a depth of maximum dose (1.5 cm for 6 MV and 3.2 cm for 18 MV). Thus, after conversion DR_{100} (in cGy/sec) is the average dose rate under the calibration condition, while $InstDR_{100}$ (in cGy/sec) is the instantaneous dose rate at a 5-cm depth in the miniphantom at SAD = 100 cm and 10×10 cm^2 collimator setting. $S_c(10) = 1$ is the collimator scatter factor for a collimator setting of 10×10 cm^2, $S_p(4)$ is the phantom scatter factor for cross section of 4×4 cm^2, TMR(4,5) is the tissue maximum ratio for a field size of 4 cm^2 at a depth of 5 cm in the miniphantom.[3,24] Siemens Primus linear accelerator was used for both pulsed radiation beams. The PW and PRF were 2.8 μs and 263 Hz for 6 MV and 3.20 μs and 200 Hz for 18 MV, respectively. The average dose rate (DR) for the Siemens Primus accelerator was 297 MU/min (6 MV) and 490 MU/min (18 MV) at a SDD of 100 cm for 10×10-cm^2 field size. The instantaneous dose rates at a depth of 5 cm in a miniphantom for SDD=100 cm and field size of 4×4 cm^2 were approximately 6169 cGy/s and 13977 cGy/s for 6 and 18 MV, respectively.

3. Field Size Dependence

The field size dependence correction factors (FS CF) were measured by taking the diode readings on the surface of the polystyrene phantom and ion chamber at d_{max} of the same phantom (1.6 cm for 6 MV and 3.2 cm for 18 MV) at 100-cm SSD. The field size was changed between 4×4 cm^2 to 40×40 cm^2. The diode and ion chamber readings were collected for different field sizes and were normalized to diode and ion chamber readings of 10×10 cm^2 field size. The field size correction factors (FS CF), normalized at a field

size of 10×10 cm^2, were calculated by taking the inverse of normalized ratios between the diode readings (M_{diode}) and the ion chamber readings (M_{ion}):

$$FS \quad CF = \frac{(M_{diode} / M_{ion})_{10\times10}}{(M_{diode} / M_{ion})_{FS}} \tag{65}$$

FS CF = 1 at field size=10×10 cm^2 and is a function of field size.

4. Angular Dependence

The angular dependence was determined by placing the diode on a polystyrene phantom at SSD=100 cm and field size of 10 cm^2. The diode readings were taken by rotating the gantry angle form –75° to +75°. The diode readings at different angles were normalized to the diode readings at gantry angle of 0°. The angular dependence was determined for the energy for which the detector is designed.

The angular dependence correction factors (ANG. CF) were determined by taking the ratio of diode reading (M_{diode}) at gantry angle of 0° (perpendicular to the detector) to the diode readings (M_{diode}) at different gantry angles.

$$ANG \quad CF = \frac{(M_{diode})_{0^0}}{(M_{diode})_{ANG}}. \tag{66}$$

5. Temperature Dependence

Temperature dependence of n-type Pt-doped unirradiated Isorad-3 and QED diodes was measured under pulsed (6 MV and 18 MV) radiation. Diodes were placed individually in a 30×30×30 cm^2 large water phantom at 5-cm depth in water so that the point of measurement was beyond the range of contamination electrons. The water surface was 100 cm from the x-ray target and the field size was set to 10×10 cm^2. The diodes were

placed in very thin plastic to make them waterproof. Four aquarium water heaters were placed on the corners of the water phantom to raise the temperature of the water. A water pump was used to homogenize the temperature. A digital thermometer was used to determine the actual water temperature. The temperature was cooled downed to 10^{o}C using ice and was slowly increase from 10^{o}C to 35^{o}C at a rate of approximately 0.25°C/minute. After the water temperature was raised, the water pump was turned on to circulate the water for at least 10 to 15 minutes. Once the temperature in the phantom was completely stabilized, the radiation was applied. One hundred-monitor units were applied for each diode reading. Three to four readings were taken and the average value was used for analyzing the data. Leakage was measured for each temperature and was subtracted from the reading. Since the water volume was large, the temperature remained constant during the measurement. The water temperature was recorded at each successive step. The sensitivity vs. temperature was measured between 10-35° C. The data was normalized to 22° C.

The charge collected by the diode was measured for each temperature and normalized to the linear fit value at 22°C. The charge was not measured at 22°C, instead the expected charge value at 22°C was obtained from a linear fit to the measured data. The results were plotted as normalized charge vs. the temperature. The temperature coefficient, defined as $\frac{1}{S}\frac{dS}{dT}$ where S is the diode sensitivity was then determined by linear regression of the data. The error bar for the measurement is based on the worst deviation between measurements and the linear fit (Fig. 27) and is set to be ±0.5% for all measurements.

6. Energy Dependence (Reference 37)

The energy dependence was measured for Isorad-3 Gold, QED Gold, and QED Red diodes in our previous paper.[36] The measurements were performed in a liquid water phantom at 5-cm depth for 10 × 10-cm^2 collimator setting and source–to-detector

distance (SDD) of 100 cm. The response (nC/Gy) was normalized to Co-60 beam after corrections for the dose rate and temperature dependences for each diode. A thin sleeve was used to protect the diode detector. The output of the linear accelerator was calibrated using AAPM TG51[54] protocol.

6.4 Results and Discussion

Prior to the implementation of diode in-vivo dosimetry, it is necessary to assess the effect of different parameters which affects the diode sensitivity. Generally, in clinic, the entrance dose is calculated from the diode reading, multiplied by its calibration factor and the product of different correction factors which affects the diode sensitivity. In this paper, different correction factors were measured for new n-type pt-doped unirradiated Isorad-3 and QED diodes under pulsed radiation (6 MV and 18 MV). Since no literature exist for these types of diodes, the dosimetric characteristics of these diode detectors are compared with other commercially available diode detectors being used in the clinics.

The SSD CF, normalized to SSD=100 cm, varied from 0.989 to 1.007 for Isorad-3 Gold diode (measured under 6MV) and 0.977 to 1.017 Isorad-3 Red (measured under 18 MV) diode. The correction factors varied between 0.979 –1.016 for QED Gold (measured under 6MV) diode and 0.984-1.023 for QED Red (measured under 18 MV) diode. Figure 23 shows SSD dependence of the silicon diode detectors under pulsed radiation.

There are a number of studies of SSD CF published in the literature. Zhu has shown that the SSD CF for unirradiated Isorad (n-type, original design) diodes varies between 0.960-1.02 for 6 MV and 0.940-1.02 for 18 MV, when the SSD was changed from 70 cm to 130 cm.[38] The preirradiated QED (p-type) varies by 2.0% under 6 MV and 4.0% under 18 MV when the SSD changed from 70 to 130 cm.[38] Huang et. al. have reported, preirradiated Isorad-p (p-type) and QED (p-type) to show variation of 10% and ~5%, respectively under both 6 MV and 18 MV for the SSD change in between 70-120 cm.[37] Colussi et. al. has shown variation in SSD CF of ~6.5% for both QED (p-type) and Isorad

(p-type) under 18 MV. Jornet et. al. and Geroge et. al. has reported SSD CF change by 5.0% under 18 MV for EDP30 (p-type) for SSD change in 80 –120 cm. [31,34]

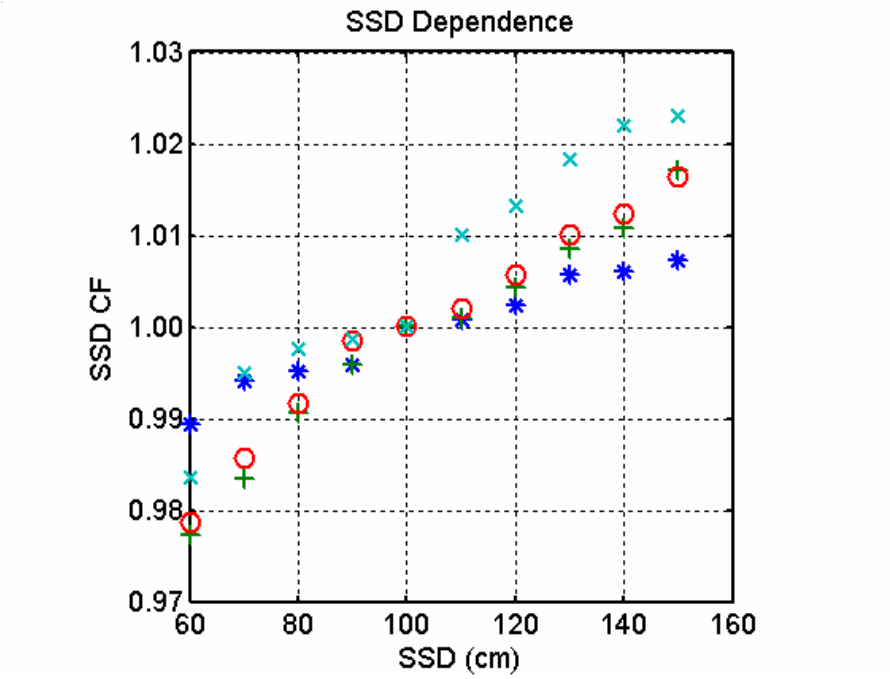

Figure 23. SSD dependence of pt-doped diode detectors.
* - Isorad-3 Gold (6 MV), + - Isorad-3 Red (18MV) , O - QED Gold (6 MV), x - QED Red (18 MV).

In comparison, we have seen much smaller variation in SSD CF for both n-type pt doped Isorad-3 and QED diodes. The SSD CF for n-type Isorad-3 Gold varied by ~2.0% (under 6 MV) and ~3.0% for Isorad-3 Red (under 18 MV) when the SSD was changed from 60-150 cm. The SSD CF was within 4.0% (6 and 18 MV) for both n-type QED diodes under the same SSD change. The pt-doped n-type unirradiated Isorad-3 and QED showed less variation in SSD CF compared to other commercially available n-type and p-type diode detectors.

The dose rate dependence, normalized to 10000 cGy/sec, varied between 0.980 (1490 cGy/s) – 1.005 (38990 cGy/s) for Isorad-3 Gold, 0.994 (1490 cGy/s) – 1.001 (38990 cGy/s) for Isorad-3 Red, 0.964 (1460 cGy/s) – 1.014 (39060 cGy/s) for QED Gold, and

0.967 (1460 cGy/s) – 1.014 (39060 cGy/s) for QED Red diode. The dose rate dependence was smaller for these n-type Pt-doped diodes as compared to previous n-type Isorad and p-type QED diodes. Figure 24 shows the dose rate dependence for these diodes.

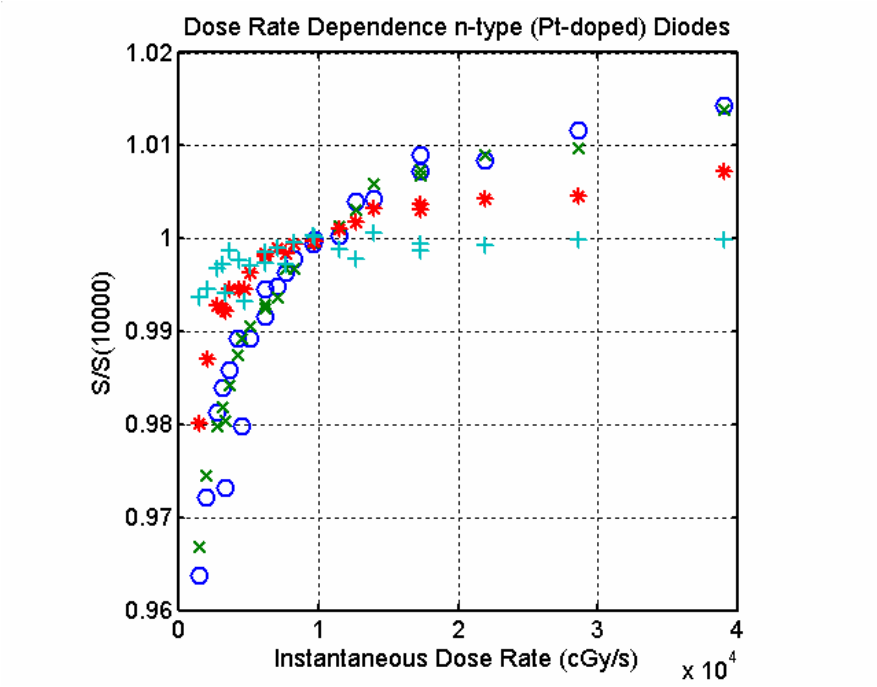

Figure 24. Dose rate dependence of pt-doped diode detectors (6 and 18 MV).
* - Isorad-3 Gold, + - Isorad-3 Red, O - QED Gold, and x - QED Red.

The dose rates has been reported to be a problem in n-type semiconductor detectors but not for pre-irradiated p-type diodes.[7] It has been reported that the p-type Si detector pre-irradiated to 25 kGy displays a flat dose rate dependence.[27] Also, it has been shown that the response of n-type detector shows more dose rate dependence than p-type detectors.[6] The linearity of p-type detector depends upon the resistivity or doping level of the diode (higher the doping level, lower the resistivity and vice versa).[27] A high doped (low resistivity) p-type detector shows linear response. Accumulative dose generally reduces dose rate dependence for p-type diodes. [29] However, in a recent paper by Wilkins, it has been shown that one of the pre-irradiated (Scanditronix) p-type diodes showed increased dose rate dependence after high level of accumulative irradiation (~25 kGy).[30] This could

be caused by neutron irradiation since it seemed to only happen when the diode was irradiated by photon energies higher than 10 MV and does not always happen when irradiated to 25 kGy by low energy photons.

The new n-type unirradiated Isorad-3 and the QED diodes have substantially smaller dose rate dependence than other n-type diodes. These diodes are doped by platinum. Heavily platinum doped diodes have very small dose rate dependence due to very small minority-carrier lifetime (< 0.3 μs).[29]

The field size correction factors (FS CF), normalized to field size of 10 cm^2, varied from 0.985 to 1.007 for Isorad-3 Gold (measured under 6 MV) and 0.962 to 1.034 for Isorad-3 Red (measured under 18 MV) diode for field sizes between 4-40 cm^2. The field size correction factors varied from 0.995 to 1.007 for QED Gold (measured under 6 MV) and 0.981 to 1.007 for QED Red (measured under 18 MV) diode for the same change in field size. Table 13. and Fig. 25 shows the field size correction factors for these diodes.

For diodes used in-vivo dosimetry, the field size dependence is mainly due to the different irradiation conditions between the diode and the ion chamber. The diode is generally placed on the surface, it normally lacks an overlaying layer and it's reading is more dependent on head scatter as compared to the phantom scatter.[31,59] Therefore, the diode under responds as the field size is increased.[34,37,59-61]

Table 13. The field size correction factors for different diodes.

Field Size (cm^2)	Isorad-3 Gold (6 MV)	Isorad-3 Red (18 MV)	QED Gold (6 MV)	QED Red (18 MV)
4	0.985	0.962	0.995	0.981
6	0.992	0.981	0.998	0.993
8	0.996	0.990	0.999	0.998
10	1.000	1.000	1.000	1.000
12	1.000	1.005	1.001	1.003
15	1.004	1.012	1.001	1.005
20	1.006	1.018	1.002	1.006
25	1.008	1.021	1.003	1.006
30	1.007	1.025	1.004	1.006
40	1.007	1.034	1.005	1.007

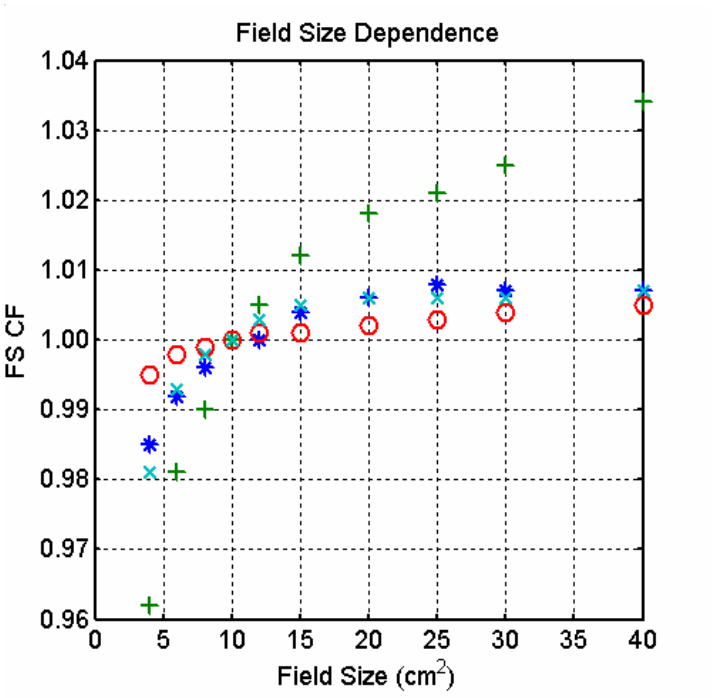

Figure 25. Field size dependence correction factors for different diodes.
* - Isorad-3 Gold (6 MV),+ - Isorad-3 Red (18MV), O - QED Gold (6 MV), x - QED Red (18 MV).

The field size dependence has reported to be more problem for cylindrical design as compared to the flat design at higher energy beams where there might not be adequate buildup on the diode.[8,38] Zhu has reported FS CF varied in between 0.950-106 for the previous n-type Isorad diode and 0.970-1.040 for the p-type QED diode under 18 MV.[38] The FS CF ranged between 0.990-1.020 for both n-type Isorad and p-type QED diode under 6 MV beam for field size between 4-40 cm.[38] Wolff et.al. has also observed variation between 0.975-1.04 for n-type Isorad under high energy beam and 0.99-1.015 for 6 MV.[60] The other authors have reported similar results for the p-type Isorad-p and p-type QED diodes.[8] Also, it has been reported that the flat design EDP30 diode's correction factors were in the opposite direction ranging between 1.002-0.965 when the field size was varied between 6-40 cm^2.[34] They have concluded that the buildup material placed on the top of the diode was not thick enough to have the electronic equilibrium.[31,37]

The new n-type pt-doped Isorad-3 and QED diodes field size correction factors increase with an increase in field size. The Isorad-3 Gold and QED Gold shows smaller correction factors under 6MV than the Isorad-3 and QED Red diodes measured under 18 MV beam. The FS CF under 6MV beam, were between 0.985 to 1.007 for Isorad-3 Gold and 0.995-1.007 for QED Red diodes. Under 18 MV, the FS CF for Isorad-3 Red and QED Red shows variation between 0.962 to 1.034 and 0.981-1.007, respectively for field sizes between 4-40-cm^2. The new cylindrical design Isorad-3 diodes show similar field size correction factors as compared to the previous cylindrical Isorad (both n- and p-type). Also, the flat design n-type QED diodes show similar FS CF as compared to the p-type QED diodes.

The ANG. CF, measured with a square field size of 10-cm^2, was within 2.6% for Isorad-3 Gold, 1.2% for Isorad-3 Red, 7.5% for QED Gold and 2.7% for QED Red diode for angles between -75^o and +75^o (Fig. 26). The Isorad-3 diodes do show smaller angular dependence than the QED diodes due to the construction of the diode.

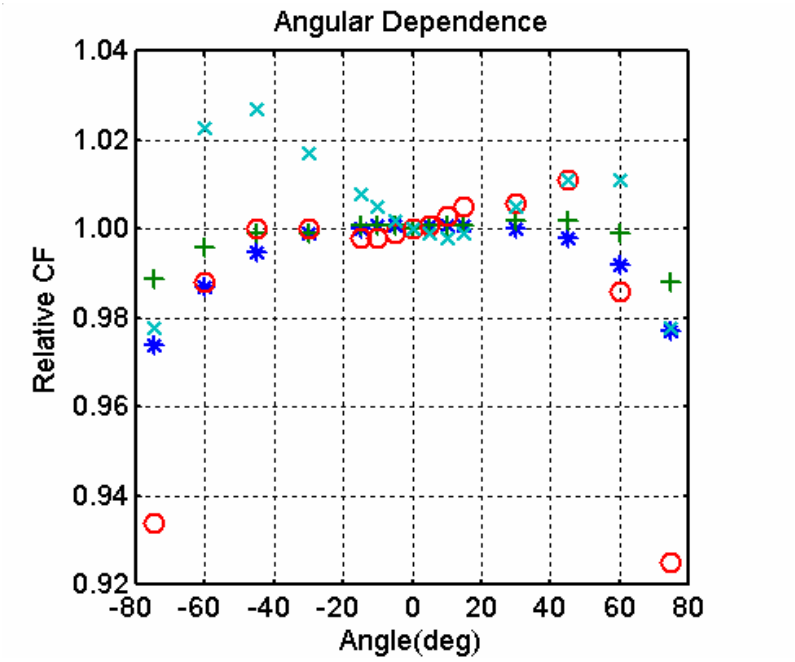

Figure 26. Angular dependence for different diode detectors.
* - Isorad-3 Gold (6 MV), + - Isorad-3 Red (18MV) , O - QED Gold (6 MV), x - QED Red (18 MV).

The diode used in in-vivo dosimetry is placed on the patient's skin. The diode reading per monitor unit (MU) depends on its orientation with respect to the incident direction of the beam. The angular dependence is caused mainly by the detector construction and by the back scattering from the patient. In general, the cylindrical design shows smaller angular dependence than the flat detector.[38] The cylindrical design gives much less angular dependence than the flat design detector.[19,38] Flat design (QED and EDP30) can give more than 5% change in the angular dependence correction factors.[34,38]

In this study, we have seen similar phenomenon in the n-type cylindrical Isorad-3 and the flat design QED diodes. The flat design QED diodes did show larger angular dependence than the cylindrical Isorad-3 diodes. The Isorad-3 diode showed the variation within 2.0% for gantry angles of +/-60^{o}. The QED diode showed dependence within 3.5% for the same angle range.

The temperature coefficient of the new n-type diode detectors increases linearly. The temperature coefficient was (0.475±0.055)%/ °C for Isorad-3 and (0.63±0.02)%/ °C for QED diodes under pulsed (6 MV and 18 MV) radiation (Table 14). Figure 27 shows the temperature dependence of these detectors under pulsed radiation. These diodes show larger temperature coefficients as compared to other commercially available n-type detectors.[24]

Table 14. Temperature Coefficient (%/^{o}C) for different diodes.

Diode	6 MV (%/^{o}C)	18 MV (%/^{o}C)
Isorad-3 Gold	0.52	0.51
Isorad-3 Red	0.43	0.43
QED Gold	0.63	0.65
QED Red	0.66	0.62

The radiation current generated in the diode depends on the temperature of the diodes. Most of the diode detectors commercially used have positive temperature coefficient (i.e. sensitivity increases with increase in temperature). The SVWT tends to increase with

accumulated dose because more traps are generated. Welsh and Reinstein have recently quantified the rising time of temperature and the equilibrium temperature for many commercial diodes.[25] Depending upon the temperature coefficient for a particular diode, it can produce 3-5% inaccuracy in dose measurements.[27] It has been reported that the change in sensitivity for diodes used commercially varies between 0.1 to +0.5 %^{o}C.[22-24,34]

In a recent paper, the temperature dependence for n-type and p-type diodes were extensively studied.[24] It was shown that the n-type unirradiated diode show smaller temperature dependence under pulsed radiation, however the temperature coefficients varied between different energies and individual diode.[24] The temperature coefficient for Pt-doped diodes was larger than the previous n-type diodes measured under pulsed radiation.[24] The n-type Isorad-3 and QED have shown temperature dependence between 0.43%/^{o}C – 0.65%/^{o}C. These diode detectors have shown little larger temperature coefficient as compared to other commercially available diodes.[24]

The energy dependence data was taken from our previous paper. The energy dependence, normalized to Co-60 beam, varied by 34% for Isorad-3 Gold, 21% for n-type QED Gold, and 24% for n-type QED Red for nominal accelerating potential between Co-60 and 15 MV.[36] In that paper, the Monte Carlo simulation were used to verify the results for diodes with different buildup thicknesses and materials. In that paper, it was concluded that the material around the Si die such as buildup material causes the energy dependence.[36]

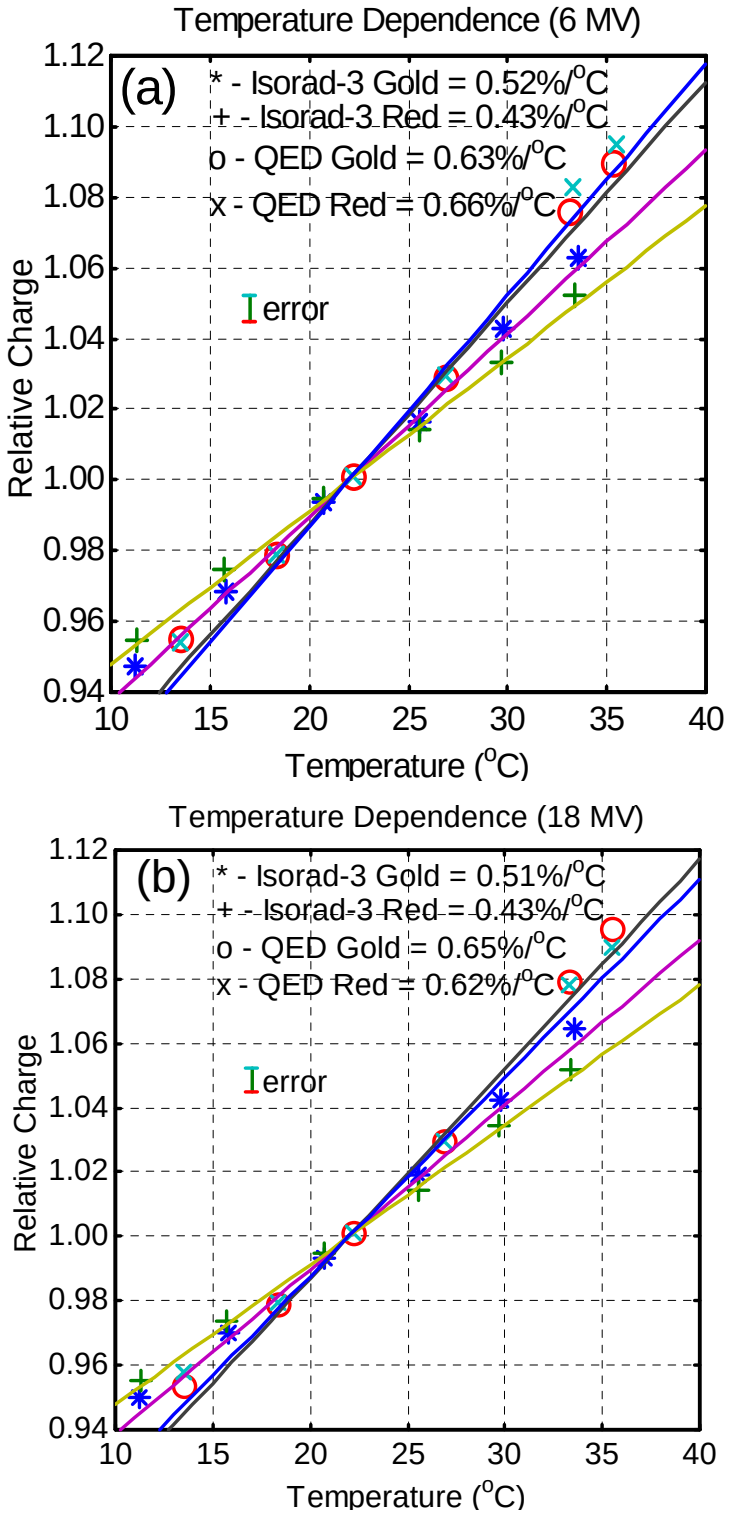

Figure 27. Temperature dependence for different diode detectors.
(a) 6 MV (b) 18 MV, * - Isorad-3 Gold, + - Isorad-3 Red, O - QED Gold, and x - QED Red.

6.5 Conclusion

In this study, dosimetric characteristics of commercially available new pt-doped n-type Isorad-3 and QED silicon diode detectors were experimentally studied. The SSD, dose rate, field size, angular, temperature, and energy dependence were studied. The SSD correction factors were smaller for these new n-type pt-doped diodes under pulsed radiation as compared to other n-type diodes and some p-type diodes. The field size correction factors (FS CF), normalized to field size of 10 cm^2, varied from 0.962 to 1.034 for all the diodes. The angular dependence measured with a square field size of 10-cm^2, was within 2.6% for Isorad-3 and within 7.5% for QED diodes for angles between -75^o and +75^o. The sensitivity vs. temperature was measured at 5-cm depth in a large water phantom between 10 – 35°C was linear with temperature coefficient of (0.475±0.055)%/ °C for Isorad-3 and (0.64±0.02)%/°C for QED diodes under pulsed radiation (6 MV and 18 MV). The new n-type Pt-doped unirradiated diodes do show better dosimetric characteristics as compared to previous n-type and p-type (Isorad) and p-type (QED) diodes.

CHAPTER 7 CONCLUDING REMARKS

This dissertation presents the first systematic and quantitative study of dosimetric characteristics for most of the commercial radiation diodes (n-type and p-type) under different radiation beams. In order to achieve the best possible accuracy between the prescribed dose and the measured dose, proper correction factors for temperature, dose rate or SDD, and energy need to be applied to the diode measurements. They are extensively studied in this work. Other relevant dosimetric characteristics were also studied for some of the diodes.

The diode detector is used as a relative radiation dosimeter mainly due to it's dependence upon the temperature, dose rate, and energy.[1,3,54,55] The transient electric and radiation properties have to be quantified by fundamental physics quantities in order to use the diode detector as an absolute dosimeter. This work has systematically quantified the dose rate dependence on temperature coefficient, dose rate dependence, and energy dependence.

This dissertation presented some preliminary results that will potentially enable a diode detector to act as an absolute dosimeter. To do so, we present theoretically the correlation between the dose and the measured quantities (radiation current) using the fundamental physics quantities. The sensitivity, *S*, of the bare diode detector is defined as the radiation current per unit absorbed dose. Under continuous radiation, we get:

$$S_{diode} = \frac{M_{diode}}{D_{diode}} = K\sqrt{\kappa\tau} \qquad (67)$$

Where M_{diode} is the total charge collected by the diode during irradiation and D_{diode} is the absorbed dose in the silicon diode, κ is the diffusion coefficient (cm^2/s), τ is the excess carrier minority carrier lifetime(s) and K can be defined as:[24,28,29]

$$K = Ae\frac{\rho}{e\beta\left(\frac{W}{e}\right)} = \frac{A\rho}{\beta\left(\frac{W}{e}\right)} \tag{68}$$

A is the cross-section area of the diode (in cm^2). β is the dose-to-kerma ratio.[3] ρ is density of silicon W/e is the energy required to produce an electron-hole pair for silicon.[1] All the quantities are determined by fundamental physics quantities. For pulsed radiation, one needs to solve the non-linear differential equation (equation 17). If the Si diode is buried inside buildup materials, its energy dependence will change significantly.[36] Under that condition:

$$S = \frac{M_{diode}}{D} = \frac{M_{diode}}{D_{diode}} \cdot P = S_{diode} \cdot P \tag{69}$$

M_{diode} is the charge collected in nC by the silicon diode detector. S_{diode} is the sensitivity of the bare diode defined in nC/cGy. P is the perturbation factor which depends upon the thickness and type of the buildup material used. The perturbation factor, P, can be modeled using radiation transport codes (e.g. MC simulation). Chapter 5 demonstrated that this can be done, independent of diode electrical properties.[36]

In summary, some of the future works to enable a diode detector as an absolute dosimeter includes:

- Solving the non-linear differential equation in 1D, 2D, and 3D.
- Characterizing the basic electric properties of a 3 dimensional diode detector.
- Detailed MC modeling of a diode detector including all the involved buildup structures.

- Coupling the radiation transport with electric transport equations.

The emphasis of this dissertation is on the use of the diode detector for dosimetry of photon beams. The use of the diode detector for electron beams is also feasible but is beyond the scope of this study.

REFERENCES

[1]F. H. Attix, *Introduction to radiological physics and radiation dosimetry*. (John Wiley & Sons, New York 1986).

[2]H. Johns and J. Cunnigham, *The physics of radiology*, 4th ed. (Charles Thomas, 1983).

[3]F. M. Khan, *The physics of radiation therapy*, 2nd ed. (Lippincott Wiliams & Wilkins, Baltimore, 1994).

[4]E. B. Podgorsak, *Radiation oncology physics: A handbook for teachers and students*. (IAEA, Vienna, 2005).

[5]G. Rikner and E. Grusell, "Effects of radiation damage on p-type silicon detectors." Phys. Med. Biol. 28, 1261-1267 (1983).

[6]G. Rikner, "Silicon diode as detectors in relative dosimetry of photon, electron, and proton radiation fields." Ph.D. Thesis, Uppsala University, Sweden (1983).

[7]G. Rikner and E. Grusell, "General specifications for silicon semiconductors for use in radiation dosimetry." Phys. Med. Biol. 32, 1109-1117 (1987).

[8]V. Colussi, A. Beddar, T. Kinsella, and C. Sibata, "In-vivo dosimetry using a single diode for megavoltage photon beam radiotherapy: Implementation and response characterization." J. App. Clin. Med. Phys. 2, 210-218 (2001).

[9]E. M. Essers and B. J. Munheer, "In vivo dosimetry during external photon beam radiotherpay." Int. J. Radiat. Oncol. Biol. Phys. 43, 245-259 (1999).

[10]D. P. Fontenla, R. Yaparpalvi, C. S. Chui, and E. Briot, "The use of diode dosimetry in quality improvement of patient care in radiation therapy." Med. Dosim. 21, 235-241 (1996).

[11]J. H. Lanson, M. Essers, G. J. Meijer, A. Minken, G. J. Uiterwaal, and B. J. Mijnheer, "In vivo dosimetry during conformal radiotherapy: Requirements for and finding of a routine procedure." Radiother. and Oncol. 52, 51-59 (1999).

[12]G. Lunens, J. V. Dam, A. Dutreix, and E. Schueren, "Quality assurance in radiotherapy by in vivo dosimetry. 1. Entrance dose measurements, a reliable procedure." Radiother. and Oncol. 17, 141-151 (1990).

[13]G. Lunens, J. Verstraete, A. Dutreix, and E. V. d. Schueren, "Assessment of dose inhomogeneity at target level by in-vivo dosimetry: Can the recommended 5% accuracy in the dose delivered to the target volume be fulfilled in daily practice?" Radiother. and Oncol. 25, 242-250 (1992).

[14]M. Voordeckers, H. Gossens, J. Rutten, and W. V. d. Bogaert, "The implementation of in vivo dosimetry in a small radiotherapy department." Radiother. and Oncol. 47, 45-48 (1998).

[15]E. Yorke, R. Alecu, L. Ding, D. Fontenla, A. Kalend, D. Kaurin, M. E. Masterson-McGary, G. Marinello, T. Matzen, A. S. Saini, J. Shi, W. Simon, T. C. Zhu, and X. R. Zhu, "*Diode in-vivo dosimetry for patients receiving external beam radiation therapy*." Report No. 87, (AAPM, Madison, 2005).

[16]G. J. Kutcher, L. Coia, M. Gillin, W. F. Hanson, S. Leibel, R. J. Morton, J. R. Palta, J. A. Purdy, L. E. Reinstein, G. K. Svensson, M. Weller, and L. Wingfield, "Comprehensive QA of radiation therapy: Report of AAPM Radiation Therapy Committee Task Group 40." Med. Phys. 21, 581-618 (1994).

[17]IAEA, "*Investigation of an accidental exposure of radiotherapy patients in Panama, Report of a Team of Experts*." (IAEA, Vienna, 2001).

[18]A. Adeyemi and J. Lord, "An audit of radiotherapy patient dose measured with in vivo semiconductor detectors." Br. J. Radiol. 70, 399-408 (1997).

[19]R. Alecu, M. Alecu, and T. Ochran, "A method to improve the effectiveness of diode in-vivo dosimetry." Med. Phys. 25, 746-749 (1998).

[20]S. Heukelomi, J. H. Lanson, and B. J. Mijnheer, "In vivo dosimetry during pelvic treatments." Radiother. and Oncol. 25, 111-120 (1992).

[21]B. Nilson, B. Ruden, and B. Sorcini, "Characteristics of silicon diodes as patient dosimeters in external radiation therapy." Radiother. and Oncol. 11, 279-288 (1988).

[22]J. V. Dam, G. Leunens, and A. Dutreix, "Correlation between temperature and dose rate dependence of semiconductor response; influence of accumulated dose." Radiother. and Oncol. 19, 345-351 (1990).

[23]E. Grusell and G. Rikner, "Evaluation of temperature effects in p-type silicon detectors." Phys. Med. Biol. 31, (1986).

[24]A. S. Saini and T. C. Zhu, "Temperature dependence of commercially available diode detectors." Med. Phys. 29 (4), 622-630 (2002).

[25]K. T. Welsh and L. E. Reinstein, "The thermal characteristics of different diodes on in vivo patient dosimetry." Med. Phys. 28 (5), 844-849 (2001).

[26]E. Grusell and G. Rikner, "Radiation damage induced dose rate nonlinearity in an n-type silicon detector." Acta. Radiol. Oncol. 23, 465-469 (1984).

[27]E. Grusell and G. Rikner, "Linearity with dose rate of low resistivity p-type silicon semiconductor detectors." Phys. Med. Biol. 38, 785-792 (1993).

[28]A. S. Saini and T. C. Zhu, "Dose rate and SDD Dependence of commercially available diode detectors." Med. Phys. 31 (4), 914-924 (2004).

[29]J. Shi, W. E. Simon, and T. C. Zhu, "Modeling the instantaneous dose rate dependence of radiation diode detector." Med. Phys. 30 (9), 2509-2519 (2003).

[30]D. Wilkins, X. A. Li, and L. Greig, "The effect of dose rate dependence of p-type silicon detector on linac relative dosimetry." Med. Phys. 24, 879-881 (1997).

[31]D. Georg, B. Ost, M. Hoornaert, P. Pilette, J. V. Dam, M. V. Dyke, and D. Huyskens, "Buildup modification of commercial diodes for entrance dose measurements in 'higher energy' photon beams." Radiother. and Oncol. 51, 249-256 (1999).

[32]S. C. Klevenhagen, "Temeprature response of silicon surface barrier semiconductor detector operated in the dc-short circuit configuration." Acta. Radiol. 12, 124-144 (1973).

[33]J. Shi, "Characteristics of the Si diode as a radiation detector for the application of in-vivo dosimetry." M.S. Thesis, Florida Institute of Technology, Melbourne (1995).

[34]N. Jornet, M. Ribas, and T. Eudaldo, "In vivo dosimetry: Intercomparison between p-type based and n-type based diodes for the 16-25 MV range." Med. Phys. 2, 210-218 (2000).

[35]P. A. Jursinic, "Implementation of an in-vivo diode dosimetry program and changes in diode characteristics over a 4-year clinical history." Med. Phys. 28, 1718-1726 (2001).

[36]A. S. Saini and T. C. Zhu, "Energy dependence of commercially available diode detectors for in-vivo dosimetry." Med. Phys. 34 (5), 1704-1711 (2007).

[37]K. Huang, W. B. Jr., and O. Hidalgo-Salvatierra, "Chacterization of an in vivo diode dosimetry system for clinical use." J. App. Clin. Med. Phys. 4, 132-142 (2003).

[38]X. R. Zhu, "Entrance dose measurements for in-vivo diode dosimetry: Comparison of correction factors for two types of commercial silicon diode detectors." J. App. Clin. Med. Phys. 1, 100-107 (2000).

[39]J. V. Dam, G. Marinello, and H. Mayles, *Methods for in vivo dosimetry in external radiotherapy*. (Leuven -Apeldoorn, 1994).

[40]R. O. Carlson, Y. S. Sun, and H. B. Assalit, "Lifetime control in silicon power devices by electron or gamma irradiation." IEEE Trans. on Elect. Dev. ED-24 (8), 1103-1108 (1977).

[41]R. L. Dixon and K. E. Ekstrand, "Gold and platinum doped radiation resistant silicon diode detectors." Proceedings of the VIII International Conference on Solid State Dosimetry, 527-530 (1986).

[42]R. Pirret, *Advanced semiconductors fundamentals*, 2nd ed. (Prentice Hall, Upper Saddle River, 1994).

[43]B. Streetman, *Solid state electronic devices.* (Prentice Hall, 1990).

[44]M. Tyagi, *Introduction to semiconductor materials and devices*, 2nd ed. (John Wiley & Sons, New York, 1991).

[45]T. F. Wunch and C. L. Axness, "Modeling the time-dependent transient radiation response of semiconductor junctions." IEEE Trans. Nucl. Sci. 39, 2158-2168 (1992).

[46]J. J. Wirth and S. C. Rogers, "The transient response of transistor and diodes to ionizing radiation." IEEE Trans. Nucl. Sci. NS-11, 24-38 (1964).

[47]I. Kawrakow, "Accurate condensed history Monte Carlo simulation of electron transport. I. EGSnrc, the new EGS4 version." Med. Phys. 27, 485-498 (2000).

[48]D. W. O. Rogers, I. Kawrakow, J. P. Seuntjens, and B. R. B. Walters, "*NRC User Codes for EGSnrc*." (National Reasearch Council of Canada, Ottawa, 2000).

[49]ICRU37, "*Stopping powers for electrons and positrons*." (ICRU, Washington D.C., 1984).

[50]P. N. Mobit, A. E. Nahum, and P. Mayles, "An EGS4 Monte Carlo examination of general cavity theory." Phys Med. Biol. 42, 1319-1334 (1997).

[51]T. C. Zhu, B. E. Bjärngard, Y. Xiao, and C. J. Yang, "Modeling the output ratio in air for Megavoltage photon beams." Med. Phys. 28, 925-937 (2001).

[52]R. Sjogren and M. Karlsson, "Influence of electron contamination on in vivo surface dosimetry for high-energy photon beams." Med. Phys. 25, 916-921 (1998).

[53]G. Rikner and E. Grusell, "Correction factors in in-vivo dosimetry, with reference to entrance dose measurements." Radiother. and Oncol. 37, S19 (1995).

[54]TG51, "AAPM's TG-51 protocol for clinical reference dosimetry of high-energy photon and electron beams." Med. Phys. 26, 1847-1870 (1999).

[55]TG21, "A protocol for the determination of absorbed dose from high-energy photon and electron beams." Med. Phys. 10 (6), 741-771 (1983).

[56]A. S. Saini, T. C. Zhu, and I. Rebo, "Dosimetric Evaluation of new n-type Pt-doped QED diode detectors." Med. Phys. A177, (2003).

[57]R. Mohan, C. Chui, and L. Lidofsky, "Energy and angular distributions of photons from medical linear accelerators." Med. Phys. 12, 592-597 (1985).

[58]ICRU24, "*Determination of absorbed dose in a patient irradiated by beams of X- and Gamma rays in radiotherapy procedures*." (ICRU, Washington, D.C., 1976).

[59]J. G. Wierzbick and D. S. Waid, "Large discrepancies between calculated d_{max} and diode reading for small field sizes and small SSDs of 15 MV photon beams." Med. Phys. 25, 245-246 (1998).

[60]T. Wolff, S. Carter, K. Langmack, N. Twyman, and P. Dendy, "Characterization and use of a commercial n-type diode system." Br. J. of Radiol. 71, 1168-1177 (1998).

[61]R. Alecu, T. Loomis, J. Alecu, and T. Ochran, "Guidelines on the implementation of diode dosimetry programs for photon and electron external beam therapy'." Med. Dosim. 24, 05-12 (1999).

APPENDICES

Appendix A Mat Lab Codes for Temperature Dependence Study (Paper I)

Figure 6 (a) Paper I

```
% Temperature dependence of the Isorad 1 Gold unirradiated diode (norm. to 22°C)
x1=[15 18.35 21.4 25.25 29 32.1 35.1 38.85];
y1=[12.731 12.918 13.093 13.314 13.532 13.725 13.918 14.156];
yref1=interp1(x1,y1,22);
y1=y1./yref1;
% 6MV
x2=[14.45 17.75 21.3 25.3 29.25 33.75 37.45];
y2=[11.194 11.1976 11.272 11.2909 11.3099 11.3206 11.3516];
yref2=interp1(x2,y2,22);
y2=y2./yref2;
% 20 MV
x3=[14.45 17.75 21.3 25.3 29.25 33.75 37.45];
y3=[14.95625 14.9505 15.01313 15.01594 15.04696 15.09262 15.12263];
yref3=interp1(x3,y3,22);
y3=y3./yref3;
% Find out the slopes
p1=polyfit(x1,y1,1);
p2=polyfit(x2,y2,1);
p3=polyfit(x3,y3,1);
x=10:40;
y1f=polyval(p1,x);
y2f=polyval(p2,x);
y3f=polyval(p3,x);
% plot out the results
xerr=[17 17];
yerr=1.065.*[1 1.007];
xerr1=[xerr(1)*(1-.02) xerr(1)*(1+.02)];
yerr1=[yerr(1) yerr(1)];
xerr2=xerr1;
yerr2=[yerr(2) yerr(2)];
plot(x1,y1,'o',x2,y2,'+',x3,y3,'x',x,y1f,x,y2f,x,y3f,xerr,yerr,xerr1,yerr1,xerr2,yerr2)
xlabel('Temperature (^oC)')
ylabel('Relative Charge')
title('ISORAD Gold 1 Unirradiated Diode')
axis('square')
axis([10 40 0.94 1.08])
grid
gtext(['Error'])
gtext(['o - Co-60 = ' num2str(p1(1)*100,2) ' %/^oC'])
gtext(['+ - 6 MV = ' num2str(p2(1)*100,2) ' %/^oC'])
gtext(['x - 20 MV = ' num2str(p3(1)*100,2) ' %/^oC'])
```

Appendix A (Continued)

```
Figure 6 (b) Paper I
%       Temperature dependence of the Isorad Gold2 unirradiated diode
%       All the data is normalized to 22 degrees
x1=[16.05 19.35 22.3 24.2 27.15 30.2 33 36 39.15];
y1=[16.0253 16.1247 16.2325 16.2768 16.3497 16.4236 16.4896 16.556 16.651];
yref1=interp1(x1,y1,22);
y1=y1./yref1;
% 6MV
x2=[11.55 14.5 17.8 20.8 23.7 27 30.15 33.15 35.9 39.15];
y2=[6.7757 6.7997 6.8046 6.8188 6.8476 6.8845 6.8482 6.9169 6.8965 6.9250];
yref2=interp1(x2,y2,22);
y2=y2./yref2;
% 20 MV
x3=[11.55 14.5 17.8 20.8 23.7 27 30.15 33.15 35.9 39.15];
y3=[10.3027 10.3097 10.3396 10.3678 10.3926 10.4385 10.4612 10.4869 10.5105
10.5920];
yref3=interp1(x3,y3,22);
y3=y3./yref3;
% Find out the slopes
p1=polyfit(x1,y1,1);
p2=polyfit(x2,y2,1);
p3=polyfit(x3,y3,1);
x=10:40;
y1f=polyval(p1,x);
y2f=polyval(p2,x);
y3f=polyval(p3,x);
xerr=[17 17];
yerr=1.065.*[1 1.007];
xerr1=[xerr(1)*(1-.02) xerr(1)*(1+.02)];
yerr1=[yerr(1) yerr(1)];
xerr2=xerr1;
yerr2=[yerr(2) yerr(2)];
plot(x1,y1,'o',x2,y2,'+',x3,y3,'x',x,y1f,x,y2f,x,y3f,xerr,yerr,xerr1,yerr1,xerr2,yerr2)
xlabel('Temperature (^oC)')
ylabel('Relative Charge')
title('ISORAD Gold 2 Unirradiated Diode')
axis('square')
axis([10 40 0.94 1.08])
grid
gtext(['error'])
gtext(['o - Co-60 = ' num2str(p1(1)*100,2) ' %/^oC'])
gtext(['+ - 6 MV = ' num2str(p2(1)*100,2) ' %/^oC'])
gtext(['x - 20 MV = ' num2str(p3(1)*100,2) ' %/^oC'])
```

Appendix A (Continued)

Figure 7 Paper I

```
% Temperature dependence of the Isorad Red preirradiated diode
% All the data is normalized to 22 degrees
x1=[11.95 15.85 20.4 25.15 29.17 33.3 37.2];
y1=[9.109 9.254 9.406 9.567 9.724 9.853 9.992];
yref1=interp1(x1,y1,22);
y1=y1./yref1;
% 6MV
x2=[11.5 15.8 20.3 25.3 29.7 33.15 36.9];
y2=[3.598 3.648 3.683 3.722 3.755 3.779 3.818];
yref2=interp1(x2,y2,22);
y2=y2./yref2;
% 20 MV
x3=[11.5 15.8 20.3 25.3 29.7 33.15 36.9];
y3=[5.408 5.449 5.506 5.567 5.613 5.655 5.701];
yref3=interp1(x3,y3,22);
y3=y3./yref3;
% Find out the slopes
p1=polyfit(x1,y1,1);
p2=polyfit(x2,y2,1);
p3=polyfit(x3,y3,1);
x=10:40;
y1f=polyval(p1,x);
y2f=polyval(p2,x);
y3f=polyval(p3,x);
% plot out the results
xerr=[17 17];
yerr=1.065.*[1 1.007];
xerr1=[xerr(1)*(1-.02) xerr(1)*(1+.02)];
yerr1=[yerr(1) yerr(1)];
xerr2=xerr1;
yerr2=[yerr(2) yerr(2)];
plot(x1,y1,'o',x2,y2,'+',x3,y3,'x',x,y1f,x,y2f,x,y3f,xerr,yerr,xerr1,yerr1,xerr2,yerr2)
xlabel('Temperature (C)')
ylabel('Relative Charge')
title('ISORAD Red Preirradiated Diode')
axis('square')
axis([10 40 0.94 1.08])
grid
gtext(['error'])
gtext(['o - Co-60 = ' num2str(p1(1)*100) ' %/C'])
gtext(['+ - 6 MV = ' num2str(p2(1)*100) ' %/C'])
gtext(['x - 20 MV = ' num2str(p3(1)*100) ' %/C'])
```

Appendix A (Continued)

Figure 8 Paper I

```
% Temperature dependence of the QED unirradiated p-type photon diode
% Co-60 data, on Theratronics Phoenix at 80 cm SSD
x1=[12.8 18.65 24.7 31.15];
y1=[79 80.2 82 84.03];
yref1=interp1(x1,y1,22);
y1=y1./yref1;
% 6MV (200 MU/min)
x2=[11.45 14.1 19.2 24.2 28.5 31.7];
y2=[502 505 513 520 526.5 529.5];
yref2=interp1(x2,y2,22);
y2=y2./yref2;
% 15 MV (300 MU/min)
x3=[11.45 14.1 19.2 24.2 28.5 31.7];
y3=[564.5 567.5 575 583 589 593];
yref3=interp1(x3,y3,22);
y3=y3./yref3;
% Find out the slopes
p1=polyfit(x1,y1,1);
p2=polyfit(x2,y2,1);
p3=polyfit(x3,y3,1);
x=10:40;
y1f=polyval(p1,x);
y2f=polyval(p2,x);
y3f=polyval(p3,x);
% plot out the results
plot(x1,y1,'o',x2,y2,'+',x3,y3,'x',x,y1f,x,y2f,x,y3f)
xlabel('Temperature (C)')
ylabel('Relative Charge')
title('Unirradiated p-type Diode')
axis('square')
grid
gtext(['+ - Co-60 MV = ' num2str(p1(1)*100) ' %/C'])
gtext(['+ - 6 MV = ' num2str(p2(1)*100) ' %/C'])
gtext(['x - 15 MV = ' num2str(p3(1)*100) ' %/C'])
```

Appendix A (continued)

Figure 9 (a) Paper I

```
% Temperature dependence of the QED Red preirradiated diode
% Co-60
x1=[10.25 14.37 18.8 21.6 25.9 29.6 33.9];
y1=[60.4 61.0 61.8 62.3 63.13 63.83 64.55];
yref1=interp1(x1,y1,22);
y1=y1./yref1;
% 6MV
x2=[10.1 14.6 18.95 22.6 26.4 30.6 34.4];
y2=[85.9 86.9 87.95 88.8 89.9 91.1 91.95];
yref2=interp1(x2,y2,22);
y2=y2./yref2;
% 15 MV
x3=[10.1 14.6 18.95 22.6 26.4 30.6 34.4];
y3=[102.6 103.8 105.0 106.15 107.4 108.8 109.86];
yref3=interp1(x3,y3,22);
y3=y3./yref3;
% Find out the slopes
p1=polyfit(x1,y1,1);
p2=polyfit(x2,y2,1);
p3=polyfit(x3,y3,1);
x=8:40;
y1f=polyval(p1,x);
y2f=polyval(p2,x);
y3f=polyval(p3,x);
xerr=[17 17];
yerr=1.065.*[1 1.007];
xerr1=[xerr(1)*(1-.02) xerr(1)*(1+.02)];
yerr1=[yerr(1) yerr(1)];
xerr2=xerr1;
yerr2=[yerr(2) yerr(2)];
plot(x1,y1,'o',x2,y2,'+',x3,y3,'x',x,y1f,x,y2f,x,y3f,xerr,yerr,xerr1,yerr1,xerr2,yerr2)
xlabel('Temperature (C)')
ylabel('Relative Charge')
title('QED Red Preirradiated p-type Diode')
axis('square')
axis([10 40 0.94 1.08])
grid
gtext(['error'])
gtext(['o - Co-60 = ' num2str(p1(1)*100) ' %/C'])
gtext(['+ - 6 MV = ' num2str(p2(1)*100) ' %/C'])
gtext(['x - 15 MV = ' num2str(p3(1)*100) ' %/C'])
```

Appendix A (Continued)

Figure 9 (b) Paper I

```
% Temperature dependence of the QED Blue preirradiated diode
% Co-60
x1=[10.75 13.2 16.9 20.8 25 29.8 34];
y1=[73.8 74.23 75.1 76.0 76.9 78.1 79.1];
yref1=interp1(x1,y1,22);
y1=y1./yref1;
% 6MV
x2=[10.65 14.75 18.8 22.75 26.87 31.6 35.2];
y2=[103.9 105.0 106.25 107.6 109.16 110.7 111.83];
yref2=interp1(x2,y2,22);
y2=y2./yref2;
% 15 MV
x3=[10.65 14.75 18.8 22.75 26.87 31.6 35.2];
y3=[109.75 111.05 112.3 113.7 115.38 116.86 118.1];
yref3=interp1(x3,y3,22);
y3=y3./yref3;
% Find out the slopes
p1=polyfit(x1,y1,1);
p2=polyfit(x2,y2,1);
p3=polyfit(x3,y3,1);
x=8:40;
y1f=polyval(p1,x);
y2f=polyval(p2,x);
y3f=polyval(p3,x);
xerr=[17 17];
yerr=1.065.*[1 1.007];
xerr1=[xerr(1)*(1-.02) xerr(1)*(1+.02)];
yerr1=[yerr(1) yerr(1)];
xerr2=xerr1;
yerr2=[yerr(2) yerr(2)];
plot(x1,y1,'o',x2,y2,'+',x3,y3,'x',x,y1f,x,y2f,x,y3f,xerr,yerr,xerr1,yerr1,xerr2,yerr2)
xlabel('Temperature (C)')
ylabel('Relative Charge')
title('QED Blue Preirradiated p-type Diode')
axis('square')
axis([10 40 0.94 1.08])
grid
gtext(['error'])
gtext(['o - Co-60 = ' num2str(p1(1)*100) ' %/C'])
gtext(['+ - 6 MV = ' num2str(p2(1)*100) ' %/C'])
gtext(['x - 15 MV = ' num2str(p3(1)*100) ' %/C'])
```

Appendix A (Continued)

Figure 10 (a) Paper I

```
% Temperature dependence of the Scanditronix EDP30 diode
x1 =[14 17.45 21.3 25.5 29.2 33.5 37.3];
y1=[3.489 3.534 3.582 3.638 3.693 3.757 3.816];
yref1=interp1(x1,y1,22);
y1=y1./yref1;
% 6MV
x2=[11.7 16.2 19.7 24 28.2 32.3 36.5];
y2=[2.414 2.444 2.475 2.518 2.562 2.605 2.627];
yref2=interp1(x2,y2,22);
y2=y2./yref2;
% 20 MV
x3=[11.7 16.2 19.7 24 28.2 32.3 36.5];
y3=[3.441 3.48 3.511 3.571 3.629 3.681 3.734];
yref3=interp1(x3,y3,22);
y3=y3./yref3;
% Find out the slopes
p1=polyfit(x1,y1,1);
p2=polyfit(x2,y2,1);
p3=polyfit(x3,y3,1);
x=10:50;
y1f=polyval(p1,x);
y2f=polyval(p2,x);
y3f=polyval(p3,x);
% plot out the results
xerr=[17 17];
yerr=1.065.*[1 1.007];
xerr1=[xerr(1)*(1-.02) xerr(1)*(1+.02)];
yerr1=[yerr(1) yerr(1)];
xerr2=xerr1;
yerr2=[yerr(2) yerr(2)];
plot(x1,y1,'o',x2,y2,'+',x3,y3,'x',x,y1f,x,y2f,x,y3f,xerr,yerr,xerr1,yerr1,xerr2,yerr2)
xlabel('Temperature (C)')
ylabel('Relative Charge')
title('Scanditronix EDP30 diode')
axis('square')
axis([10 40 0.94 1.08])
grid
gtext(['error'])
gtext(['o - Co-60 = ' num2str(p1(1)*100) ' %/C'])
gtext(['+ - 6 MV = ' num2str(p2(1)*100) ' %/C'])
gtext(['x - 20 MV = ' num2str(p3(1)*100) ' %/C'])
```

Appendix A (Continued)

Figure 10 (b) Paper I

```
% Temperature dependence of the Scanditronix EDP10 diode
%Co-60
x1 =[12.6 16.25 20.5 25.3 29.25 33 36.1];
y1=[2.901 2.94 2.984 3.037 3.078 3.121 3.157];
yref1=interp1(x1,y1,22);
y1=y1./yref1;
% 6MV
x2=[12.3 16.35 20.3 24.25 28.25 32.5 36.25];
y2=[2.212 2.238 2.269 2.303 2.339 2.38 2.415];
yref2=interp1(x2,y2,22);
y2=y2./yref2;
% 20 MV
x3=[12.3 16.35 20.3 24.25 28.25 32.5 36.25];
y3=[2.603 2.635 2.669 2.703 2.738 2.776 2.813];
yref3=interp1(x3,y3,22);
y3=y3./yref3;
% Find out the slopes
p1=polyfit(x1,y1,1);
p2=polyfit(x2,y2,1);
p3=polyfit(x3,y3,1);
x=10:50;
y1f=polyval(p1,x);
y2f=polyval(p2,x);
y3f=polyval(p3,x);
xerr=[17 17];
yerr=1.065.*[1 1.007];
xerr1=[xerr(1)*(1-.02) xerr(1)*(1+.02)];
yerr1=[yerr(1) yerr(1)];
xerr2=xerr1;
yerr2=[yerr(2) yerr(2)];
plot(x1,y1,'o',x2,y2,'+',x3,y3,'x',x,y1f,x,y2f,x,y3f,xerr,yerr,xerr1,yerr1,xerr2,yerr2)
xlabel('Temperature (C)')
ylabel('Relative Charge')
title('Scanditronix EDP10 diode')
axis('square')
axis([10 40 0.94 1.08])
grid
gtext(['error'])
gtext(['o - Co-60 = ' num2str(p1(1)*100) ' %/C'])
gtext(['+ - 6 MV = ' num2str(p2(1)*100) ' %/C'])
gtext(['x - 20 MV = ' num2str(p3(1)*100) ' %/C'])
```

Appendix B Mat Lab Codes for Dose Rate Dependence Study (Paper II)

File name: invsq1. Save the following file as invsq1.m and run it along with figures. For example if this file is on c drive. Write cd c:\ in mat lab and then run the other files.

```
function [z, xv]=invsq1(x,y,xf);
% z=INVSQ(x,y) will do an inverse-square law fit to the input data
% (x, y) and generate the virtual sourse position xv, the fitted y positions z for xf.
x1=x;
y1=ones(size(y))./sqrt(y);
p=polyfit(x1,y1,1);
D=p(1).*p(1);
xv=-p(2)./p(1);
z=D.*ones(size(xf))./(xf-xv).^2;
z=z./z(find(xf==100));
return
```

Appendix B (Continued)

Figure 12 Paper II

```
% This program analyze the Dose Rate and SDD-dependence of diodes
% Ion chamber data for Veridose Green diode
xionv=[80 90 100 110 130 150 175.3 205.8];
yionv6=[1.5652 1.2363 1.0000 0.8245 0.5895 0.4418 0.3236 0.2346];
yionv18=[1.561 1.2342 1.0000 0.8253 0.5900 0.4420 0.3242 0.2353];
[yionv6f, xvion6v]=invsq1(xionv,yionv6,xionv);
[yionv18f, xvion18v]=invsq1(xionv,yionv18,xionv);
% Veridose Green diode n-type data
xvergreen=[80 90 100 110 130 150 175.3 205.8];
yvergreen6=[1.5796 1.2410 1.0000 0.8236 0.5863 0.4383 0.3205 0.2322];
yvergreen18=[1.5737 1.2408 1.0000 0.8249 0.5868 0.4390 0.3208 0.2319];
qvergreen6f=yvergreen6./yionv6f;
qvergreen18f=yvergreen18./yionv18f;
% Ion chamber data for QED n-type pt doped diodes
xionq=[60 70 80 90 100 110 120 130 140 150 175.1 205.1];
yionq6=[2.7985 2.0451 1.5588 1.2349 1.0000 0.8220 0.6910 0.5887 0.5073 0.4406
0.3249 0.2352];
yionq18=[2.7989 2.0441 1.5593 1.2322 1.0000 0.8215 0.6910 0.5881 0.5073 0.4407
0.3252 0.2359];
[yionq6f, xvion6q]=invsq1(xionq,yionq6,xionq);
[yionq18f, xvion18q]=invsq1(xionq,yionq18,xionq);
% QED Red Pt doped n-type unirradiated diode data
xqed2n=[60 70 80 90 100 110 120 130 140 150 175.1 205.1];
yqed2n6=[2.8404 2.0729 1.5779 1.2410 1.0000 0.8235 0.6892 0.5848 0.5027 0.4367
0.3184 0.2300];
yqed2n18=[2.8166 2.0565 1.5707 1.2375 1.0000 0.8220 0.6891 0.5851 0.5027 0.4372
0.3195 0.2306];
```

Appendix B (Continued)

```
qqed2n6f=yqed2n6./yionq6f;
qqed2n18f=yqed2n18./yionq18f;
% Ion chamber data measured for Isorad Gold n-type (#1)
xiongold2=[60 70 80 90 100 110 120 130 140 150 172.8 203.2];
yion6=[2.8028 2.0532 1.5702 1.2384 1.0000 0.8255 0.6932 0.5908 0.5100 0.4437 0.3332
0.2422];
yion18=[2.7957 2.0505 1.5681 1.2352 1.0000 0.8261 0.6930 0.5918 0.5101 0.4444
0.3337 0.2428];
[yion6f, xvion6]=invsq1(xiongold2,yion6,xiongold2);
[yion18f, xvion18]=invsq1(xiongold2,yion18,xiongold2);
% Isorad Gold #1 diode data
xisoold=[60 70 80 90 100 110 120 130 140 150 172.8 203.2];
yisoold6=[2.8265 2.0664 1.5755 1.2369 1.0000 0.8243 0.6909 0.5882 0.5060 0.4396
0.3297 0.2374];
yisoold18=[2.8120 2.0559 1.5722 1.2361 1.0000 0.8259 0.6930 0.5908 0.5083 0.4421
0.3316 0.2395];
qisoold6=yisoold6./yion6f;
qisoold18=yisoold18./yion18f;
% Ion chamber data for Isorad Red diode
xionred2=[60 70 80 90 100 110 120 130 140 150 172.8 203.2];
yion6red_2=[2.8028 2.0532 1.5702 1.2384 1.0000 0.8255 0.6932 0.5908 0.5100 0.4437
0.3332 0.2422];
yion18red_2=[2.7957 2.0505 1.5681 1.2352 1.0000 0.8261 0.6930 0.5918 0.5101 0.4444
0.3337 0.2428];
[yion6redf_2, xvion6red]=invsq1(xionred2,yion6red_2,xionred2);
[yion18redf_2, xvion18red]=invsq1(xionred2,yion18red_2,xionred2);
% Isorad Red diode data
xisored2=[60 70 80 90 100 110 120 130 140 150 172.8 203.2];
```

Appendix B (Continued)

```
yisored6_2=[2.898 2.1051 1.5914 1.2482 1.0000 0.8186 0.6834 0.5787 0.4963 0.4305
0.3221 0.2304];
yisored18_2=[2.8306 2.0679 1.5792 1.2377 1.0000 0.8207 0.6870 0.5808 0.4984 0.4320
0.3217 0.2302];
qisored6f_2=yisored6_2./yion6redf_2;
qisored18f_2=yisored18_2./yion18redf_2;
% Ion chamber data for Isorad 3 Gold pt doped diode
xiongold3=[60 70 80 90 100 110 120 130 140 150 172.8 203.1];
yion6gold3=[2.7994 2.0501 1.5651 1.2352 1.0000 0.8255 0.6931 0.5910 0.5084 0.4431
0.3318 0.2412];
yion18gold3=[2.7865 2.0485 1.5612 1.2325 1.0000 0.8260 0.6939 0.5900 0.5092 0.4437
0.3327 0.2418];
[yion6gold3f, xvion6gold3]=invsq1(xiongold3,yion6gold3,xiongold3);
[yion18gold3f, xvion18gold3]=invsq1(xiongold3,yion18gold3,xiongold3);
% Isorad 3 Gold pt doped data
xiso3gold=[60 70 80 90 100 110 120 130 140 150 172.8 203.1];
yiso3gold6=[2.8140 2.059 1.5698 1.2366 1.0000 0.8241 0.6906 0.5880 0.5056 0.4403
0.3295 0.2366];
yiso3gold18=[2.8003 2.049 1.5664 1.2360 1.0000 0.8242 0.6913 0.5886 0.5071 0.4414
0.3311 0.2390];
qiso3gold6f=yiso3gold6./yion6gold3f;
qiso3gold18f=yiso3gold18./yion18gold3f;
% correction factors
qiso3gold6f=1./qiso3gold6f;
qiso3gold18f=1./qiso3gold18f;
qisored6f_2=1./qisored6f_2;
qisored18f_2=1./qisored18f_2;
qisoold6=1./qisoold6;
```

Appendix B (Continued)

```
qisoold18=1./qisoold18;
%qisonew6f=1./qisonew6f;
%qisonew20f=1./qisonew20f;
%qisored6f=1./qisored6f;
%qisored20f=1./qisored20f;
qvergreen6f=1./qvergreen6f;
qvergreen18f=1./qvergreen18f;
qqed2n6f=1./qqed2n6f;
qqed2n18f=1./qqed2n18f;
figure(1)
h=plot(xiongold2,qisoold6,'o',xionred2,qisored6f_2,'+',xiongold3,qiso3gold6f,'>',xionv,q
vergreen6f,'<',xionq,qqed2n6f,'x','markersize',10,'linewidth',2);
set(h,'linewidth',2);
xlabel('SDD (cm)','fontsize',13)
ylabel('SDD CF','fontsize',13)
title('6MV, open, SDD Dependence (n-type)','fontsize',13)
axis('square')
grid on
axis([60 220 0.96 1.08])
set(gca,'fontsize',13,'linewidth',1.5,'yticklabel',['0.96'; '0.98'; '1.00'; '1.02'; '1.04'; '1.06';
'1.08'],'xtick',[60 80 100 120 140 160 180 200 220])
gtext('(a)','fontsize',20);
figure(2)
h=plot(xiongold2,qisoold18,'o',xionred2,qisored18f_2,'+',xiongold3,qiso3gold6f,'>',
xionv,qvergreen18f,'<',xionq,qqed2n18f,'x','markersize',10,'linewidth',2);
set(h,'linewidth',2);
xlabel('SDD (cm)','fontsize',13)
ylabel('SDD CF','fontsize',13)
```

Appendix B (Continued)

```
title('18MV, open, SDD Dependence (n-type)','fontsize',13)
axis('square')
grid on
axis([60 220 0.96 1.08])
set(gca,'fontsize',13,'linewidth',1.5)
gtext('(b)','fontsize',20);
```

Appendix B (Continued)

Figure 13 Paper II

```
% This program analyze dose rate and SDD dependence for p-type diodes
% Ion chamber data for EDP10-3G diode
xione10=[60 70 80 90 100 110 120 130 140 150 172.8 203];
yion6e10=[2.7984 2.0496 1.5652 1.2361 1.0000 0.8245 0.6931 0.5905 0.5085 0.4424
0.3343 0.2420];
yion18e10=[2.7903 2.0431 1.5614 1.2311 1.0000 0.8239 0.6911 0.5898 0.5079 0.4429
0.3339 0.2425];
% This fitting is only used for the EDP 10-3G diode
[yion6e10f, xvion6]=invsq1(xione10,yion6e10,xione10);
[yion18e10f, xvion18]=invsq1(xione10,yion18e10,xione10);
% Ion chamber data for the EDP30 diode
xione=[80 100 130 150 173.75 201.35 370.2];
yion6e=[1.5763 1 0.5857 0.4384 0.3263 0.2414 0.0711];
yion20e=[1.5779 1 0.5867 0.4390 0.3251 0.2409 0.0716];
% This fitting is only used for the EDP 30 diode
[yion6ef, xvion6]=invsq1(xione,yion6e,xione);
[yion20ef, xvion20]=invsq1(xione,yion20e,xione);
% Ion chamber data for Isorad Red (p-type, EDP20-3G diodes
xion=[80 90 100 110 130 150 175.3 205.8];
yion6=[1.557 1.236 1.000 0.824 0.589 0.442 0.324 0.235];
yion18=[1.558 1.234 1.000 0.825 0.590 0.442 0.324 0.235];
% This fitting is only used for the EDP 20-3G and Isorad Red (p-type)diode
[yion6f, xvion6]=invsq1(xion,yion6,xion);
[yion18f, xvion18]=invsq1(xion,yion18,xion);
% Ion chamber data for QED Blue and QED Red p-type diodes
xionq=[80 90 100 110 130 140 179.4 202.6];
yion6q=[1.5677 1.2359 1.0000 0.8270 0.5911 0.5093 0.3096 0.2436];
yion15q=[1.5642 1.2342 1.00000 0.8268 0.5913 0.5090 0.3105 0.2444];
```

Appendix B (Continued)

```
 [yion6qf, xvion6]=invsq1(xionq,yion6q,xionq);
[yion15qf, xvion15]=invsq1(xionq,yion15q,xionq);
% EDP10-3G diode data
xedp10=[60 70 80 90 100 110 120 130 140 150 172.8 203];
yedp106=[2.8101 2.0551 1.5711 1.2402 1.0000 0.8231 0.6913 0.5879 0.5065 0.4408
0.3319 0.2407];
yedp1018=[2.8068 2.0527 1.5699 1.2397 1.0000 0.8232 0.6911 0.5882 0.5062 0.4405
0.3323 0.2410];
qedp106f=yedp106./yion6e10f;
qedp1018f=yedp1018./yion18e10f;
% EDP30 diode data
xedp30=[80 100 130 150 173.75 201.35 370.2];
yedp306=[1.5717 1 .5889 .4371 .3296 .2424 0.0708];
yedp3020=[1.5761 1 .5873 .4400 .3291 .2433 0.0717];
qedp306f=yedp306./yion6ef;
qedp3020f=yedp3020./yion20ef;
% EDP20-3G diode data
xedp20=[80 90 100 110 130 150 175.3 205.8];
yedp206=[1.562 1.238 1.000 0.825 0.589 0.444 0.323 0.235];
yedp2018=[1.559 1.236 1.000 0.824 0.588 0.444 0.324 0.235];
qedp206f=yedp206./yion6f;
qedp2018f=yedp2018./yion18f;
% Isorad Red (p-type) diode data
xisored=[80 90 100 110 130 150 175.3 205.8];
yisored6=[1.583 1.246 1.000 0.821 0.581 0.433 0.315 0.227];
yisored18=[1.596 1.248 1.000 0.817 0.578 0.429 0.312 0.224];
qisored6f=yisored6./yion6f;
qisored18f=yisored18./yion18f;
```

Appendix B (Continued)

```
% QED Red (p-type) diode data
xqedred=[80 90 100 110 130 140 179.4 202.6];
yqedred6=[1.5748 1.2389 1.0000 0.8225 0.5865 0.5052 0.3067 0.2404];
yqedred15=[1.576 1.238 1.000 0.8228 0.5854 0.5058 0.3062 0.2405];
qqedred6f=yqedred6./yion6qf;
qqedred15f=yqedred15./yion15qf;
% QED Blue (p-type) diode data
xqedblue=[80 90 100 110 130 140 179.4 202.6];
yqedblue6=[1.5733 1.2384 1.0000 0.8207 0.5855 0.5038 0.3051 0.2392];
yqedblue15=[1.578 1.240 1.000 0.8219 0.5849 0.5025 0.3043 0.2375];
qqedblue6f=yqedblue6./yion6qf;
qqedblue15f=yqedblue15./yion15qf;
% Correction Factors
% 6 MV
qedp206f=1./qedp206f;
qisored6f=1./qisored6f;
qedp106f=1./qedp106f;
qqedred6f=1./qqedred6f;
qqedblue6f=1./qqedblue6f;
% 15,18,or 20 MV
qedp2018f=1./qedp2018f;
qisored18f=1./qisored18f;
qedp1018f=1./qedp1018f;
qqedred15f=1./qqedred15f;
qqedblue15f=1./qqedblue15f;
figure(1)
h=plot(xion,qedp206f,'x',xisored,qisored6f,'*',xione10,qedp106f,'d',xqedred,qqedred6f,'^',
xqedblue,qqedblue6f,'v','markersize',10,'linewidth',2)
```

Appendix B (Continued)

```
set(h,'linewidth',2);
xlabel('SDD (cm)','fontsize',13)
ylabel('SDD CF','fontsize',13)
title('6MV, open, SDD Dependence (p-type)','fontsize',13)
axis('square')
axis([60 220 0.96 1.08])
grid on
set(gca,'fontsize',13,'linewidth',1.5,'yticklabel',['0.96'; '0.98'; '1.00'; '1.02'; '1.04'; '1.06';
'1.08'],'xtick',[60 80 100 120 140 160 180 200 220])
gtext('(a)','fontsize',20);
figure(2)
h=plot(xion,qedp2018f,'x',xisored,qisored18f,'*',xione10,qedp1018f,'d',xqedred,qqedred1
5f,'^', xqedblue,qqedblue15f,'v','markersize',10,'linewidth',2)
set(h,'linewidth',2);
xlabel('SDD (cm)','fontsize',13)
ylabel('SDD CF','fontsize',13)
title('15MV or 18 MV, open, SDD Dependence (p-type)','fontsize',13)
axis('square')
axis([60 220 0.96 1.08])
grid on
set(gca,'fontsize',13,'linewidth',1.5,'yticklabel',['0.96'; '0.98'; '1.00'; '1.02'; '1.04'; '1.06';
'1.08'],'xtick',[60 80 100 120 140 160 180 200 220])
gtext('(b)','fontsize',20);
```

Appendix B (Continued)

Figure 14 Paper II

```
% This program analyze the dose rate and SDD dependence of diodes under Co
% Ion chamber data for all (3) diodes
xion=[80 100 130 183.6 206.6];
yion=[1.568 1 .5897 .2980 .2348];
% Data for Isorad Red (n-type)diode
xisored=xion;
yisored=[1.57 1 0.5886 0.2961 0.2328]
qisored=yisored./yion
% Data for Isorad Gold #2 diode
xisoold=xion;
yisoold=[1.573 1 0.5883 0.2966 0.2331];
qisoold=yisoold./yion;
% Data for EDP30 diode
xedp30=xion;
yedp30=[1.569 1 0.5899 0.2960 0.2332];
qedp30=yedp30./yion;
% SDD CF
isoold=1./qisoold;
isored=1./qisored;
edp30=1./qedp30;
figure(1)
h=plot(xisoold,isoold,'o',xisored,isored,'*',xedp30,edp30,'d','markersize',10);
set(h,'linewidth',2);
xlabel('SDD (cm)','fontsize',13)
ylabel('SDD CF','fontsize',13)
title('Co-60, open, SDD Dependence','fontsize',13)
axis('square')
axis([60 220 0.96 1.08])
grid on
set(gca,'fontsize',13,'linewidth',1.5,'yticklabel',['0.96'; '0.98'; '1.00'; '1.02'; '1.04'; '1.06';
        '1.08'],'xtick',[60 80 100 120 140 160 180 200 220])
```

Appendix B (Continued)

```
Figure 15 Paper II
% This program will analyze the Dose rate dependence of diodes
% Ion Chamber  and and Diode Data
% Isorad Red (preirradiated) diode #3 May 8, 2003 measured on Primus 6 and 18 MV
ssdionred_2=[60 70 80 90 100 110 120 130 140 150 172.8 203.2];
yion6red_2=[2.8028 2.0532 1.5702 1.2384 1.0000 0.8255 0.6932 0.5908 0.5100 0.4437
        0.3332 0.2422];
yion18red_2=[2.7957 2.0505 1.5681 1.2352 1.0000 0.8261 0.6930 0.5918 0.5101 0.4444
        0.3337 0.2428];
xisored6_2= yion6red_2.*6169;
xisored18_2= yion18red_2.*13977;
yisored6_2=[2.898 2.1051 1.5914 1.2482 1.0000 0.8186 0.6834 0.5787 0.4963 0.4305
        0.3221 0.2304];
yisored18_2=[2.8306 2.0679 1.5792 1.2377 1.0000 0.8207 0.6870 0.5808 0.4984 0.4320
        0.3217 0.2302];
% Normalize to the corresponding ion chamber value
Sxisored6_2=xisored6_2;
Sxisored6_2=invsq1(ssdionred_2,yion6red_2,ssdionred_2).*6169;
Sisored6_2=yisored6_2./invsq1(ssdionred_2,yion6red_2,ssdionred_2);
Sxisored18_2=xisored18_2;
Sxisored18_2=invsq1(ssdionred_2,yion18red_2,ssdionred_2).*13977;
Sisored18_2=yisored18_2./invsq1(ssdionred_2,yion18red_2,ssdionred_2);
% Isorad Gold #2 measured on May 8, 2003 (Isorad old n-type unirradiated diode
        measured on Primus
ssdionold_2=[60 70 80 90 100 110 120 130 140 150 172.8 203.2];
yion6_2=[2.8028 2.0532 1.5702 1.2384 1.0000 0.8255 0.6932 0.5908 0.5100 0.4437
        0.3332 0.2422];
yion18_2=[2.7957 2.0505 1.5681 1.2352 1.0000 0.8261 0.6930 0.5918 0.5101 0.4444
        0.3337 0.2428];
yisoold6_2=[2.8265 2.0664 1.5755 1.2369 1.0000 0.8243 0.6909 0.5882 0.5060 0.4396
        0.3297 0.2374];
yisoold18_2=[2.8120 2.0559 1.5722 1.2361 1.0000 0.8259 0.6930 0.5908 0.5083 0.4421
        0.3316 0.2395];
% normalize to the corresponding ion chamber value
Sxisoold6_2=invsq1(ssdionold_2,yion6_2,ssdionold_2).*6169;
Sisoold6_2=yisoold6_2./invsq1(ssdionold_2,yion6_2,ssdionold_2);
Sxisoold18_2=invsq1(ssdionold_2,yion18_2,ssdionold_2).*13977;
Sisoold18_2=yisoold18_2./invsq1(ssdionold_2,yion18_2,ssdionold_2);
% Data for Isorad 3 Gold pt doped n-type unirradiated diode
ssdioniso3=[60 70 80 90 100 110 120 130 140 150 172.8 203.1];
yion6iso3=[2.7994 2.0501 1.5651 1.2352 1.0000 0.8255 0.6931 0.5910 0.5084 0.4431
        0.3318 0.2412];
```

Appendix B (Continued)

```
yion18iso3=[2.7865 2.0485 1.5612 1.2325 1.0000 0.8260 0.6939 0.5900 0.5092 0.4437
        0.3327 0.2418];
yiso3gold6=[2.8140 2.059 1.5698 1.2366 1.0000 0.8241 0.6906 0.5880 0.5056 0.4403
        0.3295 0.2366];
yiso3gold18=[2.8003 2.049 1.5664 1.2360 1.0000 0.8242 0.6913 0.5886 0.5071 0.4414
        0.3311 0.2390];
% normalize to the corresponding ion chamber value
Sxiso3gold6=invsq1(ssdioniso3,yion6iso3,ssdioniso3).*6169;
Siso3gold6=yiso3gold6./invsq1(ssdioniso3,yion6iso3,ssdioniso3);
Sxiso3gold18=invsq1(ssdioniso3,yion18iso3,ssdioniso3).*13977;
Siso3gold18=yiso3gold18./invsq1(ssdioniso3,yion18iso3,ssdioniso3);
% Ion chamber data for the QED Blue and Red p-type diodes measured on Siemens KD2
ssdionq=[80 90 100 110 130 140 179.4 202.6];
xionq6=[9911 7813 6322 5228 3736 3219 1957 1540];
xionq15=[17907 14129 11448 9465 6769 5827 3554 2798];
yionq6=[6.2623 4.937 3.9945 3.3033 2.361 2.0343 1.2366 0.9732];
yionq15=[6.953 5.486 4.445 3.675 2.6283 2.2626 1.3800 1.0864];
yionq6=yionq6./3.9945;
yionq15=yionq15./4.445;
% QED Blue p-type data
ssdqedblue=[80 90 100 110 130 140 179.4 202.6];
xqedblue6=[9911 7813 6322 5228 3736 3219 1957 1540];
xqedblue15=[117907 14129 11448 9465 6769 5827 3554 2798];
yqedblue6=[171.96 135.36 109.3 89.7 64.0 55.06 33.35 26.15];
yqedblue15=[188.7 148.3 119.6 98.3 69.96 60.1 36.4 28.4];
yqedblue6=yqedblue6/109.3;
yqedblue15=yqedblue15/119.6;
% normalize to the corresponding ion chamber value
Sxqedblue6=invsq1(ssdionq,yionq6,ssdionq).*6322;
Sqedblue6=yqedblue6./invsq1(ssdionq,yionq6,ssdionq);
Sxqedblue15=invsq1(ssdionq,yionq15,ssdionq).*11448;
Sqedblue15=yqedblue15./invsq1(ssdionq,yionq15,ssdionq);
% QED Red p-type data
ssdqedred=[80 90 100 110 130 140 179.4 202.6];
xqedred6=[9911 7813 6322 5228 3736 3219 1957 1540];
xqedred15=[17907 14129 11448 9465 6769 5827 3554 2798];
yqedred6=[140.16 110.26 89.0 73.2 52.2 44.96 27.3 21.4];
yqedred15=[175.0 137.4 111.03 91.36 65 56.0 34.0 26.7];
yqedred6=yqedred6./89.0;
yqedred15=yqedred15/111.03;
% normalize to the corresponding ion chamber value
Sxqedred6=invsq1(ssdionq,yionq6,ssdionq).*6322;
Sqedred6=yqedred6./invsq1(ssdionq,yionq6,ssdionq);
```

Appendix B (Continued)

```
Sxqedred15=invsq1(ssdionq,yionq15,ssdionq).*11448;
Sqedred15=yqedred15./invsq1(ssdionq,yionq15,ssdionq);
% Ion chamber data for Isorad Red p-type, EDP20-3G, Veridose Green diodes
ssdionprimus=[80 90 100 110 130 150 175.3 205.8];
xion6primus=[9702 7702 6231 5135 3670 2754 2019 1464];
xion18primus=[22220 17599 14262 11766 8414 6304 4621 3352];
yion6primus=[1.557 1.2363 1.0000 0.8245 0.5895 0.4418 0.3236 0.2346];
yion18primus=[1.558 1.2342 1.0000 0.8253 0.5900 0.4420 0.3242 0.2353];
% Ion chamber data - same data as above except it has new data for 80 cm SSD taken on
      6/28/03
ssdionprimusv=[80 90 100 110 130 150 175.3 205.8];
yion6primusv=[1.5652 1.2363 1.0000 0.8245 0.5895 0.4418 0.3236 0.2346];
yion18primusv=[1.561 1.2342 1.0000 0.8253 0.5900 0.4420 0.3242 0.2353];
% Data for EDP20-3G p-type diode
xedp20=[80 90 100 110 130 150 175.3 205.8];
yedp206=[1.562 1.238 1.000 0.825 0.589 0.444 0.323 0.235];
yedp2018=[1.559  1.236 1.000 0.824 0.588 0.444 0.324 0.235];
% Normalize to the corresponding ion chamber value
Sxedp206=invsq1(ssdionprimus,yion6primus,ssdionprimus).*6169;
Sedp206=yedp206./invsq1(ssdionprimus,yion6primus,ssdionprimus);
Sxedp2018=invsq1(ssdionprimus,yion18primus,ssdionprimus).*13977;
Sedp2018=yedp2018./invsq1(ssdionprimus,yion18primus,ssdionprimus);
% Isorad-p red (preirradiated, p-type) diode
xisoredp=[80 90 100 110 130 150 175.3 205.8];
yisoredp6=[1.583 1.246 1.000 0.821 0.581 0.433 0.315 0.227];
yisoredp18=[1.596 1.248 1.000 0.817 0.578 0.429 0.312 0.224];
% Normalize to the corresponding ion chamber value
Sxisoredp6=invsq1(ssdionprimus,yion6primus,ssdionprimus).*6169;
Sisoredp6=yisoredp6./invsq1(ssdionprimus,yion6primus,ssdionprimus);
Sxisoredp18=invsq1(ssdionprimus,yion18primus,ssdionprimus).*13977;
Sisoredp18=yisoredp18./invsq1(ssdionprimus,yion18primus,ssdionprimus);
xvergreen=[80 90 100 110 130 150 175.3 205.8];
yvergreen6=[1.5796 1.2410 1.0000 0.8236 0.5863 0.4383 0.3205 0.2322];
yvergreen18=[1.5737 1.2408 1.0000 0.8249 0.5868 0.4390 0.3208 0.2319];
% Normalize to the corresponding ion chamber value
Sxvergreen6=invsq1(ssdionprimusv,yion6primusv,ssdionprimusv).*6169;
Svergreen6=yvergreen6./invsq1(ssdionprimusv,yion6primusv,ssdionprimusv);
Sxvergreen18=invsq1(ssdionprimusv,yion18primusv,ssdionprimusv).*13977;
Svergreen18=yvergreen18./invsq1(ssdionprimusv,yion18primusv,ssdionprimusv);
% Ion chamber for QED Red n-type pt doped diode
ssdionq2=[60 70 80 90 100 110 120 130 140 150 175.1 205.1];
yion6q=[2.7985 2.0451 1.5588 1.2349 1.0000 0.8220 0.6910 0.5887 0.5073 0.4406
      0.3249 0.2352];
```

Appendix B (Continued)

```
yion18q=[2.7989 2.0441 1.5593 1.2322 1.0000 0.8215 0.6910 0.5881 0.5073 0.4407
        0.3252 0.2359];
xion6q=yion6q.*6169;
xion18q=yion18q.*13977;
% Data for QED Red pt doped n-type diode
xqed2n=[60 70 80 90 100 110 120 130 140 150 175.1 205.1];
yqed2n6=[2.8404 2.0729 1.5779 1.2410 1.0000 0.8235 0.6892 0.5848 0.5027 0.4367
        0.3184 0.2300];
yqed2n18=[2.8166 2.0565 1.5707 1.2375 1.0000 0.8220 0.6891 0.5851 0.5027 0.4372
        0.3195 0.2306];
% Normalize to the corresponding ion chamber value
Sxqed2n6=invsq1(ssdionq2,yion6q,ssdionq2).*6169;
Sqed2n6=yqed2n6./invsq1(ssdionq2,yion6q,ssdionq2);
Sxqed2n18=invsq1(ssdionq2,yion18q,ssdionq2).*13977;
Sqed2n18=yqed2n18./invsq1(ssdionq2,yion18q,ssdionq2);
% Ion chamber data for EDP10-3G diode on Siemens Primus
ssdione=[60 70 80 90 100 110 120 130 140 150 172.8 203];
yione6=[2.7984 2.0496 1.5652 1.2361 1.0000 0.8245 0.6931 0.5905 0.5085 0.4424
        0.3343 0.2420];
yione18=[2.7903 2.0431 1.5614 1.2311 1.0000 0.8239 0.6911 0.5898 0.5079 0.4429
        0.3339 0.2425];
% Data for EDP10-3G diode
ssdedp10=[60 70 80 90 100 110 120 130 140 150 172.8 203];
xedp106=[6215 3943 2309 1729 1287 952 280];
xedp1018=[14663 9293 5452 4080 3021 2239 665];
yedp106=[2.8101 2.0551 1.5711 1.2402 1.0000 0.8231 0.6913 0.5879 0.5065 0.4408
        0.3319 0.2407];
yedp1018=[2.8068 2.0527 1.5699 1.2397 1.0000 0.8232 0.6911 0.5882 0.5062 0.4405
        0.3323 0.2410];
% Normalize to the corresponding ion chamber value
Sxedp106=invsq1(ssdione,yione6,ssdione).*6169;
Sedp106=yedp106./invsq1(ssdione,yione6,ssdione);
Sxedp1018=invsq1(ssdione,yione18,ssdione).*13977;
Sedp1018=yedp1018./invsq1(ssdione,yione18,ssdione);
% Normalize all Sensitivity to that for dose rate of 4000 for linac and 1.6 for Co
Siso3gold6=Siso3gold6./interp1(Sxiso3gold6,Siso3gold6,4000);
Siso3gold18=Siso3gold18./interp1(Sxiso3gold18,Siso3gold18,4000);
Sisoold6_2=Sisoold6_2./interp1(Sxisoold6_2,Sisoold6_2,4000);
Sisoold18_2=Sisoold18_2./interp1(Sxisoold18_2,Sisoold18_2,4000);
Sisored6_2=Sisored6_2./interp1(Sxisored6_2,Sisored6_2,4000);
Sisored18_2=Sisored18_2./interp1(Sxisored18_2,Sisored18_2,4000);
Sedp106=Sedp106./interp1(Sxedp106,Sedp106,4000);
Sedp1018=Sedp1018./interp1(Sxedp1018,Sedp1018,4000);
```

Appendix B (Continued)

```
Sqedred6=Sqedred6./interp1(Sxqedred6,Sqedred6,4000);
Sqedred15=Sqedred15./interp1(Sxqedred15,Sqedred15,4000);
Sqedblue6=Sqedblue6./interp1(Sxqedblue6,Sqedblue6,4000);
Sqedblue15=Sqedblue15./interp1(Sxqedblue15,Sqedblue15,4000);
Sedp206=Sedp206./interp1(Sxedp206,Sedp206,4000);
Sedp2018=Sedp2018./interp1(Sxedp2018,Sedp2018,4000);
Sisoredp6=Sisoredp6./interp1(Sxisoredp6,Sisoredp6,4000);
Sisoredp18=Sisoredp18./interp1(Sxisoredp18,Sisoredp18,4000);
Svergreen6=Svergreen6./interp1(Sxvergreen6,Svergreen6,4000);
Svergreen18=Svergreen18./interp1(Sxvergreen18,Svergreen18,4000);
Sqed2n6=Sqed2n6./interp1(Sxqed2n6,Sqed2n6,4000);
Sqed2n18=Sqed2n18./interp1(Sxqed2n18,Sqed2n18,4000).*0.997;
% Combining the data for low and high energies for each diode
xiso3gold=[Sxiso3gold6, Sxiso3gold18];
iso3gold=[Siso3gold6, Siso3gold18.*.998];
xisoold_2=[Sxisoold6_2, Sxisoold18_2];
isoold_2=[Sisoold6_2, Sisoold18_2.*1.003];
xisored_2=[Sxisored6_2, Sxisored18_2];
isored_2=[Sisored6_2, Sisored18_2.*1.005];
xvergreen=[Sxvergreen6,Sxvergreen18];
vergreen=[Svergreen6,Svergreen18];
xedp20=[Sxedp206,Sxedp2018];
edp20=[Sedp206,Sedp2018];
xisoredp=[Sxisoredp6,Sxisoredp18];
isoredp=[Sisoredp6,Sisoredp18];
xedp10=[Sxedp106,Sxedp1018];
edp10=[Sedp106,Sedp1018];
xqedred=[Sxqedred6,Sxqedred15];
qedred=[Sqedred6,Sqedred15];
xqedblue=[Sxqedblue6,Sxqedblue15];
qedblue=[Sqedblue6,Sqedblue15];
xqed2n=[Sxqed2n6,Sxqed2n18];
qed2n=[Sqed2n6,Sqed2n18];
% For Isorad Gold #2 n-type unirr measured on May 8, 2003
xf=0:4*10^4;
beta1=2.94*10^(-5);
beta2=3.03*10^(-4);
beta1=2.47*10^(-5); % refit
beta2=2.36*10^(-4);
s1a=((beta1*xf));
s1b=(1+(beta2*xf));
s1=s1a./s1b;
s2=((beta1*4000))/(1+(beta2*4000));
```

Appendix B (Continued)

```
yf1=sqrt((1+s1)/(1+s2));
% For Isorad-3 Gold
beta1=6.42*10^(-4);
beta2=15.6*10^(-4);
beta1=9.58*10^(-6);
beta2=1.88*10^(-4);
s1a=((beta1*xf));
s1b=(1+(beta2*xf));
s1=s1a./s1b;
s2=((beta1*4000))/(1+(beta2*4000));
yf2=sqrt((1+s1)/(1+s2));
% For Isorad Red #2, n-type preirr measured on May 8, 2003
beta1=6.40*10^(-5);
beta2=1.73*10^(-4);
s1a=((beta1*xf));
s1b=(1+(beta2*xf));
s1=s1a./s1b;
s2=((beta1*4000))/(1+(beta2*4000));
yf3=sqrt((1+s1)/(1+s2));
% For Isorad Veridose Green
beta1=1.59*10^(-5);
beta2=1.73*10^(-4);
beta1=8.22*10^(-6);
beta2=7.63*10^(-5);
s1a=((beta1*xf));
s1b=(1+(beta2*xf));
s1=s1a./s1b;
s2=((beta1*4000))/(1+(beta2*4000));
yf4=sqrt((1+s1)/(1+s2));
% For QED Red (n-type) Pt-dopes
beta1=6.03*10^(-5);
beta2=3.63*10^(-4);
beta1=5.80*10^(-5); % refit
beta2=3.68*10^(-4);
s1a=((beta1*xf));
s1b=(1+(beta2*xf));
s1=s1a./s1b;
s2=((beta1*4000))/(1+(beta2*4000));
yf5=sqrt((1+s1)/(1+s2));
% for Isorad 3 Gold measured on May 8, 2003
beta1=3.4*10^(-5);
beta2=4.6*10^(-4);
s1a=((beta1*xf));
```

Appendix B (Continued)

```
s1b=(1+(beta2*xf));
s1=s1a./s1b;
s2=((beta1*4000))/(1+(beta2*4000));
yf6=sqrt((1+s1)/(1+s2));
% For EDP30
beta1=3.06*10^(-7);
beta2=0;
beta1=1.83*10^(-7);
beta2=2.06*10^(-6);
beta1=2.9*10^(-6);
beta2=1.0*10^(-4);
s1a=((beta1*xf));
s1b=(1+(beta2*xf));
s1=s1a./s1b;
s2=((beta1*4000))/(1+(beta2*4000));
yf1p=sqrt((1+s1)/(1+s2));
% For EDP10-3G
beta1=2.268*10^(-6);
beta2=3.196*10^(-5);
s1a=((beta1*xf));
s1b=(1+(beta2*xf));
s1=s1a./s1b;
s2=((beta1*4000))/(1+(beta2*4000));
yf1p=sqrt((1+s1)/(1+s2));
xf1=0:2.2*10^4;
% for EDP20-3G
beta1=1.0*10^(-9);
beta2=0;
beta1=5.3*10^(-7);
beta2=9.6*10^(-6);
beta1=1.05*10^(-6);
beta2=2.5*10^(-4);
s1a=((beta1*xf1));
s1b=(1+(beta2*xf1));
s1=s1a./s1b;
s2=((beta1*4000))/(1+(beta2*4000));
yf2p=sqrt((1+s1)/(1+s2));
xf2=0:1.8*10^4;
% For QED Blue p-type
beta1=1.0*10^(-5);
beta2=5.52*10^(-5);
beta1=8.26*10^(-6);  % refit
beta2=2.90*10^(-5);
```

Appendix B (Continued)

```
s1a=((beta1*xf2));
s1b=(1+(beta2*xf2));
s1=s1a./s1b;
s2=((beta1*4000))/(1+(beta2*4000));
yf3p=sqrt((1+s1)/(1+s2));
% For QED Red p-type
beta1=4.67*10^(-6);
beta2=1.07*10^(-5);
s1a=((beta1*xf2));
s1b=(1+(beta2*xf2));
s1=s1a./s1b;
s2=((beta1*4000))/(1+(beta2*4000));
yf4p=sqrt((1+s1)/(1+s2));
% For Isorad Red (p-type)
beta1=1.97*10^(-5);
beta2=4.86*10^(-5);
beta1=2.11*10^(-5);
beta2=5.41*10^(-5);
s1a=beta1*xf1;
s1b=1+(beta2*xf1);
s1=s1a./s1b;
s2=(beta1*4000)/(1+(beta2*4000));
yf5p=sqrt((1+s1)/(1+s2));
%for EDP30 diode
dedp30=0:3*10^4;
beta11=6.0*10^(-7);
beta22=0;
ss1a=beta11*dedp30;
ss1b=1+(beta22*dedp30);
ss1=ss1a./ss1b;
ss2=1+(beta11*4000)/(1+(beta22*4000));
ss=sqrt((1+ss1)/ss2);
figure(1)
h=plot(xisoold_2,isoold_2,'o',xisored_2,isored_2,'+',xiso3gold,iso3gold,'>',xvergreen,ver
        green,'<',xqed2n,qed2n,'x','markersize',10)
hold on
plot(xf,yf1,'-',xf,yf2,'-',xf,yf6,'-',xf,yf3,'-',xf,yf4,'-',xf,yf5,'linewidth',2);
hold off
set(h,'linewidth',2);
xlabel('Instantaneous dose rate (cGy/s)','Fontsize',13);
ylabel('S/S(4000)','Fontsize',13);
set(gca,'linewidth',1.2,'Fontsize',13);
title('Dose Rate Dependence (n-type)','fontsize',13);
```

Appendix B (Continued)

```
axis('square');
axis([0 40000 0.92 1.1]);
grid on;
set(gca,'fontsize',13,'linewidth',1.5)
gtext('(a)','fontsize',20);
figure(2)
h=plot(xedp10,edp10,'d',xedp20,edp20,'x',xqedblue,qedblue,'v',xqedred,qedred,'^',xisored
        p,isoredp,'*','markersize',10)
hold on
plot(xf,yf1p,'-',xf1,yf2p,'-',xf2,yf3p,'-',xf2,yf4p,'-',xf1,yf5p,'-','linewidth',2);
hold off
set(h,'linewidth',2);
xlabel('Instantaneous dose rate (cGy/s)','Fontsize',13);
ylabel('S/S(4000)','Fontsize',13);
set(gca,'linewidth',1.2,'Fontsize',13);
title('Dose Rate Dependence (p-type)','fontsize',13);
axis('square');
axis([0 40000 0.92 1.1]);
grid on;
set(gca,'fontsize',13,'linewidth',1.5)
gtext('(b)','fontsize',20);
```

Appendix B (Continued)

Figure 16 Paper II

```
% This program analyzes the Dose rate dependence of diodes
% Ion chamber for Isorad Gold #2 diode and EDP30 diode on Varian
ssdion=[70 80 90 100 110 120 130 137];   % checked ok.
xion8=[15223 11934 9394 7575 6237 5225 4437 3987];
xion18=[34856 27365 21531 17361 14279 11953 10139 9107];
yion8=[2.0096 1.5754 1.2402 1.0000 0.8234 0.6897 0.5857 0.5263];
yion18=[2.0077 1.5762 1.2402 1.0000 0.8225 0.6885 0.5840 0.5246];
% Isorad Gold #2 diode data
ssdisoold=[70 80 90 100 110 120 130 137];
xisoold8=[15223 11934 9394 7575 6237 5225 4437 3987];
xisoold18=[34856 27365 21531 17361 14279 11953 10139 9107];
qisoold8=[2525.5 1960.1 1524.7 1217.3 993.9 826.8 698.95 625.9];
qisoold18=[2787.45 2151 1663.65 1322.65 1075.8 892.2 752.1 673.1];
yisoold8=qisoold8./qisoold8(4);
yisoold18=qisoold18./qisoold18(4);
% Normalize to the corresponding ion chamber value
Sxisoold8=xion8;
Sisoold8=yisoold8./yion8;
Sxisoold18=xion18;
Sisoold18=yisoold18./yion18;
% Data for EDP30 diode
ssdedp30=[70 80 90 100 110 120 130 137];
xedp30=[15223 11934 9394 7575 6237 5225 4437 3987];
xedp30=[34856 27365 21531 17361 14279 11953 10139 9107];
qedp308=[1151 902.75 709.65 571.6 470.35 393.45 333.75 299.65];
qedp3018=[1409.15 1104.7 867.25 698.9 574.9 481.05 408.15 367.5];
yedp308=qedp308./qedp308(4);
yedp3018=qedp3018./qedp3018(4);
% Normalize to the corresponding ion chamber value
Sxedp308=xion8;
Sxedp3018=xion18;
Sedp308=yedp308./yion8;
Sedp3018=yedp3018./yion18;
xr=10000;
% Normalize all Sensitivity to that for dose rate of 10000 cGy/s for Varian linac
Sisoold8=Sisoold8./interp1(Sxisoold8,Sisoold8,xr);
Sisoold18=Sisoold18./interp1(Sxisoold18,Sisoold18,xr);
Sedp308=Sedp308./interp1(Sxedp308,Sedp308,15000);
Sedp3018=Sedp3018./interp1(Sxedp3018,Sedp3018,15000);
% Combining the data for low and high energies for each diode
xisoold=[Sxisoold8,Sxisoold18];
```

Appendix B (Continued)

```
isoold=[Sisoold8,Sisoold18];
xedp30=[Sxedp308; Sxedp3018]%
edp30=[Sedp308, Sedp3018];
% For EDP30 diode
dedp30=0:4*10^4;
beta11=6.0*10^(-7);
beta22=0;
ss1a=beta11*dedp30;
ss1b=1+(beta22*dedp30);
ss1=ss1a./ss1b;
ss2=1+(beta11*xr)/(1+(beta22*xr));
ss=sqrt((1+ss1)/ss2);
Sref1=sqrt(ss2);
% For Isorad Gold #2 diode fitting
disoold=0:4*10^4;
beta111=2.3*10^(-5);
beta222=3.8*10^(-5);
sss1a=beta111*disoold;
sss1b=1+(beta222*disoold);
sss1=sss1a./sss1b;
sss2=1+(beta111*xr)/(1+(beta222*xr));
sss=sqrt((1+sss1)/sss2);
Sref2=sqrt(sss2);
figure(1)
plot(Sxisoold8,Sisoold8.*Sref2,'o',Sxisoold18,Sisoold18.*Sref2,'x','markersize',10,'linewi
        dth',2)
hold on
plot(Sxisoold8,Sedp308.*Sref1,'o',Sxisoold18,Sedp3018.*Sref1,'x','markersize',10,'linewi
        dth',2)
plot(disoold,sss.*Sref2,'r-',dedp30,ss.*Sref1,'r-','linewidth',2);
hold off
xlabel('Instantaneous dose rate (cGy/s)','Fontsize',13);
ylabel('S/S(0)','Fontsize',13);
set(gca,'linewidth',1.5,'Fontsize',13);
title('Dose Rate Dependence (n-type)');
axis('square');
axis([0 40000 0.95 1.20]);
grid on;
gtext('(a)','fontsize',20);
figure(2)
plot(Sxisoold8,Sisoold8,'o',Sxisoold18,Sisoold18,'x','markersize',10,'linewidth',2)
hold on
plot(Sxisoold8,Sedp308,'o',Sxisoold18,Sedp3018,'x','markersize',10,'linewidth',2)
```

Appendix B (Continued)

```
plot(disoold,sss,'r-',dedp30,ss,'r-','linewidth',2);
hold off
xlabel('Instantaneous dose rate (cGy/s)','Fontsize',13);
ylabel('S/S(10000)','Fontsize',13);
set(gca,'linewidth',1.5,'Fontsize',13);
title('Dose Rate Dependence (n-type)');
axis('square');
axis([0 40000 0.92 1.10]);
grid on;
gtext('(b)','fontsize',20);
```

Appendix B (Continued)

```
Figure 17 Paper II
% This program analyze the SDD-dependence of diodes on the surface
% This data is taken the same day and measured vertically up to 150 cm
% The ion chamber data for 6 MV was taken at 1.6 cm depth and for 18 MV at 3.2 cm
        %depth with markus chamber
% SDD comparison symbol only - data measured on the surface, symbol with line - data
        %measured in a miniphantom
%====================Surface Data Set  ======================
% Ion chamber used for Isorad Red n-type diode
xioniso=[60 70 80 90 100 110 120 130 140 150];
yion6iso=[2.7564 2.0260 1.5552 1.2315 1.0000 0.8267 0.6964 0.5941 0.5128 0.4472];
        %at 1.6 cm
yion18iso=[2.7728 2.0316 1.5582 1.2321 1.0000 0.8284 0.6962 0.5934 0.5116 0.4455];
        % at 3.2 cm
% Data for Isorad Red n-type (on the surface)
xiso=[60 70 80 90 100 110 120 130 140 150];
yisored6=[2.8769 2.0968 1.5895 1.2440 1.0000 0.8181 0.6843 0.5798 0.4961 0.4310];
yisored18=[2.7971 2.0500 1.5684 1.2386 1.0000 0.8220 0.6853 0.5793 0.4968 0.4296];
qisored6=yion6iso./yisored6;
qisored18=yion18iso./yisored18;
%===============Data from the in mini phantom set =================
% Data for Isorad Red n-type measured in a minphantom on primus
% Ion chamber for Isorad red n-type diode
xionred2=[60 70 80 90 100 110 120 130 140 150];
yion6red_2=[2.8028 2.0532 1.5702 1.2384 1.0000 0.8255 0.6932 0.5908 0.5100 0.4437];
yion18red_2=[2.7957 2.0505 1.5681 1.2352 1.0000 0.8261 0.6930 0.5918 0.5101
        0.4444];
[yion6redf_2, xvion6red]=invsq1(xionred2,yion6red_2,xionred2);
[yion18redf_2, xvion18red]=invsq1(xionred2,yion18red_2,xionred2);
% Data for Isorad Red n-type diode in a minphantom
xisored2=[60 70 80 90 100 110 120 130 140 150 172.8 203.2];
yisored6_2=[2.898 2.1051 1.5914 1.2482 1.0000 0.8186 0.6834 0.5787 0.4963 0.4305];
yisored18_2=[2.8285 2.0679 1.5792 1.2377 1.0000 0.8207 0.6870 0.5808 0.4984
        0.4320];
qisored6f_2=yion6redf_2./yisored6_2;
qisored18f_2=yion18redf_2./yisored18_2;
%====================Surface Data set====================
% Ion chamber data for QED Red n-type diode (pt)
xionq=[60 70 80 90 100 110 120 130 140 150];
yion6q=[2.7564 2.0260 1.5552 1.2315 1.0000 0.8267 0.6964 0.5941 0.5128 0.4472];
yion18q=[2.7878 2.0451 1.5666 1.2365 1.0000 0.8303 0.6984 0.5960 0.5145 0.4477];
% Data for QED Red (n-type) diode
```

Appendix B (Continued)

```
xqed=[60 70 80 90 100 110 120 130 140 150]
yqedred6=[2.8122 2.0577 1.5724 1.2395 1.0000 0.8260 0.6934 0.5904 0.5084 0.4426 ];
yqedred18=[2.8346 2.0689 1.5727 1.2367 1.0000 0.8250 0.6920 0.5881 0.5061 0.4384];
qqedred6=yion6q./yqedred6;
qqedred18=yion18q./yqedred18;
% ==============Mini phantom data set for QED Red (n-type) diode=======
% Data for Ion chamber for QED Red n-type pt doped diode
xionq=[60 70 80 90 100 110 120 130 140 150];
yionq6=[2.7985 2.0451 1.5588 1.2349 1.0000 0.8220 0.6910 0.5887 0.5073 0.4406];
yionq18=[2.7989 2.0441 1.5593 1.2322 1.0000 0.8215 0.6910 0.5881 0.5073 0.4407];
[yionq6f, xvion6q]=invsq1(xionq,yionq6,xionq);
[yionq18f, xvion18q]=invsq1(xionq,yionq18,xionq);
% Data for QED Red n-type pt-doped diode
xqed2n=[60 70 80 90 100 110 120 130 140 150];
yqed2n6=[2.8404 2.0729 1.5779 1.2410 1.0000 0.8235 0.6892 0.5848 0.5027 0.4367];
yqed2n18=[2.8166 2.0565 1.5707 1.2375 1.0000 0.8220 0.6891 0.5851 0.5027 0.4372];
qqed2n6=yionq6f./yqed2n6;
qqed2n18=yionq18f./yqed2n18;
%=====================Surface Data set=========================
% ion chamber data for Isorad 3 Gold Diode
xioniso3=[60 70 80 90 100 110 120 130 140 150];
yion6iso3=[2.7678 2.0346 1.5558 1.2297 1.0000 0.8271 0.6957 0.5939 0.5133 0.4471];
% at 1.6 cm
yion18iso3=[2.7878 2.0451 1.5666 1.2365 1.0000 0.8303 0.6984 0.5960 0.5145 0.4477];
% at 3.2 cm on 9/17/03
% Data for Isorad -3 Gold diode on surface
xiso3=[60 70 80 90 100 110 120 130 140 150]
yiso3gold6=[2.7977 2.0465 1.5633 1.2348 1.0000 0.8264 0.6941 0.5905 0.5102 0.4439];
% Isorad 3 Gold
yiso3gold18=[2.8437 2.0722 1.5741 1.2379 1.0000 0.8250 0.6941 0.5898 0.5077
        0.4416];
% Isorad 3 Gold under 18 on surf on 9/17/03
qiso3gold6=yion6iso3./yiso3gold6;
qiso3gold18=yion18iso3./yiso3gold18;
% ==================mini phantom data set for Isorad 3 Gold diode=====
% Ion chamber data for Isorad 3 Gold diode
xiongold3=[60 70 80 90 100 110 120 130 140 150];
yion6gold3=[2.7994 2.0501 1.5651 1.2352 1.0000 0.8255 0.6931 0.5910 0.5084 0.4431];
yion18gold3=[2.7865 2.0485 1.5612 1.2325 1.0000 0.8260 0.6939 0.5900 0.5092
        0.4437];
[yion6gold3f, xvion6gold3]=invsq1(xiongold3,yion6gold3,xiongold3);
[yion18gold3f, xvion18gold3]=invsq1(xiongold3,yion18gold3,xiongold3);
% Data for Isorad 3 Gold diode
```

Appendix B (Continued)

```
xiso3gold=[60 70 80 90 100 110 120 130 140 150];
yiso3gold6=[2.8140 2.059 1.5698 1.2366 1.0000 0.8241 0.6906 0.5880 0.5056 0.4403];
yiso3gold18=[2.8003 2.049 1.5664 1.2360 1.0000 0.8242 0.6913 0.5886 0.5071 0.4414];
qiso3gold6f=yion6gold3f./yiso3gold6;
qiso3gold18f=yion18gold3f./yiso3gold18;
%================Surface data set ============================
% Ion Chamber data for EDP10-3G diode
xionedp=[60 70 80 90 100 110 120 130 140 150];
yion6edp=[2.7734 2.0319 1.5590 1.2347 1.0000 0.8277 0.6969 0.5955 0.5139 0.4483];
% measured at 1.6048 depth on 9/10/03
yion18edp=[2.7728 2.0316 1.5582 1.2321 1.0000 0.8284 0.6962 0.5934 0.5116 0.4455];
% EDP10 under 18 MV on surface
% Data for EDP10-3G diode
xedp=[60 70 80 90 100 110 120 130 140 150];
yedp106=[2.8162 2.0505 1.5672 1.2373 1.0000 0.8278 0.6958 0.5926 0.5115 0.4457];
yedp1018=[2.8729 2.0660 1.5706 1.2364 1.0000 0.8228 0.6898 0.5867 0.5054 0.4395];
qedp106=yion6edp./yedp106;
qedp1018=yion18edp./yedp1018;
% ==============mini phantom data setfor EDP10-3G diode=============
% Ion chamber data for EDP10-3G diode
xione10=[60 70 80 90 100 110 120 130 140 150];
yion6e10=[2.7984 2.0496 1.5652 1.2361 1.0000 0.8245 0.6931 0.5905 0.5085 0.4424];
yion18e10=[2.7903 2.0431 1.5614 1.2311 1.0000 0.8239 0.6911 0.5898 0.5079 0.4429];
%This fitting is only used for the EDP 10-3G diode
[yion6e10f, xvion6]=invsq1(xione10,yion6e10,xione10);
[yion18e10f, xvion18]=invsq1(xione10,yion18e10,xione10);
% Data for EDP10-3G diode
xedp10=[60 70 80 90 100 110 120 130 140 150];
yedp106f=[2.8101 2.0551 1.5711 1.2402 1.0000 0.8231 0.6913 0.5879 0.5065 0.4408];
yedp1018f=[2.8068 2.0527 1.5699 1.2397 1.0000 0.8232 0.6911 0.5882 0.5062 0.4405];
qedp106f=yion6e10f./yedp106f;
qedp1018f=yion18e10f./yedp1018f;
%====================Figures=========================
figure(1)
h=plot(xioniso,qisored6,'b+-',xionred2,qisored6f_2,'b+--',xionq,qqedred6,'rx-
        ',xionq,qqed2n6,'rx--',xioniso3,qiso3gold6,'g>-',xiongold3,qiso3gold6f,'g>--
        ',xionedp,qedp106,'kd-',xione10,qedp106f,'kd--');
set(h,'linewidth',2);
set(h,'markersize',10);
xlabel('SDD (cm)','fontsize',13);
ylabel('SDD CF','fontsize',13);
title('SDD Dependence, 6 MV','fontsize',13);
set(gca,'fontsize',13,'linewidth',1.5,'yticklabel',['0.95';'0.96'; '0.97'; '0.98'; '0.99';'1.00';
```

Appendix B (Continued)

```
'1.01'; '1.02'; '1.03'; '1.04'],'xtick',[60 80 100 120 140 160])
axis('square');
axis([60 160 0.95 1.04]);
grid on;
gtext('(a)','fontsize',20);
figure(2)
h=plot(xioniso,qisored18,'b+-',xionred2,qisored18f_2,'b+--',xionq,qqedred18,'rx-
        ',xionq,qqed2n18,'rx--',xioniso3,qiso3gold18,'g>-',xiongold3,qiso3gold18f,'g>--
        ',xionedp,qedp1018,'kd-',xione10,qedp1018f,'kd--');
set(h,'linewidth',2);
set(h,'markersize',10);
xlabel('SDD (cm)','fontsize',13);
ylabel('SDD CF','fontsize',13);
title('SDD Dependence, 18 MV','fontsize',13);
set(gca,'fontsize',13,'linewidth',1.5,'yticklabel',['0.95';'0.96'; '0.97'; '0.98'; '0.99';'1.00';
        '1.01'; '1.02'; '1.03'; '1.04'],'xtick',[60 80 100 120 140 160])
axis('square');
axis([60 160 0.95 1.04]);
grid on;
gtext('(b)','fontsize',20);
```

Appendix C Mat Lab Codes for Energy Dependence Study (Paper III)

Figure 19 and Figure 20 Paper III

```
%This program will analyze the Dose rate dependence of diodes
xr=0;
%Dose rate correction data
%for Isorad Gold 3 diode fitting
disogold3=0:4*10^4;
beta1=9.6*10^(-6);
beta2=1.9*10^(-4);
s1a=beta1*disogold3;
s1b=1+(beta2*disogold3);
s1=s1a./s1b;
s2=1+(beta1*xr)/(1+(beta2*xr));
s=sqrt((1+s1)/s2);
%for EDP203g diode
dedp20=0:4*10^4;
beta11=1.0*10^(-6);
beta22=2.5*10^(-4);
ss1a=beta11*dedp20;
ss1b=1+(beta22*dedp20);
ss1=ss1a./ss1b;
ss2=1+(beta11*xr)/(1+(beta22*xr));
ss=sqrt((1+ss1)/ss2);
Sref1=sqrt(ss2);
%for EDP10-3G diode
dedp10=0:4*10^4;
beta111=2.3*10^(-6);
beta222=3.2*10^(-5);
sss1a=beta111*dedp10;
sss1b=1+(beta222*dedp10);
sss1=sss1a./sss1b;
sss2=1+(beta111*xr)/(1+(beta222*xr));
sss=sqrt((1+sss1)/sss2);
Sref2=sqrt(sss2);
%for verisodes diodes
dvergreen=0:4*10^4;
beta1ver=8.2*10^(-6);
beta2ver=7.6*10^(-5);
s1aver=beta1ver*dvergreen;
s1bver=1+(beta2ver*dvergreen);
s1ver=s1aver./s1bver;
s2ver=1+(beta1ver*xr)/(1+(beta2ver*xr));
sver=sqrt((1+s1ver)/s2ver);
```

Appendix C (Continued)

```
Srefver=sqrt(s2ver);
%for QED n-type diodes (QEd Gold n-will be used for both pt diode)
dqedn=0:4*10^4;
beta1qedn=5.8*10^(-5);
beta2qedn=3.8*10^(-4);
s1aqedn=beta1qedn*dqedn;
s1bqedn=1+(beta2qedn*dqedn);
s1qedn=s1aqedn./s1bqedn;
s2qedn=1+(beta1qedn*xr)/(1+(beta2qedn*xr));
sqedn=sqrt((1+s1qedn)/s2qedn);
Srefqedn=sqrt(s2qedn);
%for Isorad Red n-type (the old style) diodes
disored=0:4*10^4;
beta1isored=6.1*10^(-5);
beta2isored=1.6*10^(-4);
s1aisored=beta1isored*disored;
s1bisored=1+(beta2isored*disored);
s1isored=s1aisored./s1bisored;
s2isored=1+(beta1isored*xr)/(1+(beta2isored*xr));
sisored=sqrt((1+s1isored)/s2isored);
Srefisored=sqrt(s2isored);
% For QED Blue p-type
dqedbluep=0:4*10^4;
beta1qedbluep=8.3*10^(-6);
beta2qedbluep=2.9*10^(-5);
s1aqedbluep=beta1qedbluep*dqedbluep;
s1bqedbluep=1+(beta2qedbluep*dqedbluep);
s1qedbluep=s1aqedbluep./s1bqedbluep;
s2qedbluep=1+(beta1qedbluep*xr)/(1+(beta2qedbluep*xr));
sqedbluep=sqrt((1+s1qedbluep)/s2qedbluep);
Srefqedbluep=sqrt(s2qedbluep);
%For QED Red p-type
dqedredp=0:4*10^4;
beta1qedredp=4.7*10^(-6);
beta2qedredp=1.1*10^(-5);
s1aqedredp=beta1qedredp*dqedredp;
s1bqedredp=1+(beta2qedredp*dqedredp);
s1qedredp=s1aqedredp./s1bqedredp;
s2qedredp=1+(beta1qedredp*xr)/(1+(beta2qedredp*xr));
sqedredp=sqrt((1+s1qedredp)/s2qedredp);
Srefqedredp=sqrt(s2qedredp);
```

Appendix C (Continued)

```
% For edp30 old type
dedp30=0:4*10^4;
beta1edp30=4.7*10^(-6);
beta2edp30=1.1*10^(-5);
s1aedp30=beta1edp30*dedp30;
s1bedp30=1+(beta2edp30*dedp30);
s1edp30=s1aedp30./s1bedp30;
s2edp30=1+(beta1edp30*xr)/(1+(beta2edp30*xr));
sedp30=sqrt((1+s1edp30)/s2edp30);
Srefedp30=sqrt(s2edp30);
% Instan. dose rate correction
insdr = [1.23 6999 12137 15169 13907]
driso3gold=interp1(disogold3, s, insdr)
dredp203g=interp1(dedp20, ss, insdr)
dredp103g=interp1(dedp10, sss, insdr)
drvergreen=interp1(dvergreen, sver, insdr)
drqedn=interp1(dqedn, sqedn, insdr)
drisored=interp1(disored, sisored, insdr)  %the older n-type
drqedredp=interp1(dqedredp, sqedredp, insdr)
dredp30=interp1(dedp30, sedp30, insdr)
%====================================
%energy=[1.25, 6, 10, 15, 18]
energy=[1.25, 4.9, 8.9, 13.22, 15]
mu=100
%time-1min
% dose at 5cm depth at SAD=100cm, for 10x10 fs
dr=83.37;
tmrco=.878;
isco=1.01;
output=1;
doseco=dr*tmrco*isco;
%dr=1cgy/mu at dmax at ssd setup
% Oncor
tmr6x=.922;
is6x=1.02819;
output6x=1.011;
dose6x = tmr6x*is6x*mu/output6x
% Oncor
tmr10x=.963;
is10x=1.0465;
output10x=1.012;
dose10x = tmr10x*is10x*mu/output10x
% Iokd
```

Appendix C (Continued)

```
tmr15x=.986;
is15x=1.0506;
output15x=1.001;
dose15x = tmr15x*is15x*mu/output15x
% Primus
tmr18x=.994;
is18x=1.065;
output18x=1.02;
dose18x = tmr18x*is18x*mu/output18x
dose=[doseco dose6x dose10x dose15x dose18x]
% Charge Reading (measured Data)
edp103g=[21.197 25.08 26.94 27.74 28.80]
edp203g=[20.265 24.18 27.03          28.36 30.00]
edpelectron3g=[22.05 27.39 28.80 28.92 29.97]
pfd=[24.82 31.77 33.28 33.30 34.05];
vergreen=[98.7 130.53 158.23 171.80          188.57];
veryellow=[129.5 170.50 190.70 196.88 211.53];
verelectron=[114.87 155.8 167.47 166.40 178.19];
qedgoldn=[22.55 28.50 32.25 33.70 35.99];
qedredn=[23.37 27.6 31.28 32.71 35.38];
iso3gold=[16.27 21.25  24.85 26.28 28.10];
iso3golda=[17.6 23.167 27.277 28.64 30.67];
% Temperature Correction (used from the temp dependence paper and measured data) .
edp10tc=0.25
edp20tc=0.25
edpelectrontc=0.25
pfdtc=0.25
vergreentc=0.5
veryellowtc=0.5
verelectrontc=0.5 % verisode coefficient needed
qedgoldntc=0.63
qedredntc=0.66
iso3goldtc = 0.515
temp=[23.5 22.8 22.8 19 19];
edp103gt=edp103g-(([temp]-22)*edp10tc)
edp203gt=edp203g-(([temp]-22)*edp20tc)
edpelectron3gt=edpelectron3g-(([temp]-22)*edpelectrontc)
pfdt=pfd-(([temp]-22)*pfdtc)
vergreent=vergreen-(([temp]-22)*vergreentc)
veryellowt=veryellow-(([temp]-22)*veryellowtc)
verelectront=verelectron-(([temp]-22)*verelectrontc)
qedgoldnt=qedgoldn-(([temp]-22)*qedgoldntc)
qedrednt=qedredn-(([temp]-22)*qedredntc)
```

Appendix C (Continued)

```
iso3goldt=iso3gold-(([temp]-22)*iso3goldtc)
iso3goldat=iso3golda-(([temp]-22)*iso3goldtc)
%nc/cGy
edp103gnc=edp103gt./dose;
edp203gnc=edp203gt./dose;
edpelectron3gnc=edpelectron3gt./dose;
pfdnc=pfdt./dose;
vergreennc=vergreent./dose;
veryellownc=veryellowt./dose;
verelectronnc=verelectront./dose;
qedgoldnnc=qedgoldnt./dose;
qedrednnc=qedrednt./dose;
iso3goldnc=iso3goldt./dose;
iso3goldanc=iso3goldat./dose;
% normalized n/Gy to Co-60 beam
edp103gnc_norm = edp103gnc./edp103gnc(1);
edp203gnc_norm = edp203gnc./edp203gnc(1);
edpelectron3gnc_norm=edpelectron3gnc./edpelectron3gnc(1);
pfdnc_norm=pfdnc./pfdnc(1);
vergreennc_norm=vergreennc./vergreennc(1);
veryellownc_norm=veryellownc./veryellownc(1);
verelectronnc_norm=verelectronnc./verelectronnc(1);
qedgoldnnc_norm=qedgoldnnc./qedgoldnnc(1);
qedrednnc_norm=qedrednnc./qedrednnc(1);
iso3goldnc_norm=iso3goldnc./iso3goldnc(1);
iso3goldanc_norm=iso3goldanc./iso3goldanc(1);
%After correcting for the d.r dependence
edp103gnc_norm = edp103gnc_norm./dredp103g;
edp203gnc_norm = edp203gnc_norm./dredp203g;
edpelectron3gnc_norm = edpelectron3gnc_norm./dredp203g;
pfdnc_norm=pfdnc_norm./dredp203g;
vergreennc_norm=vergreennc_norm./drvergreen;
veryellownc_norm=veryellownc_norm./drvergreen;
verelectronnc_norm=verelectronnc_norm./drvergreen;
qedgoldnnc_norm=qedgoldnnc_norm./drqedn;
qedrednnc_norm=qedrednnc_norm./drqedn;
iso3goldnc_norm=iso3goldnc_norm./driso3gold;
iso3goldanc_norm=iso3goldanc_norm./driso3gold;
figure(1)
plot(energy, edp103gnc_norm,'mo-',energy,edp203gnc_norm,'x--
        ',energy,edpelectron3gnc_norm,'r+:',energy,pfdnc_norm,'g*-
        ',energy,vergreennc_norm,'rv--','markersize',10,'linewidth',2)
hold on
```

Appendix C (Continued)

```
plot(energy, veryellownc_norm,'m^-.',energy,verelectronnc_norm,'p-
        ',energy,qedgoldnnc_norm,'>-',energy,qedrednnc_norm,'r<-
        ','markersize',10,'linewidth',2)
hold on
plot(energy,iso3goldnc_norm,'s-
        ',energy,iso3goldanc_norm,'d:','markersize',10,'linewidth',2)
hold off
h = legend('EDP10^3^G','EDP20^3^G','EDP2^3^G','PFD','Veridose Green','Veridose
        Yellow','Veridose Electron','QED Gold (n-type)','QED Red (n-type)','Isorad 3
        Gold #1','Isorad 3 Gold #2',0);
xlabel('Nominal Accelerating Potential (MV)','Fontsize',13);
ylabel('Normalized Sensitivity','Fontsize',13);
set(gca,'linewidth',1.5,'Fontsize',13);
title('Energy Dependence');
axis('square');
axis([0 20 0.70 1.50]);
grid on;
%============Data for Figure (2)===========
nenergy=[1.25 4.8 6.25 16 17];
% nc/Gy
isoelectron=[1.174      1.136 1.111     1.052 1.063];
isored=[0.6395          0.6969 0.7308 0.9396 0.9874];
edp10=[0.2639           0.2517 0.253    0.2626 0.2668];
qedelectronp=[0.6839 0.6565 0.6436 0.6203 0.6176]
qedbluep=[0.5818        0.5614 0.5495 0.5469 0.5516];
% qedgold=[0.4449    0.396   .4187   0.4712 0.4641];
qedredp=[0.4699         0.4581 0.4619 0.5319 0.5521];
%Normalized sensitivty
isoelectron=isoelectron./isoelectron(1);
isored=isored./isored(1);
edp10=edp10./edp10(1);
qedelectronp=qedelectronp./qedelectronp(1);
qedbluep=qedbluep./qedbluep(1);
%qedgold=qedgold./qedgold(1);
qedredp=qedredp./qedredp(1);
% Instan. dose rate correction
insdr1 = [1.9 4480 7575 17361 9789]
drqedbluep=interp1(dqedbluep, sqedbluep, insdr1)
drqedredp=interp1(dqedredp, sqedredp, insdr1)
drisored=interp1(disored, sisored, insdr1)  %the older n-type
dredp30=interp1(dedp30, sedp30, insdr1)
isoelectron = isoelectron./drisored;
isored=isored./drisored;
```

Appendix C (Continued)

```
edp10=edp10./dredp30;
qedelectronp=qedelectronp./drqedbluep;
qedbluep=qedbluep./drqedbluep;
qedredp=qedredp./drqedredp;

figure(2)
plot(nenergy, isoelectron,'o-',nenergy,isored,'x-
        ',nenergy,edp10,'+:',nenergy,qedelectronp,'*-',nenergy,qedbluep,'v--
        ',nenergy,qedredp,'^-','markersize',10,'linewidth',2)
h = legend('Isorad Electron','Isorad Red','EDP10','QED Electron (p-type)','QED Blue (p-
        type)','QED Red (p-type)',0);
xlabel('Nominal Accelerating Potential (MV)','Fontsize',13);
ylabel('Normalized Sensitivity','Fontsize',13);
set(gca,'linewidth',1.5,'Fontsize',13);
title('Energy Dependence');
axis('square');
axis([0 20 0.70 1.50]);
grid on;

% Differences
edp103g=((max(edp103gnc_norm)/min(edp103gnc_norm))-1)*100
edp203g=((max(edp203gnc_norm)/min(edp203gnc_norm))-1)*100
edp2=((max(edpelectron3gnc_norm)/min(edpelectron3gnc_norm))-1)*100
pfd=((max(pfdnc_norm)/min(pfdnc_norm))-1)*100
vergreen=((max(vergreennc_norm)/min(vergreennc_norm))-1)*100
veryellow=((max(veryellownc_norm)/min(veryellownc_norm))-1)*100
verelectron=((max(verelectronnc_norm)/min(verelectronnc_norm))-1)*100
qedgoldn=((max(qedgoldnnc_norm)/min(qedgoldnnc_norm))-1)*100
qedredn=((max(qedrednnc_norm)/min(qedrednnc_norm))-1)*100
iso3goldn=((max(iso3goldnc_norm)/min(iso3goldnc_norm))-1)*100
iso3goldan=((max(iso3goldanc_norm)/min(iso3goldanc_norm))-1)*100

% differences
isoelectron=((max(isoelectron)/min(isoelectron))-1)*100
isored=((max(isored)/min(isored))-1)*100
edp10=((max(edp10)/min(edp10))-1)*100
qedelectronp=((max(qedelectronp)/min(qedelectronp))-1)*100
qedbluep=((max(qedbluep)/min(qedbluep))-1)*100
qedredp=((max(qedredp)/min(qedredp))-1)*100
perdiff=[edp103g edp203g edp2 pfd vergreen veryellow qedgoldn qedredn iso3goldn
        iso3goldan isoelectron isored qedelectronp qedbluep qedredp]
```

Appendix D Mat Lab Codes for the Dosimetric Study (Paper IV)

Figure 23 Paper IV

```
%SSD Dependence, ion data for 6 MV at 1.6 cm depth,18 MV at 3.2 cm depth with
markus chamber, diodes placed on surface with 10x10 field size at 100 SAD setup
% Ion chamber data for the QED Gold diode at 6 MV
xion=[60 70 80 90 100 110 120 130 140 150];
yion6q=[2.7576 2.0265 1.5545 1.2311 1.0000 0.8273 0.6968 0.5942 0.5132 0.4475];
% Ion chamber data for the QED Red diode at 18 MV
yion18q=[2.7878 2.0451 1.5666 1.2365 1.0000 0.8303 0.6984 0.5960 0.5145 0.4477];
% Ion chamber data for the Isorad 3 Gold diode at 6 MV
yion6iso=[2.7678 2.0346 1.5558 1.2297 1.0000 0.8271 0.6957 0.5939 0.5133 0.4471];
% Ion chamber data for the Isorad 3 Red diode at 18 MV
yion18iso=[2.7703 2.0347 1.5579 1.2317 1.0000 0.8258 0.6950 0.5931 0.5116 0.4459];
% diodes
xdiode=[60 70 80 90 100 110 120 130 140 150]
% QED Gold diode on surface under 6MV
yqedgold6=[2.8178 2.0559 1.5675 1.2330 1.0000 0.8257 0.6928 0.5883 0.5069 0.4403];
% QED Red diode on surface for 18MV-measured on 9/17/03
yqedred18=[2.8345 2.0553 1.5703 1.2381 1.0000 0.8220 0.6893 0.5853 0.5034 0.4376];
% Isorad-3 Gold diode on surface for 6MV
yisogold6=[2.7977 2.0465 1.5633 1.2348 1.0000 0.8264 0.6941 0.5905 0.5102 0.4439];
% Isorad-3 Red diode on surface for 18MV
yisored18=[2.8346 2.0689 1.5727 1.2367 1.0000 0.8250 0.6920 0.5881 0.5061 0.4384];
% SDD CF
qqedgold6=yion6q./yqedgold6;
qqedred18=yion18q./yqedred18;
qisogold6=yion6iso./yisogold6;
qisored18=yion18iso./yisored18;
figure(1)
h=plot(xdiode,qisogold6,'*',xdiode,qisored18,'+',xdiode,qqedgold6,'o',xdiode,qqedred18,'
x');
set(h,'linewidth',2);
set(h,'markersize',10);
%h=legend('QED (6-12 MV) n-type','QED(15-25 MV) n-type');
xlabel('SDD (cm)','fontsize',13);
ylabel('SDD CF','fontsize',13);
title('SDD Dependence','fontsize',13);
set(gca,'fontsize',13,'linewidth',1.5,'yticklabel',['0.97'; '0.98'; '0.99';'1.00'; '1.01';
'1.02';'1.03'],'xtick',[60 80 100 120 140 160])
axis('square');
axis([60 160 0.97 1.03]);
grid on;
```

Appendix D (Continued)

Run the file from Appendix B called invsq1.m along with Figure 24. Follow the directions at the beginning of Appendix B

```
Figure 24 Paper IV
% This program will analyze the Dose rate dependence of diodes
% Ion chamber data for QED n-type pt doped
ssdionq=[60 70 80 90 100 110 120 130 140 150 175.1 205.1];
xion6q=[17438 12744 9713 7695 6231 5122 4306 3668 3161 2746 2025 1466];
xion18q=[39917 29153 22238 17573 14262 11716 9855 8387 7235 6285 4638 3364];
yion6q=[2.7985 2.0451 1.5588 1.2349 1.0000 0.8220 0.6910 0.5887 0.5073 0.4406
0.3249 0.2352];
yion18q=[2.7989 2.0441 1.5593 1.2322 1.0000 0.8215 0.6910 0.5881 0.5073 0.4407
0.3252 0.2359];
% Ion chamber Isorad -3 pt doped diode
ssdioniso3=[60 70 80 90 100 110 120 130 140 150 172.8 203.1];
xion6iso3=[17270 12647 9655 7620 6169 5093 4276 3646 3136 2734 2047 1488];
xion18iso3=[38946 28631 21820 17226 13977 11545 9698 8246 7117 6201 4650 3380];
yion6iso3=[2.7994 2.0501 1.5651 1.2352 1.0000 0.8255 0.6931 0.5910 0.5084 0.4431
0.3318 0.2412];
yion18iso3=[2.7865 2.0485 1.5612 1.2325 1.0000 0.8260 0.6939 0.5900 0.5092 0.4437
0.3327 0.2418];
%==========Diode Data=======================
%       QED Gold (6-12 MV) pt doped n-type diode;
xqed1n6=[17438 12744 9713 7695 6231 5122 4306 3668 3161 2746 2025 1466];
xqed1n18=[39917 29153 22238 17573 14262 11716 9855 8387 7235 6285 4638 3364];
yqed1n6=[2.8420 2.0715 1.5753 1.2385 1.0000 0.8212 0.6893 0.5849 0.5030 0.4367
0.3171 0.2289];
yqed1n18=[2.8225 2.0637 1.5725 1.2394 1.0000 0.8225 0.6904 0.5867 0.5041 0.4375
0.3170 0.2293];
% normalize to the corresponding ion chamber value
Sxqed1n6=invsq1(ssdionq,yion6q,ssdionq).*6169;
Sqed1n6=yqed1n6./invsq1(ssdionq,yion6q,ssdionq);
Sxqed1n18=invsq1(ssdionq,yion18q,ssdionq).*13977;
Sqed1n18=yqed1n18./invsq1(ssdionq,yion18q,ssdionq);
% QED Red (15-25 MV) pt doped n-type unirradiated diode
xqed2n6=[17438 12744 9713 7695 6231 5122 4306 3668 3161 2746 2025 1466];
xqed2n18=[39917 29153 22238 17573 14262 11716 9855 8387 7235 6285 4638 3364];
yqed2n6=[2.8404 2.0729 1.5779 1.2410 1.0000 0.8235 0.6892 0.5848 0.5027 0.4367
0.3184 0.2300];
yqed2n18=[2.8166 2.0565 1.5707 1.2375 1.0000 0.8220 0.6891 0.5851 0.5027 0.4372
0.3195 0.2306];
```

Appendix D (Continued)

```
% Normalize to the corresponding ion chamber value
Sxqed2n6=invsq1(ssdionq,yion6q,ssdionq).*6169;
Sqed2n6=yqed2n6./invsq1(ssdionq,yion6q,ssdionq);
Sxqed2n18=invsq1(ssdionq,yion18q,ssdionq).*13977;
Sqed2n18=yqed2n18./invsq1(ssdionq,yion18q,ssdionq);
% Isorad 3 Gold (6-12 MV)pt doped n-type unirradiated diode
xiso3gold6=[17270 12647 9655 7620 6169 5093 4276 3646 3136 2734 2047 1488];
xiso3gold18=[38946 28631 21820 17226 13977 11545 9698 8246 7117 6201 4650
3380];
yiso3gold6=[2.8140 2.059 1.5698 1.2366 1.0000 0.8241 0.6906 0.5880 0.5056 0.4403
0.3295 0.2366];
yiso3gold18=[2.8003 2.049 1.5664 1.2360 1.0000 0.8242 0.6913 0.5886 0.5071 0.4414
0.3311 0.2390];
% Normalize to the corresponding ion chamber value
Sxiso3gold6=invsq1(ssdioniso3,yion6iso3,ssdioniso3).*6169;
Siso3gold6=yiso3gold6./invsq1(ssdioniso3,yion6iso3,ssdioniso3);
Sxiso3gold18=invsq1(ssdioniso3,yion18iso3,ssdioniso3).*13977;
Siso3gold18=yiso3gold18./invsq1(ssdioniso3,yion18iso3,ssdioniso3);
% Isorad 3 Red (15-25 MV)pt doped n-type unirradiated diode
xiso3red6=[17270 12647 9655 7620 6169 5093 4276 3646 3136 2734 2047 1488];
xiso3red18=[38946 28631 21820 17226 13977 11545 9698 8246 7117 6201 4650 3380];
yiso3red6=[2.8006 2.05 1.570 1.2347 1.0000 0.8244 0.6925 0.5902 0.5078 0.4419
0.3319 0.2398];
yiso3red18=[2.7875 2.0450 1.5630 1.2340 1.0000 0.8246 0.6935 0.5903 0.5085 0.4421
0.3316 0.2401];
% Normalize to the corresponding ion chamber value
Sxiso3red6=invsq1(ssdioniso3,yion6iso3,ssdioniso3).*6169;
Siso3red6=yiso3red6./invsq1(ssdioniso3,yion6iso3,ssdioniso3);
Sxiso3red18=invsq1(ssdioniso3,yion18iso3,ssdioniso3).*13977;
Siso3red18=yiso3red18./invsq1(ssdioniso3,yion18iso3,ssdioniso3);
% Normalize all Sensitivity to that for dose rate of 10000 cGy/s for Varian linac
Sqed1n6=Sqed1n6./interp1(Sxqed1n6,Sqed1n6,10000);
Sqed1n18=Sqed1n18./interp1(Sxqed1n18,Sqed1n18,10000);
Sqed2n6=Sqed2n6./interp1(Sxqed2n6,Sqed2n6,10000);
Sqed2n18=Sqed2n18./interp1(Sxqed2n18,Sqed2n18,10000);
Siso3gold6=Siso3gold6./interp1(Sxiso3gold6,Siso3gold6,10000);
Siso3gold18=Siso3gold18./interp1(Sxiso3gold18,Siso3gold18,10000);
Siso3red6=Siso3red6./interp1(Sxiso3red6,Siso3red6,10000);
Siso3red18=Siso3red18./interp1(Sxiso3red18,Siso3red18,10000);
% combining the data for low and high energies for each diode
xqed1n=[Sxqed1n6,Sxqed1n18];
qed1n=[Sqed1n6,Sqed1n18];
xqed2n=[Sxqed2n6,Sxqed2n18];
```

Appendix D (Continued)

```
qed2n=[Sqed2n6,Sqed2n18];
xiso3gold=[Sxiso3gold6,Sxiso3gold18];
iso3gold=[Siso3gold6,Siso3gold18];
xiso3red=[Sxiso3red6,Sxiso3red18];
iso3red=[Siso3red6,Siso3red18];
figure(1)
h=plot(xqed1n,qed1n,'o',xqed2n,qed2n,'x',xiso3gold,iso3gold,'*',xiso3red,iso3red,'+');
set(h,'linewidth',2);
set(h,'markersize',10);
xlabel('Instantaneous Dose Rate (cGy/s)','Fontsize',13);
ylabel('S/S(10000)','Fontsize',13);
title('Dose Rate Dependence n-type (Pt-doped) Diodes','fontsize',13);
axis('square');
axis([0 40000 0.96 1.02]);
set(gca,'fontsize',13,'linewidth',1.5)
grid on;
```

Appendix D (Continued)

Figure 25 Paper IV

```
% Field Size dependence data taken at dmax, diode on the surface, ion on dmax (1.6 cm for 6 MV and 3.2 cm for 18 MV)
%       ion chamber (for the new and old unnirradiated diodes, EDP10)
fs=[4 6 8 10 12 15 20 25 30 40];
%FS CF
iso3gold6=[0.985 0.992 0.996 1.000 1.000 1.004 1.006 1.008 1.007 1.007];% this is the ratio of ion to diode for 6X
iso3red18=[0.962 0.981 0.990 1.000 1.005 1.012 1.018 1.021 1.025 1.034]% 18 X
qedgold6=[0.995 0.998 0.999 1.000 1.001 1.001 1.002 1.003 1.004 1.005]% 6X
qedred18=[0.981 0.993 0.998 1.000 1.003 1.005 1.006 1.006 1.006 1.007];% 18x
figure(1)
h=plot(fs,iso3gold6,'*',fs, iso3red18,'+',fs,qedgold6,'o',fs,qedred18,'x');
set(h,'markersize',10);
set(h,'linewidth',2);
xlabel('Field Size (cm^2)','fontsize',13)
ylabel('FS CF','fontsize',13)
axis([0 40 0.96 1.04]);
set(gca,'fontsize',13,'linewidth',1.5,'yticklabel',['0.96'; '0.97'; '0.98'; '0.99'; '1.00';
'1.01';'1.02';'1.03';'1.04'],'xtick',[0 5 10 15 20 25 30 35 40])
title('Field Size Dependence','fontsize',13)
axis('square')
grid on
```

Appendix D (Continued)

Figure 26 Paper IV

```
% This program analyze the angular dependence of Isorad 3 and QED n-type diodes
% Angle in degrees
angle=[-75 -60 -45 -30 -15 -10 -5 0 5 10 15 30 45 60 75];
iso3gold=[0.974 0.987 0.995 0.999 1.000 1.001 1.001 1.000 1.001 1.001 1.001 1.000
0.998 0.992 0.977]; %taken under 6 X
iso3red=[0.989 0.996 0.999 0.999 1.001 1.001 1.001 1.000 1.001 1.001 1.001 1.002
1.002 0.999 0.988];% taken under 18 X
qed1n6=[0.934 0.988 1.000 1.000 0.998 0.998 0.999 1.000 1.001 1.003 1.005 1.006
1.011 0.986 0.925];%taken under 6X
qed2n18=[0.978 1.023 1.027 1.017 1.008 1.005 1.002 1.000 0.999 0.998 0.999 1.005
1.011 1.011 0.978]% taken under 18 X
figure(1)
h=plot(angle,iso3gold,'*',angle,iso3red,'+',angle,qed1n6,'o',angle,qed2n18,'x');
set(h,'linewidth',2);
set(h,'markersize',10);
xlabel('Angle(deg)','fontsize',13)
ylabel('Relative CF','fontsize',13)
title('Angular Dependence','fontsize',13)
axis('square')
axis([-80 80 0.920 1.04]);
set(gca,'fontsize',13,'linewidth',1.5,'yticklabel',['0.92'; '0.94'; '0.96'; '0.98'; '1.00';
'1.02';'1.04'],'xtick',[-80 -60 -40 -20 0 20 40 60 80])
grid on
```

Appendix D (Continued)

```
Figure 27 Paper IV
%       Temperature dependence of the IsoGold (6-12 MV) n-type unirradaited pt doped
diode
% Isorad3 Gold Data
% 6MV
x1=[11.25 15.85 20.7 25.55 29.8 33.6];
y1=[93.1 95.2 97.7 99.9 102.5 104.5];
yref1=interp1(x1,y1,22);
y1=y1./yref1;
% 18 MV
x2=[11.25 15.85 20.7 25.55 29.8 33.6];
y2=[121.2 123.8 126.7 130 133 135.8];
yref2=interp1(x2,y2,22);
y2=y2./yref2;
% Isorad 3 Red Data
% 6MV
x3=[11.3 15.7 20.7 25.6 29.7 33.4];
y3=[96 98 100 102 103.9 105.8];
yref3=interp1(x3,y3,22);
y3=y3./yref3;
% 18 MV
x4=[11.3 15.7 20.7 25.6 29.7 33.4];
y4=[137.2 139.9 142.9 145.7 148.6 151.1];
yref4=interp1(x4,y4,22);
y4=y4./yref4;
% QED Gold Data
% 6MV
x5=[13.5 18.4 22.2 26.9 33.15 35.3];
y5=[128.4 131.6 134.6 138.35 144.65 146.5];
yref5=interp1(x5,y5,22);
y5=y5./yref5;
% 18 MV
x6=[13.5 18.4 22.2 26.9 33.3 35.5];
y6=[156 160.2 163.8 168.45 176.6 179.3];
yref6=interp1(x6,y6,22);
y6=y6./yref6;
% QED Red Data
% 6MV
x7=[13.5 18.4 22.2 26.9 33.3 35.5];
y7=[124.6 127.85 130.7 134.4 141.4 143];
yref7=interp1(x7,y7,22);
y7=y7./yref7;
```

Appendix D (Continued)

```
% 18 MV
x8=[13.5 18.4 22.2 26.9 33.3 35.5];
y8=[156.2 159.7 163.2 167.9 175.8 177.7];
yref8=interp1(x8,y8,22);
y8=y8./yref8;
% Find out the slopes
p1=polyfit(x1,y1,1);
p2=polyfit(x2,y2,1);
p3=polyfit(x3,y3,1);
p4=polyfit(x4,y4,1);
p5=polyfit(x5,y5,1);
p6=polyfit(x6,y6,1);
p7=polyfit(x7,y7,1);
p8=polyfit(x8,y8,1);
x=10:40;
y1f=polyval(p1,x);
y2f=polyval(p2,x);
y3f=polyval(p3,x);
y4f=polyval(p4,x);
y5f=polyval(p5,x);
y6f=polyval(p6,x);
y7f=polyval(p7,x);
y8f=polyval(p8,x);
% Interpolate at 22C for the fitted value
y1fref=interp1(x,y1f,22);
y2fref=interp1(x,y2f,22);
y3fref=interp1(x,y3f,22);
y4fref=interp1(x,y4f,22);
y5fref=interp1(x,y5f,22);
y6fref=interp1(x,y6f,22);
y7fref=interp1(x,y7f,22);
y8fref=interp1(x,y8f,22);
% Normalize the fitted interpolated values at 22deg C
y1f=y1f./y1fref;
y2f=y2f./y2fref;
y3f=y3f./y3fref;
y4f=y4f./y4fref;
y5f=y5f./y5fref;
y6f=y6f./y6fref;
y7f=y7f./y7fref;
y8f=y8f./y8fref;
% plot out the results
figure(1)
```

Appendix D (Continued)

```
xerr=[17 17];
yerr=1.045.*[1 1.007];
xerr1=[xerr(1)*(1-.02) xerr(1)*(1+.02)];
yerr1=[yerr(1) yerr(1)];
xerr2=xerr1;
yerr2=[yerr(2) yerr(2)];
h=plot(x1,y1,'*',x3,y3,'+',x5,y5,'o',x7,y7,'x',x,y1f,x,y3f,x,y5f,x,y7f,xerr,yerr,xerr1,yerr1,x
err2,yerr2)
set(h,'linewidth',2);
set(h,'markersize',10);
xlabel('Temperature (^oC)','fontsize',13)
ylabel('Relative Charge','fontsize',13)
title('Temperature Dependence (6 MV)','fontsize',13)
axis('square');
axis([10 40 0.94 1.12])
set(gca,'fontsize',13,'linewidth',1.5,'yticklabel',['0.94'; '0.96'; '0.98'; '1.00'; '1.02';'1.04';
'1.06';'1.08'; '1.10'; '1.12'],'xtick',[10 15 20 25 30 35 40])
grid
gtext('error','fontsize',12.5)
gtext(['* - Isorad-3 Gold = ' num2str(p1(1)*100,2) '%/^oC'],'fontsize',12.5)
gtext(['+ - Isorad-3 Red = ' num2str(p3(1)*100,2) '%/^oC'],'fontsize',12.5)
gtext(['o - QED Gold = ' num2str(p5(1)*100,2) '%/^oC'],'fontsize',12.5)
gtext(['x - QED Red = ' num2str(p7(1)*100,2) '%/^oC'],'fontsize',12.5)
gtext('(a)','fontsize',20)
figure(2)
xerr=[17 17];
yerr=1.045.*[1 1.007];
xerr1=[xerr(1)*(1-.02) xerr(1)*(1+.02)];
yerr1=[yerr(1) yerr(1)];
xerr2=xerr1;
yerr2=[yerr(2) yerr(2)];
h=plot(x2,y2,'*',x4,y4,'+',x6,y6,'o',x8,y8,'x',x,y2f,x,y4f,x,y6f,x,y8f,xerr,yerr,xerr1,yerr1,x
err2,yerr2)
set(h,'linewidth',2);
set(h,'markersize',10);
xlabel('Temperature (^oC)','fontsize',13)
ylabel('Relative Charge','fontsize',13)
title('Temperature Dependence (18 MV)','fontsize',13)
axis('square');
axis([10 40 0.94 1.12])
set(gca,'fontsize',13,'linewidth',1.5,'yticklabel',['0.94'; '0.96'; '0.98'; '1.00'; '1.02';'1.04';
'1.06';'1.08'; '1.10'; '1.12'],'xtick',[10 15 20 25 30 35 40])
grid
```

Appendix D (Continued)

```
gtext('error','fontsize',12.5)
gtext(['* - Isorad-3 Gold = ' num2str(p2(1)*100,2) '%/^oC'],'fontsize',12.5)
gtext(['+ - Isorad-3 Red = ' num2str(p4(1)*100,2) '%/^oC'],'fontsize',12.5)
gtext(['o - QED Gold = ' num2str(p6(1)*100,2) '%/^oC'],'fontsize',12.5)
gtext(['x - QED Red = ' num2str(p8(1)*100,2) '%/^oC'],'fontsize',12.5)
gtext('(b)','fontsize',20)
```

ABOUT THE AUTHOR

Amarjit Saini lives with his wife Reena Saini and two kids Aren and Esha in Tampa Bay area. He completed his bachelor degree in electrical engineering at the University of South Florida in 1994. He started his graduate studies at University of Florida and received master's degree in medical health physics in 1996 from the Department of Nuclear Engineering and Radiological Sciences. After two years of clinical training in medical radiation physics at Shands Cancer Center at the University of Florida, he worked as a medical physicist at Hackensack University Medical Center in New Jersey. He became board certified in therapeutic medical physics from the American Board of Radiology in year 2000. He joined the H. Lee Moffitt Cancer as a clinical radiation physicist in year 2001 and started pursuing Ph.D. at the University of South Florida in 2002.